A Geochemical Exploration of the Sagehen Volcanic Centre, Truckee-Tahoe Region, California, U.S.A.

uOttawa

By **Christopher Angus Leo Clarke**
BSc (Hon) Geology

A Thesis submitted to the Faculty of Science in partial fulfillment of the requirements for the degree of
Master of Science

Department of Earth Sciences
Ottawa Carleton Geoscience Centre
University of Ottawa
June, 2012

Supervisor:_____ **Supervisor:**_____

Brian Cousens **Anthony Fowler**

Abstract

The assemblage of ca. 6–4 Ma volcanic rocks exposed at the Sagehen Research station in the Truckee-Tahoe region of the northern Sierra Nevada, United States, is interpreted to be, within the Ancestral Cascades volcanic arc, a Lassen-type stratovolcano complex. Sagehen is of particular importance because it is one of the few Tertiary arc volcanic centres in California which has not been heavily glaciated during the Pleistocene. The volcanic rocks are variably porphyritic or aphanitic, including abundant plagioclase with clinopyroxene and amphibole. The rocks range from basalt to basaltic-andesite to andesite in composition. Basalts are olivine- and clinopyroxene-bearing with minor phenocrysts of plagioclase. The basaltic-andesites are primarily pyroxene bearing while the andesites contain pyroxene-, plagioclase- and hornblende porphyritic phases. Sagehen arc lavas are calc-alkaline and enriched in the large ion lithophile elements and depleted in High Field Strength Elements. The basalts are depleted in Zr and Hf while the andesites are enriched with Zr and Hf relative to the middle rare earth elements. Compared to previously studied Ancestral Cascade arc samples, Sagehen region basalts have lower $^{143}Nd/^{144}Nd$ isotopic values that do not correspond to proposed mantle-lithosphere mixing lines, while the andesite samples appear to represent the interplay of these two components on a $^{87}Sr/^{86}Sr$ vs. $^{143}Nd/^{144}Nd$. The trace element data and isotopic plots suggest that the melts that produced the basalts are from subduction modified mantle wedge peridotites that ponded near the base of the lithosphere similar to the generation of other subduction related calc-alkaline lavas along convergent continental margins. The andesitic samples appear to be the result of further modification through crustal assimilation as seen in the higher isotopic Sr contents in the andesites and Ce/Sm_{pmn} vs. Tb/Yb_{pmn} plots. Finally, the proposed map units from Sylvester & Raines (2007) were found to contain various geochemical facies based on the samples collected indicating that some map units may have to be redefined or sub-divided.

Acknowledgements

I would like to thank my supervisors, Brian Cousens and Tony Fowler for their support and guidance over the last two years.

Furthermore, I would like to thank the members of the Isotope Geochemistry and Geochronology Research Centre, especially Dr. Elizabeth Ann Spencer and Dr. John Blenkinsop for their help and patience while training me to use the machinery.

I would also like to thank Jiri (George) Mrazek for preparing the polished thin sections and UC Berkeley for giving permission to work on their land.

Finally, I would like to thank my family for their support.

Table of Contents

List of Figures

List of Tables

List of Plates

1. Introduction

The Sagehen Volcanic Centre (SVC) is part of the Ancestral Cascades Arc (ACA) which is the inactive southern extension of the Modern Cascades Arc which includes the volcanic centres of Lassen, Shasta and Mt. St. Helens (Figure 1). The SVC was mapped by Sylvester and Raines (2007) with the help of undergraduate students from the University of California, Santa Barbara. The SVC is of particular importance because it is part of the Tertiary volcanic arc in north-eastern California which has not been heavily glaciated during the Pleistocene and is thus fairly well preserved geologically. Furthermore, the SVC's extrusive units are also highly constrained chronologically to within 2 Myrs of each other. This means that Sagehen can be used to 'zoom in' on a very thin slice of time where we can evaluate volcanic episodes within a set time period.

Both the Ancestral and Modern Cascades arcs belong to the Cascades Range, a 36 million year old subduction margin that extends from southern California to British Columbia and is actively consuming the Juan de Fuca and Gorda oceanic plates. The Modern Cascades Arc covers volcanism over the last 5 Myrs to the present while the Ancestral Cascades Arc includes volcanism older than 5 Myrs (Hildreth, 2007). The Cascades Range is part of a larger subduction complex termed the Pacific Ring of Fire, which almost entirely borders the Pacific Ocean, and is responsible for active volcanism/tectonism in North America, South America, New Zealand, Southeast Asia, Japan and Russia.

It is important to study past arc volcanism because the Ancestral Cascades Arc can give us a reference model for arc volcanism occurring today at Lassen Peak and other Modern Cascades Arc centres (Figure 2). Likewise, a better understanding of Tertiary arc volcanism can help us to better predict future events within the Modern Cascades Arc centres and, indeed, along other portions of the Ring of Fire where major population centres of four continents reside.

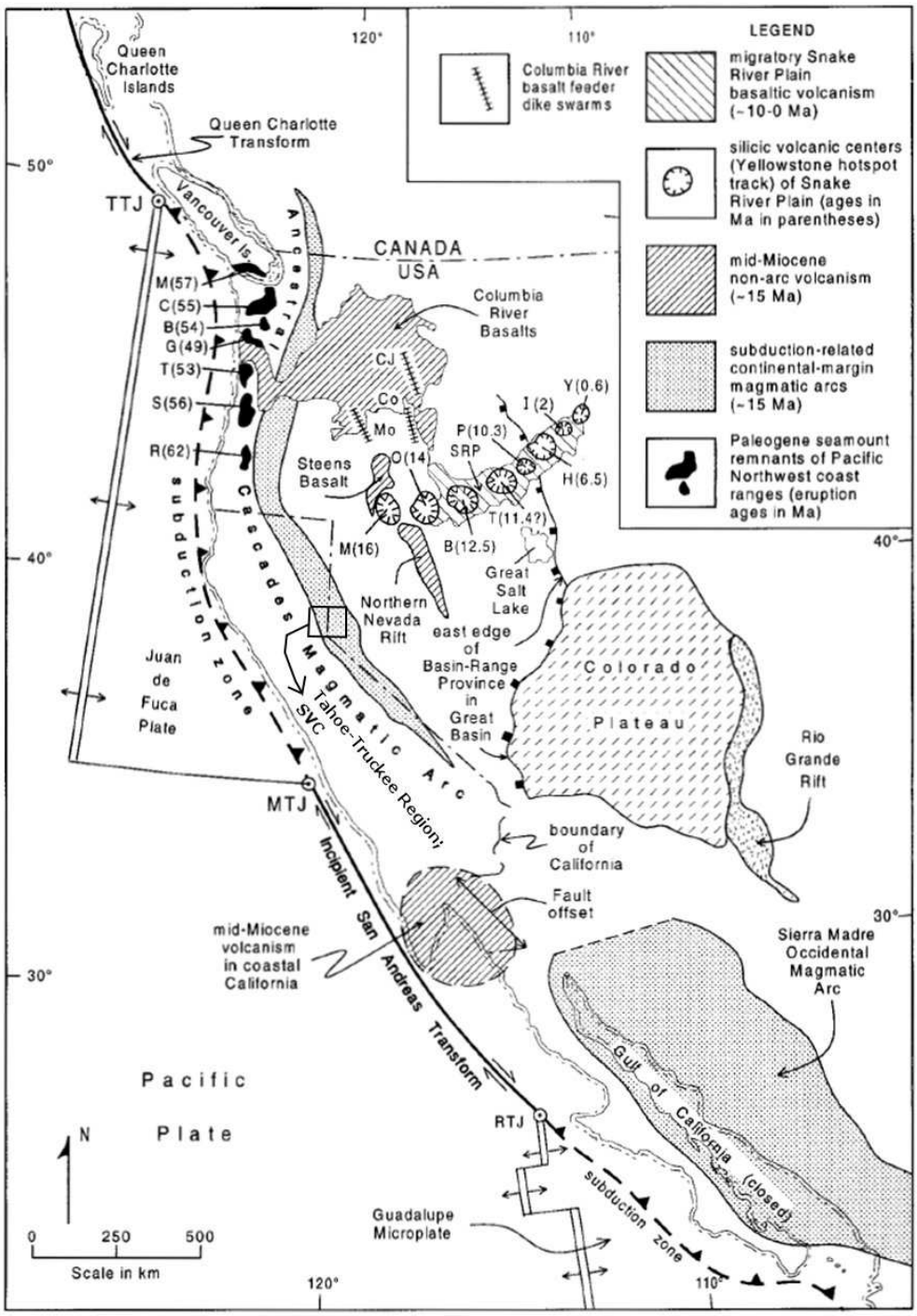

Figure 1: Geology of the Western U.S.A. during the Miocene-Pliocene showing the extent of the Ancestral Cascades arc and its relationships to other volcanic regions, notably the Basin and Range Province. Also note the location of the Mendocino Triple Junction, which has migrated northwards to its present location, off the coast parallel to the Lassen volcanic front from southern California. Modified from Dickinson, 1997.

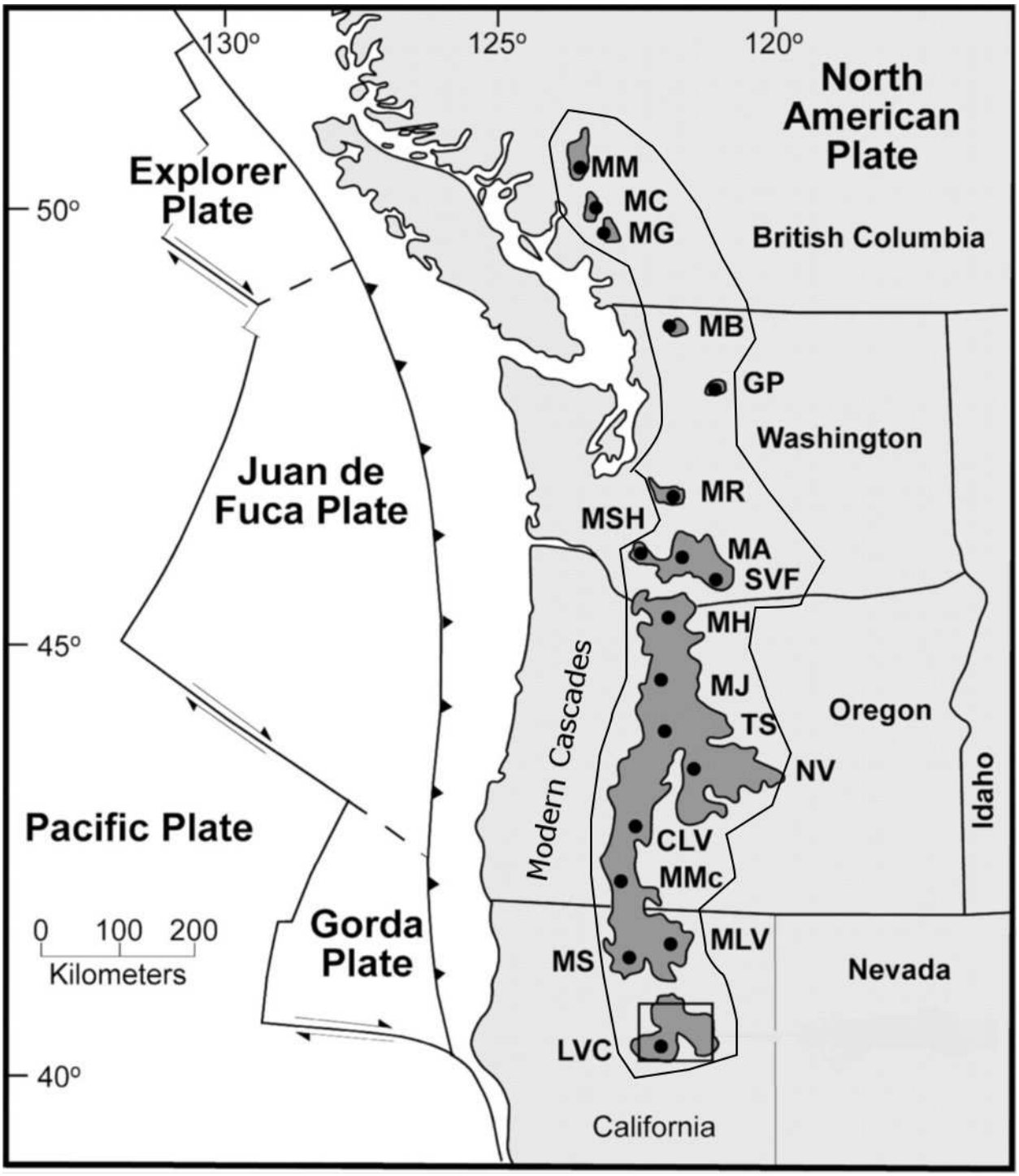

Figure 2: The Modern Cascades. MM=Mt. Meagher, MC= Mt. Cayley, MG= Mt. Garibaldi, MB= Mt. Baker, GP= Glacier Peak MR=Mt. Rainier, MSH= Mt. St. Helens, MA= Mt. Adams, MH=Mt. Hood, MJ= Mt. Jefferson, TS=Three Sisters, NV=Newberry volcanic field, CLV= Crater Lake Volcanics, MMc= Mt. McLoughlin, MLV= Medicine Lake Volcanics, MS= Mt. Shasta and the LVC = Lassen Volcanic Centre, , which is the most southern active volcano of the Modern Cascades and is therefore the closest Modern Cascades volcano to Sagehen. Modified from Hildreth, 2007.

1.1 General Characteristics of Continental Arc Volcanism

1.1.1 Subduction Zone Processes

Island arcs are proposed to be the principal sites for crustal genesis in the Phanerozoic (Holbrook et al., 1999). However, island arcs are closer in bulk composition to basalt and not andesite which is part of the 'andesite' model of continental growth. Island arcs are convergent margins of two oceanic plates, one of which is being subducted. This type of tectonic activity will generally result in a chain of volcanic islands up to several thousand kilometres long and two hundred to three hundred kilometres wide.

The Aleutian island arc is the result of the Pacific plate being subducted northwestward beneath the North American plate. The Aleutian island arc is thick enough (30 km) to generate continental crust but it has a mafic bulk composition, and lacks the seismic characteristics such as a reflective lower crust and a silicic upper crust characteristic of continental crust. The use of Zr/Y versus Y is a good discriminant between oceanic and continental arc settings beacause Zr/Y is enriched in continental crust (Pearce, 1983). The Aleutians have Zr/Y versus Y plots similar to oceanic arcs. A depleted mantle source is usually involved in the genesis of oceanic island arcs so upper convecting mantle is melted in this setting (Pearce, 1983). Holbrook et al., (1999) postulates that before or during accretion to a continental margin an island arc (like the Aleutians) would need to undergo pervasive deformation, intracrustal melting and delamination of mafic to ultramafic residium in order to transform it into a mature continental crust with an 'andesite' composition consistent with continental subduction settings (Holbrook et al., 1999).

The composition of continental mantle lithosphere i.e. its density, thickness and capacity to generate basalt varies with age. Archean mantle lithosphere is characterised by relatively low FeO abundances which are linked to komatiite extraction therefore making it less dense. Post-Archean mantle lithosphere is thought to be similar to spinel peridotite inclusions in alkali basalts which make it more likely to produce continental flood basalts and it is dense enough to be delaminated and incorporated into asthenospheric source regions of oceanic basalts (Hawkesworth et al., 1990). The Columbia River and the Deccan Flood basalts have isotope signatures consistent with derivation from sub-lithospheric, ocean island basalt (OIB) -type mantle reservoirs and were erupted on cratonic margins (Hawkesworth et al., 1990).

Observations show that average crustal compositions above Mesozoic and Cenozoic subduction zones are primarily andesitic (intermediate) with high Rb/Sr ratios relative to Bulk Earth (Ellam & Hawkesworth, 1988). This observation for Post-Archean and Post-Proterozoic lithosphere along continental margins is termed *the andesite model*. However *the andesite model* implies andesite is a primary magma since average flux values from the mantle to the crust would have to be andesitic. Hawkesworth et al., (1977) suggests from experimental evidence that andesites could be derived from melting subducted material. Isotopic and trace element data show that subduction zone magmas are derived from the mantle wedge between the subducting and over-riding plates which is likely peridotitic (Ellam & Hawkesworth, 1988). The genesis of most typical arc magmas is attributed to melting of the mantle wedge fluxed by the addition of small (<2%) amounts of slab-derived fluids (Pearce and Parkinson, l993). It is widely believed that magma sources in the mantle wedge are infiltrated by slab-derived fluids or melts before they give rise to primary magmas. If fluid is involved then it would have enriched sources in Sr and Pb relative to Nd (Vroon et al., 1993). Slab-melts rising into the hot mantle wedge are also

likely to interact with mantle peridotite (Vroon et al., 1993). Interaction of slab-melts with mantle peridotite may lower incompatible large ion lithophile element (LILE) and light rare earth element (LREE) concentrations relative to more compatible trace-elements (Stern & Kilian, 1996). Slab melts also transport Sr, Pb, and Nd into the mantle wedge. These fluid or melt additions to the mantle are termed subduction components. The LILEs are more soluble than LREEs in fluids, making the LILE more likely to be subduction components.

Volcanic arc basalts can usually be distinguished from basalts erupted in other settings by their selective enrichments in LILE and sometimes the LREEs and phosphorus and deficiencies in Nb, Ta, Ti (high field strength elements (HFSE)). The enrichment is independent of the overlying mantle wedge and is assumed to be subduction derived. Additionally, basalts erupted at active continental margins have Nb, Ta, Zr and Hf components that are not seen in oceanic island arcs. These elements are assumed to be from enriched metasomatized subcontinental lithosphere (Pearce, 1983). The subduction zone will generally provide Rb, K, Ba, Th and Sr while the lithosphere contributes portions of Ce, Sm and P and all of its Ta, Nb, Zr, Hf, Ti, Y and Yb (Pearce, 1983).

Continental volcanic rocks can be derived from both the subcontinental lithosphere and from the underlying convecting upper mantle. The concave-down pattern of incompatible elements (except Y and Yb) enriched relative to MORB is assumed to represent this (Figure 3; Pearce, 1983). Mesozoic to Cenozoic, subduction-related basalts have similar or lower Rb/Sr ratios than Bulk Earth which indicates that basaltic magmatism at subduction margins is not responsible for major fractionation of Rb/Sr between mantle and crust, since continental crust has elevated Rb/Sr ratios (Ellam & Hawkesworth, 1988). Continental mantle lithosphere has

remained isolated from the convecting mantle for long periods of geologic time (Hawkesworth et al., 1990). Mantle derived basalts enter the crust where they undergo fractional crystallization during cooling; they may also solidify in deeper regions of the crust until they are remobilized (Ellam & Hawkesworth, 1988). Ultimately the mantle-to-crust flux is differentiated into felsic material that rises into the upper crust while more mafic cumulates and/or restites remain at lower crustal depths. Andesites are therefore more likely to have been derived from fractional crystallization and crustal contamination processes rather than as primary melts of the mantle (Ellam & Hawkesworth, 1988).

The isotopic systematics of continental arc volcanism is varied but a few general observations can be gleaned. Generally "normal" modern oceanic arc isotopic signatures include $^{87}Sr/^{86}Sr$ = 0.7045-0.7055, $^{143}Nd/^{144}Nd$ = 0.51273-0.51291 and $^{206}Pb/^{204}Pb$ = 18.66-18.75 (Vroon et al., 1993). Slightly elevated $^{87}Sr/^{86}Sr$ at low $^{206}Pb/^{204}Pb$ is also regarded as a feature of continental mantle lithosphere relative to MORB due to its greater age (Hawkesworth et al., 1990).

Subduction conditions in typical volcanic arcs favour subduction of cooler, hydrated oceanic lithosphere, slab-derived fluids may promote extensive flux-melting in the wedge (Leeman et al., 2005). A general characteristic of ‘cool’ volcanic arcs is the tendency to be enriched in fluid-mobile elements. Subducted oceanic crust normally would be expected to include altered MORB and sediment, as well as fresh MORB (Stern & Kilian, 1996). However, the Cascades and other relatively warm arcs such as those along the west coast of Mexico only mildly display this slab fluid signature (Leeman et al., 2005).

High silica melts with garnet and eclogitic characteristics are more likely to be derived from adakites, volcanic rocks derived from hot hydrous descending oceanic slab (Drummond & Defant, 1990; Ducea & Saleeby, 1998). Melts as silicic as 65-69% SiO_2 cannot be produced by partial fusion of peridotites at 1.5-2 GPa even if the liquid fractions are extremely low (Ducea & Saleeby, 1998). 'Warm' arcs produce adakites (slab melts) similar to those found in the Holocene volcanic centers of the Andean Austral Volcanic Zone (AVZ; 49–54°S; (Stern & Kilian, 1996)).

The AVZ has erupted exclusively adakitic andesites and dacites characterized by low Yb and Y concentrations and high Sr/Y ratios, suggesting a source with residual garnet, amphibole and pyroxene, but little or no olivine and plagioclase (Stern & Kilian, 1996). Melting of mafic lower crust may be the source for adakites in some arcs, but such a source is inconsistent with the high magnesium number (Mg#) of AVZ adakites (Stern & Kilian, 1996). The source for Andean adakites is more likely to be subducted oceanic basalt, recrystallized to garnet-amphibolite or eclogite (Stern & Kilian, 1996). Crustal assimilation and fractional crystallization (AFC) processes and the mass contribution from the crust become more significant northwards in the Andean volcanic arc as the angle of convergence becomes more orthogonal (Stern & Kilian, 1996).

Slab windows are a part of the tectonic picture in the western U.S.A. as suggested by Dickinson & Snyder (1979). Slab windows are parts of the subducted oceanic plate that contains a mid-ocean ridge resulting in in slab detachment along the ridge. This detachment essentially creates a zone (e.g. window) where there is no slab beneath the lithosphere, putting the lithosphere in direct contact with the more hot, plastic layer of the mantle. Alkali basalt

magmatism above slab windows is a commonly accepted product of passive upwelling of asthenospheric mantle. This type of magmatism is small in volume, often long-lived (> 1 Ma) and is not usually accompanied by extensional tectonism (Farmer et al., 1995).

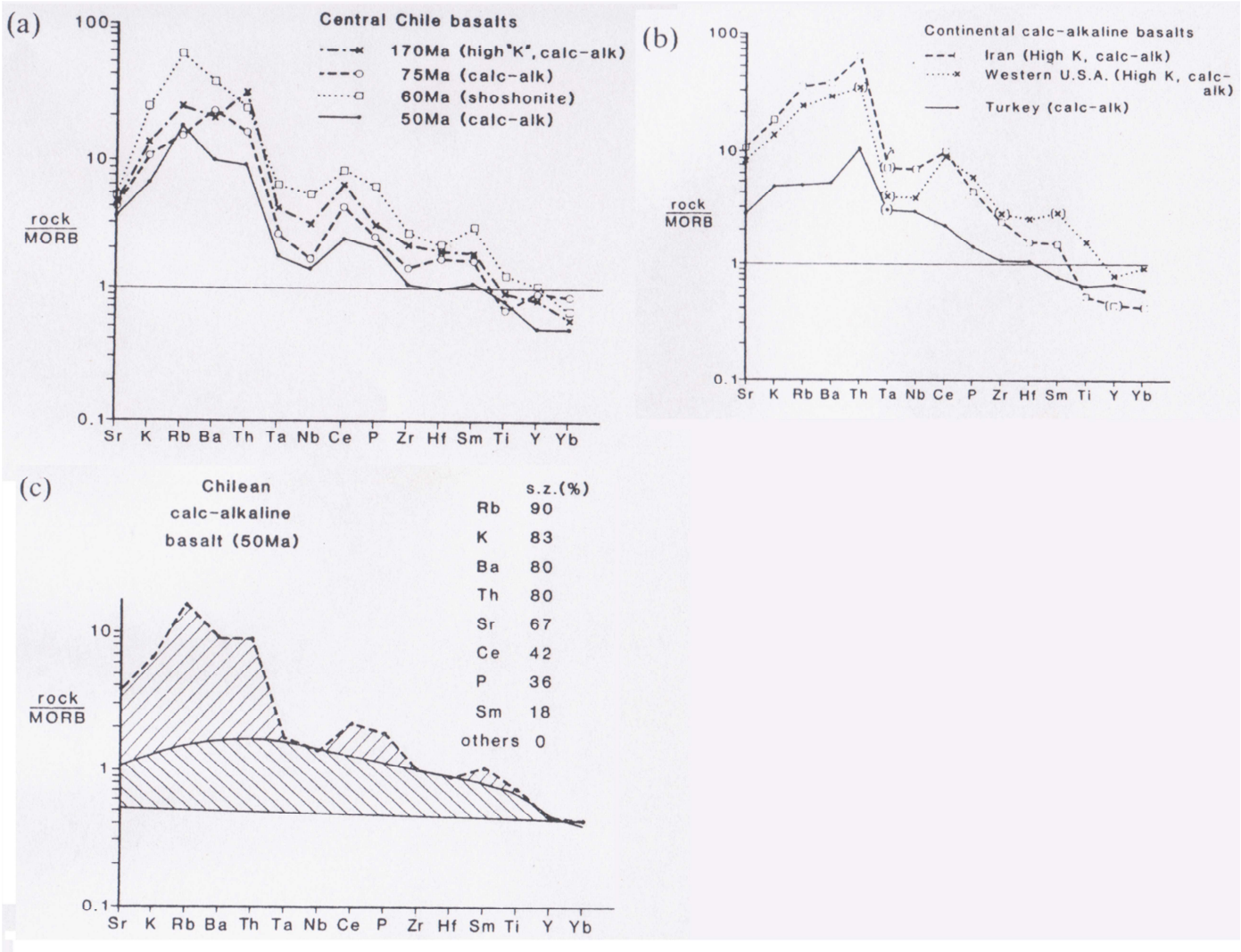

Figure 3: a) Geochemical patterns for basalts from the Central Chile convergent margin. b) Geochemical patterns for basalts from other active continental margins. c) Pearce's (1983) geochemical interpretation of a 50 Ma Chilean basalt and the relative influence of subduction component (s.z. (%)). The flat line represents the depleted mantle (MORB-type) source while the curved line above this line represents the elemental compositions that are not affected by subduction component (where they intersect the spidergram). The curved line infers the composition the basalt would have if it were derived from subcontinental lithosphere without a subduction component. Figure from Pearce, (1983).

1.1.2 Crustal Contamination/Magma Mixing

Continental crust in subduction zones can be up to 70 km thick. Newly generated mafic magma can therefore be subject to contamination by the upper and lower crust as it ascends to the surface. The crust, generally, is enriched in incompatible elements and is composed of low density felsic minerals. Felsic material, and by extension the crust, has a lower melting point than most mafic melts making crust-mantle melt mixing due to partial melting possible. This means a mafic melt contaminated with felsic material will itself become more siliceous and have a more crustal character in trace elements and isotopic ratios. Crustal contamination of basalts can be associated with the following characteristics (these are not definitive): enrichments of Th, Ba, Pb, Rb, K and Sr (sometimes) due to granitoid rock assimilation whereas Th and Ba enrichments occur for greywacke assimilation. Major element constraints limit the degree of contamination that is possible and trace element and radiogenic isotope ratios correlate with SiO_2 (Pearce, 1983).

The Southern Volcanic Zone (SVZ) in the Andes as described by Hildreth and Moorbath (1988) can be used as an example of upper crustal contamination. The SVZ extends from 33°S to 37°S, between the Andean Cordillera volcanic front and the Pacific Coast of Chile. The SVZ is a unique continental arc subduction zone in that the Nazca oceanic plate subducts beneath the SVZ at an equal angle and rate along the length of the plate segment. The composition of the continental crust is also fairly constant, while the thickness of the continental crust increases from south to north. Also, regional river discharge transfers a relatively uniform quantity and composition of sediment to the oceanic trench prior to subduction and does not strongly influence isotopic compositions (Hildreth and Moorbath, 1988). This means geochemical discrepancies can be attributed primarily to the distance traveled by the magma through the

continental crust. Hildreth and Moorbath (1988) demonstrated that K_2O has a pronounced increasing concentration moving northward along the volcanic front, while most of the other major oxides such as CaO, Al_2O_3, P_2O_5, and Na_2O do not show any variation. A Bouguer Anomaly gradient within the SVZ positively correlates with K_2O suggesting an increase in crustal thickness moving northwards. This theory on thickening is also supported by an increase in silica (SiO_2) abundance in erupted lavas, from 50-60% in the south to 58-65% in the north. A plot of K_2O vs. SiO_2 shows increasing concentrations of both K_2O and SiO_2; however K_2O is increasing slightly more quickly than SiO_2. This K_2O and SiO_2 trend remains constant despite the crystallization of silica-poor phenocrysts of olivine and pyroxene in the south, and silica-rich phenocrysts of biotite and amphibole in the north that Hildreth and Moorbath (1988) observed in the volcanic rock suites. The authors also show that both the LILE's and LREE's increase with an increasing thickness of the continental crust. Their position is supported by isotope geochemistry results: an increasing ratio of $^{87}Sr/^{86}Sr$, and a decreasing ratio of $^{143}Nd/^{144}Nd$, from south to north, which suggests an increasing continental crust contribution to magmas.

Interaction of mafic melts with the lower crust is another potential source of contamination. In general, partial melting of mafic crust produces felsic melts resulting from the intrusion of hot mafic magmas (Beard and Lofgren, 1991; Drummond & Defant, 1990; Rapp and Watson, 1995). Felsic melts are generally enriched in the LILE and light REEs, and which have negative Nb and Ta anomalies if rutile is a residual phase; if melting occurs in the garnet stability field then REE patterns in the melt may be steep with high La/Yb and Sr/Y ratios and no Eu anomaly (Martin, 1986).Magma mixing is associated with some calc-alkaline volcanic provinces (Gerlach & Grove, 1982).

Magma mixing shortly before eruption can be inferred from the presence of mafic blebs and disequilibrium mineral assemblages (Ort et al., 1996). Furthermore, magma mixing is associated with some calc-alkaline volcanic provinces (Gerlach & Grove, 1982). Evidence of magma mixing can include: reversed compositional zoning in olivines or plagioclase, glass inclusions trapped within phenocrysts and also oscillatory zoning in plagioclase (Gerlach & Grove, 1982). Trachytic textures in basaltic andesites and andesites, formed from cooling above the liquidus in lab experiments, are inferred to represent magma mixing in some volcanic suites (Gerlach & Grove, 1982). The Guatemala volcanic front (~12-16°N) has many compositional similarities to the Ancestral Cascades, especially its isotopic data (Carr et al., 1990). The explanation for the Guatemala isotopic array is mixing between two magmas; modified mantle and enriched mid-ocean ridge basalt (EMORB) mantle and crust (Carr et al., 1990). The modified mantle melt is generated beneath the volcanic field by release of fluid into the mantle wedge. The EMORB melt is generated by low-degree decompression melting of asthenosphere as it is drawn up toward the wedge corner (Carr et al., 1990).

1.1.3 Sources of Melts (Garnet versus Spinel peridotite)

Possible melt sources in volcanic continental arcs are: deep asthenosphere mantle, shallow asthenosphere mantle, metasomatized mantle wedge, subcontinental lithospheric mantle, upper and lower crust, subducted sediment or melted oceanic crust (Righter, 2000; Stern & Kilian, 1996). Possible sources of melts are hydrous phases in peridotites, hydrous eclogites and subducted oceanic sediments (Ducea & Saleeby, 1998). Peridotites have been proposed to be the main sources of Cascades melts such as those at Lassen (Clynne, 1990), Sceptor Creek (e.g.

Western Cascades; Ducea & Saleeby, 1998) and in the Tahoe-Truckee area (Cousens et al., 2008).

Garnet peridotites are from mantle depths greater than ~80 km which is where the pressure-temperature conditions for garnet peridotite is favourable (Figure 4). Garnet has high partition coefficients for the heavy REE, so melts in the garnet peridotite field have very steep REE patterns (Figure 5). Garnet peridotites from kimberlite pipes in Archean and Proterozoic basement from the Andes have low $^{143}Nd/^{144}Nd$ and high $^{87}Sr/^{86}Sr$ (Hawkesworth et al., 1990). Garnet peridotites are generally composed of 60% olivine, 20% orthopyroxene, 10% clinopyroxene and 10% garnet (Mysen, 1979).

Spinel peridotites are from intermediate mantle depths of ~40-80 km (Figure 4). Spinel has virtually zero partition coefficients for all incompatible elements, so melts of spinel peridotite have flat middle to heavy REE patterns (Figure 5). Spinel peridotites are less confined in terms of major element abundances than garnet peridotites (Hawkesworth et al., 1990). Spinel peridotite xenoliths from the Andes have high $^{143}Nd/^{144}Nd$ and low $^{87}Sr/^{86}Sr$ values which are from young lithospheric provinces (Hawkesworth et al., 1990). Spinel peridotites are generally composed of 55% olivine, 30% orthopyroxene, 10% clinopyroxene and 5% spinel (Mysen, 1979).

The model used by Reiners et al. (2000) to determine the parent magma of Washington Cascades arc basalts was a peridotite with 55% olivine, 30% orthopyroxene, 10% clinopyroxene and 2.5% garnet and 2.5% spinel. Removing the garnet and adding a comparable amount of spinel does not significantly affect the results (or by making it all garnet; Reiners et al., 2000). The peridotite can have small amounts of amphibole in it (Borg et al., 1997) but given the model

used by Reiners et al. (2000) pressures of 1-3 GPa would result in the Amphibole breaking down and reacting completely out of the modal assemblage at relatively low temperatures near the solidus. The lack of negative Ba anomalies in Reiners et al., (2000) samples also does not suggest there are large amounts of residual amphibole.

The Ba/La ratio is a measure of the role of subducted slab, especially subducted sediment since Ba is high in marine sediments (Carr et al., 1990). Within the Cascades, the role of sediment is not clearly understood with some studies suggesting small amounts of sediment can produce the geochemical signatures of the rock suites (Conrey et al., 1997) while others find little evidence of sediment in basaltic magma genesis (Leeman et al., 1990; Righter, 2000).

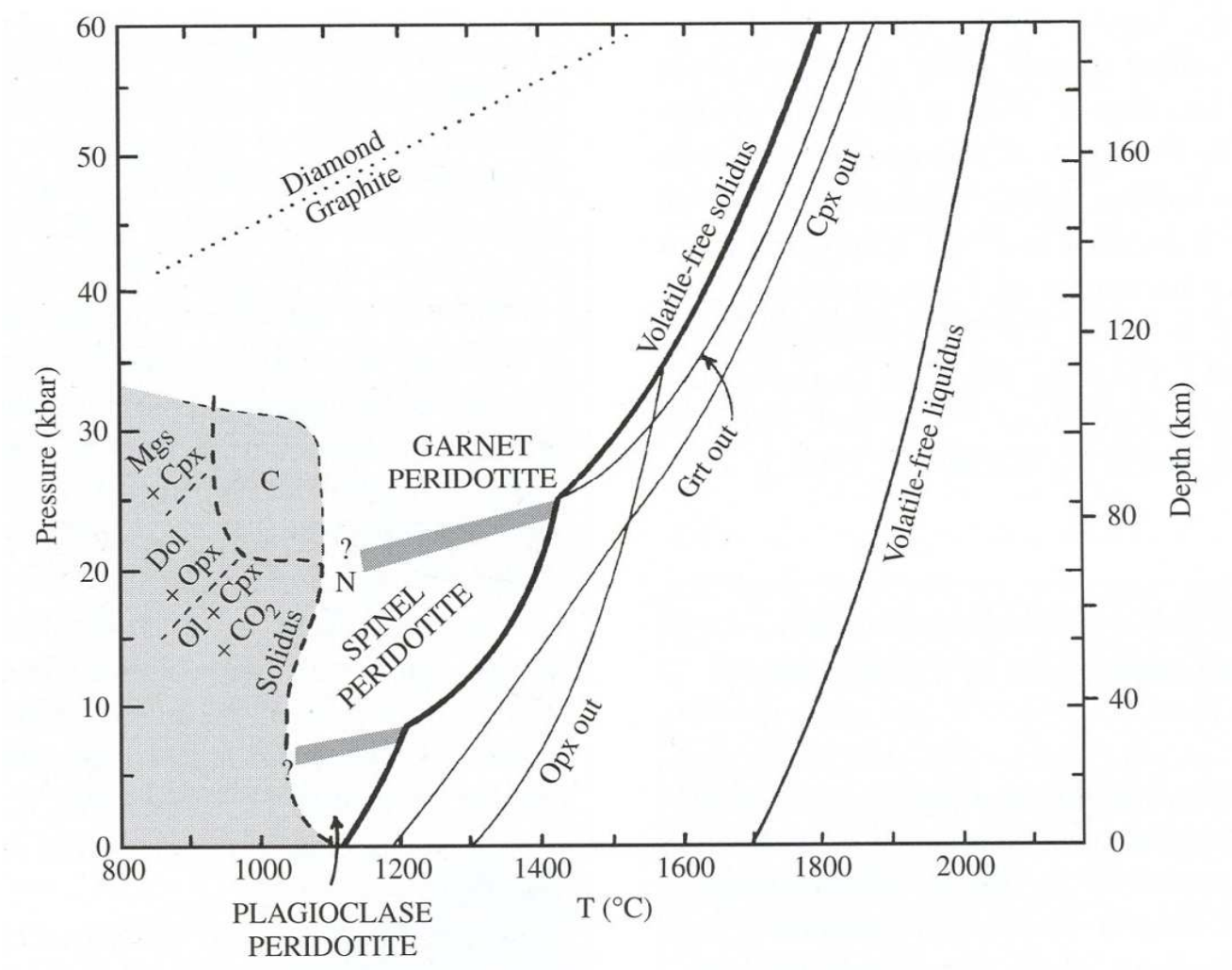

Figure 4: Phase diagram, showing stability of aluminous phases in the mantle. Modified from Wallace & Green (1988).

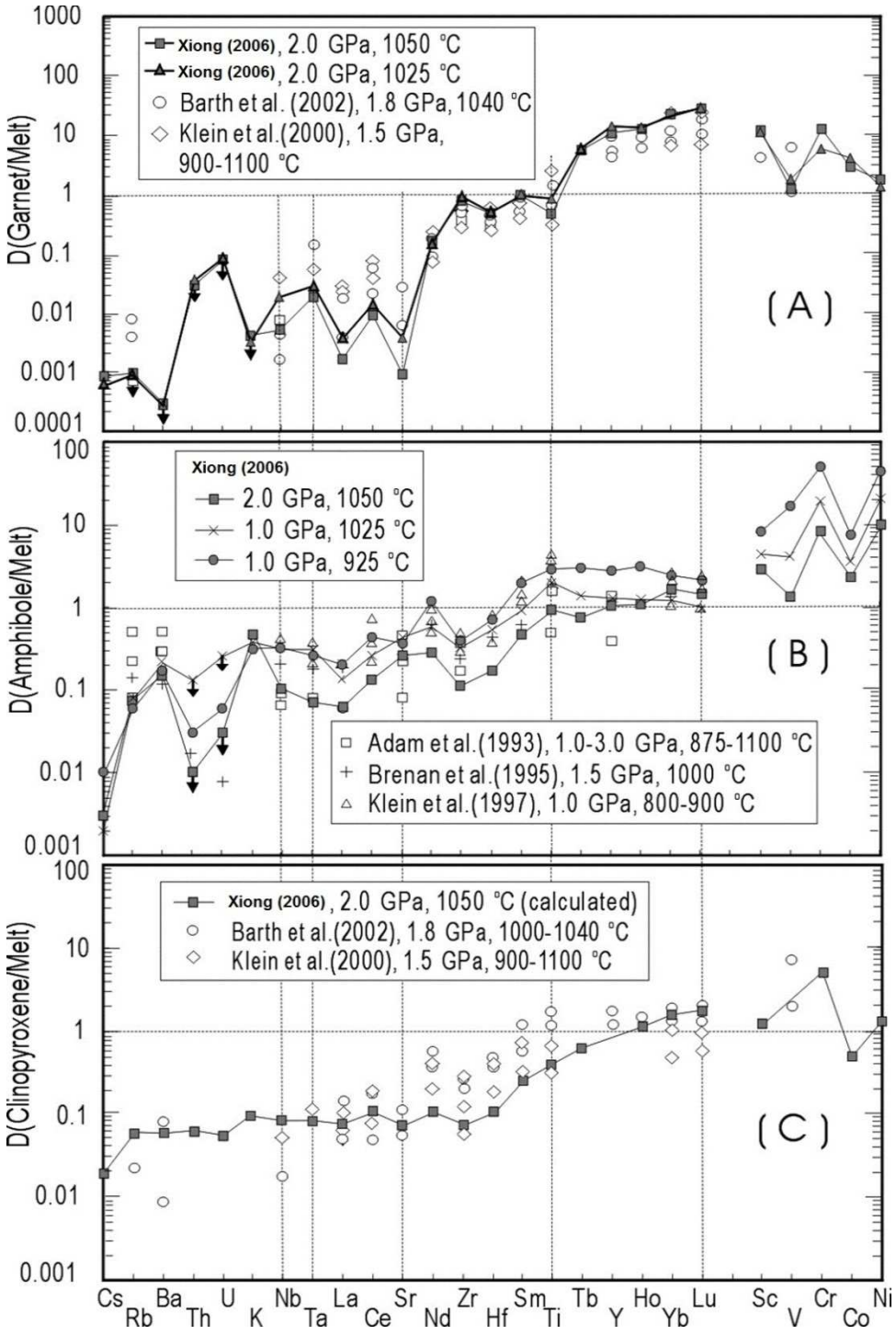

Figure 5: Typical garnet, amphibole and clinopyroxene incompatible element patterns. Melts generated from garnet peridotites will have incompatible element patterns that are the inverse of the D pattern (D= experimental partition coefficients). Figure modified from Xiong, 2006.

1.2 Ancestral and Modern Sierra Cascades Geology

The geology of the Ancestral Cascades arc in California began with subduction activity in the Mesozoic leading to the intrusion of the major granitic batholiths, notably the Sierra Nevada batholith (Dickinson, 2006). During the Laramide orogeny (Late Cretaceous to middle Eocene) arc volcanism ceased in California and Nevada which allowed the Sierra Nevada batholith to be exhumed. The cause of the cessation of arc volcanism is believed to be the result of the Juan de Fuca/Farallon plate developing a shallower dip (Figure 6; Dickinson & Snyder, 1979). At ca. 40 Ma the shallowly dipping Juan de Fuca slab re-steepened and detached from the overlying continental lithosphere (slab rollback) along a roughly north-south trend in Washington and Oregon, which is believed to have resulted in the resumption of arc volcanism in the northern Ancestral Cascades by ca. 40 Ma (Figure 6; Christiansen and Yeats, 1992). However, the Juan de Fuca slab retained a shallow dip near the trench through California, where slab rollback did not resume until much later in the Tertiary (Cousens et al., 2008). Some form of tear probably separated steep- and shallow-dipping slabs near the California-Oregon border (Cousens et al., 2008). The foundering slab beneath California pulled both southward and southwestward, with a significant component toward the trench, in an apparent slow attempt to re-establish steep subduction (Cousens et al., 2008). Ancestral Cascades arc volcanism in California did not commence until ~20 Ma.

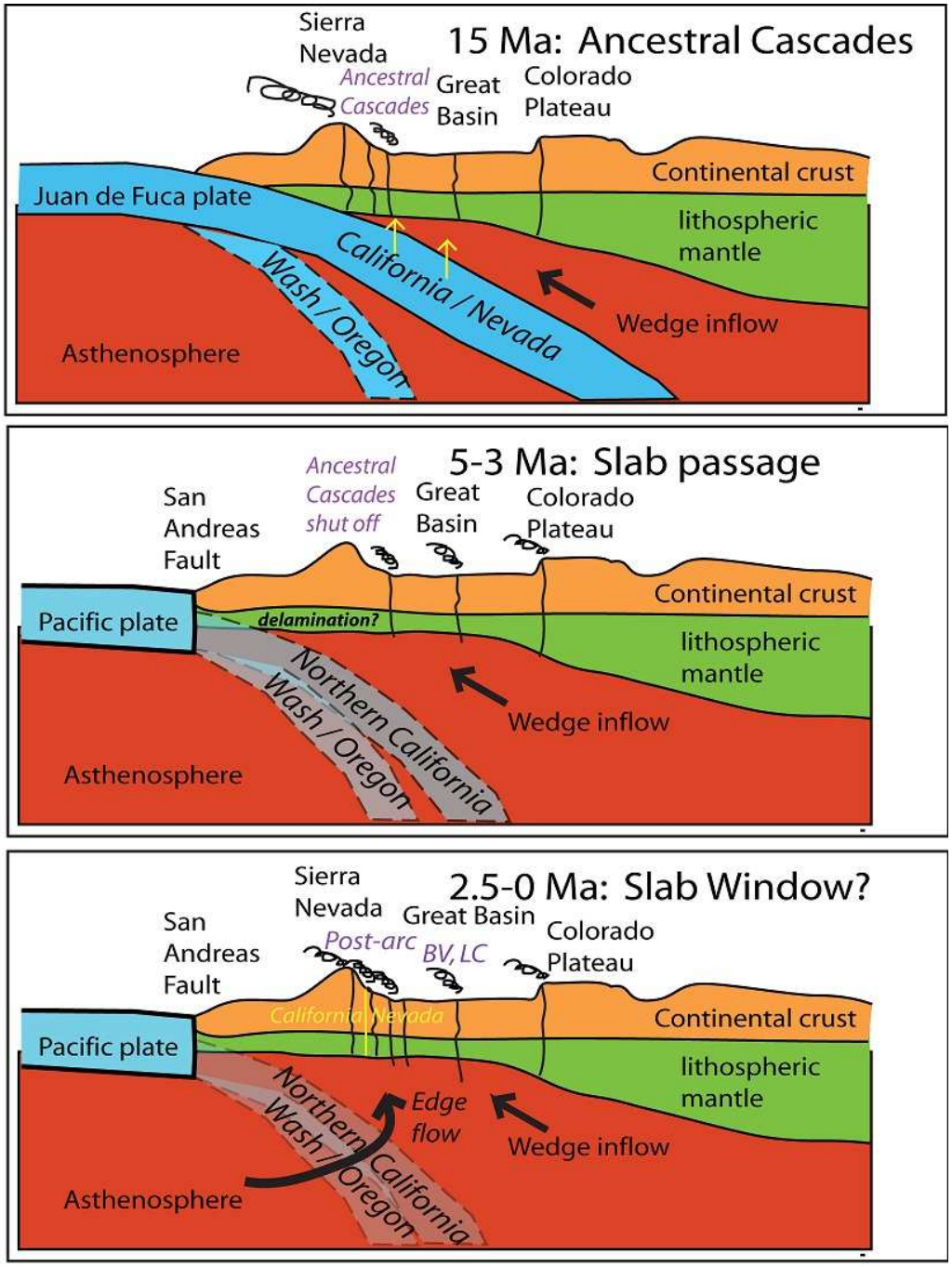

Figure 6: Model for the evolution of mantle sources for the Ancestral Cascades arc. These section represent the environment under the Tahoe area during the Miocene. The solid-line subducting plate is the shallow-dipping Juan de Fuca slab beneath northern California, whereas the dashed-line subducting plate is the steeper-dipping Juan de Fuca plate beneath Oregon and Washington (Cousens et al., 2008). Yellow arrows indicate fluids driven from the slab that drive melting of the mantle wedge and the lithospheric mantle. At 5–3 Ma, the south edge of the slab migrates north of the Lake Tahoe area, fluid flux decreases, and arc volcanism ceases. Note that both plate segments are now behind the plane of the section. Subsequent to 2.6 Ma, asthenospheric flow around the south edge of the slab (curved black arrow) adds more heat to the mantle wedge, heating the base of the lithosphere to drive post-arc melting of the lithosphere. Figure from Cousens et al. (2011).

1.2.1 Common Cascade Lava End-members

Several lava types occur in the Modern Cascades and are a common component in continental arc volcanism along the western Americas (Righter, 2000). Therefore they are pertinent to this study. These lava types have been extensively studied and categorized into the following end-members: high alumina olivine tholeiites (HAOT; Bacon et al., 1997; Gerlach & Grove, 1982), calc-alkaline basalts (CAB; Leeman et al., 2005; Righter, 2000), and intraplate basalts (Farmer et al., 1995). Although LREE enrichment can sometimes be associated with garnet melting in the residium, CABs, HAOTs, and intraplate lavas fall along an olivine-orthopyroxene-augite cotectic for the 8-12 kb range which is shallower than garnet peridotite but is within the depth range for spinel peridotite (Righter, 2000). Felsic volcanic rocks are rarely studied within the Cascade Range resulting in a lack of comprehensive analyses. The basaltic lava sequences are far more voluminous than the felsic ones, are sparsely crystalline and have little evidence of contamination or alteration, making the Cascades ideal for studying mantle sources and processes (Borg et al., 2002). Some higher silica melts (dacites and rhyolites) can be found at Medicine Lake, Glacier Peak, Mt. St. Helens, Newberry Caldera and at Lassen.

1.2.1.1 High Alumina Olivine Tholeiites (HAOT a.k.a. LKT)

HAOTs, or low potassium tholeiites (LKT), are similar to oceanic island and MORB (EMORB) lavas from within plate settings (Ba/Nb < 20) (Bacon et al., 1997; Gerlach & Grove, 1982). HAOTs are found 30-40 km trench-ward of stratovolcanoes that define the High Cascades volcanic front (Leeman et al., 2005) and because of their lows viscosity and pahoehoe textures are associated with large shield volcanoes. They are believed to be derived from deeper levels than CAB lavas (50-70 km for HAOT, 30-50 km for CAB) but they do not include slab

components (Leeman et al., 2005). High alumina olivine tholeiites are composed of Mg-rich olivine or augite and Ca-rich plagioclase (Gerlach & Grove, 1982).

The HAOTs require convective upwelling of asthenospheric wedge mantle and preclude fluid enhanced melting because they project close to the dry peridotite solidus (Leeman et al., 2005). Primitive Mantle normalized trace element patterns show MORB patterns with the exception of a flat middle to heavy REE pattern, positive Eu anomaly (not all HAOTs have this) and a small but distinctive Nb-Ta trough. Because of their MORB like chemistry and relatively flat REE patterns HAOTs are inconsistent with residual garnet in their source making decompression melting of spinel peridotite a more likely source (Leeman et al., 2005). Parental liquid temperatures for CAB are a max of 1350 °C while HAOTs are as high as 1450 °C (Leeman et al., 2005). Therefore CABs originate at lower P and T conditions than HAOTs. The most accepted explanation for the origin of HAOT lavas is decompression melting of depleted and/or enriched asthenosphere with little modification by slab contributions (Figure 7; Leeman et al., 2005; Righter, 2000).

1.2.1.2 Calc-Alkaline Basalts (CAB)

Volumetrically, CABs are more abundant than HAOTs within the Cascades (Schmidt et al., 2008) Calc-alkaline basalts have higher alkaline earth (Ba, Sr), light rare earth (La, Ce, Nd) and LREE/HFSE (Zr, Nb, Ti) enrichments than oceanic MORB. CABs are distinguished by elevated K_2O (0.6-2.2 wt%), Ba/Nb (21-100), Ba/TiO_2 (202-651), Sr/Y (29-94) but compared to HAOTs they have similar Nb/Zr ratios (Leeman et al., 2005; Righter, 2000). Because of this CABs are thought to be derived from melting of the sub arc mantle after infiltration of hydrous,

incompatible element enriched fluids. The enriched fluids lower the solidus of the peridotite producing a basaltic melt (Righter, 2000).

CAB trace element abundances reflect large degrees of melting of strongly subduction component fluxed peridotite, along with low degree of melting of subduction components consistent with being derived from relatively cold mantle. Flux melting of the mantle wedge is the dominant cause of arc magmatism in the Washington Cascades (Reiners et al., 2000). Based on the isenthalpic flux-mantle melting model, CAB trace element signatures can only be derived from melting of mantle regions with relatively low initial temperatures (Reiners et al., 2000). Parental liquid temperatures for CAB are a max of 1350 °C while HAOTs are as high as 1450 °C (Leeman et al., 2005). Therefore CABs originate at lower P (30-50 km) and T conditions than HAOTs. Leeman et al., (2005) proposes that CABs are derived melts in the shallow mantle in response to heating from ascending HAOT melts. In addition CABs do not have modern slab inputs but instead are derived from 'stored' slab derived components inherited from earlier stages of Cascadia subduction. In other words the CABs formed from melting of shallow lithospheric mantle that had been extensively metasomatized by melt or fluid infiltration over the last 40 million year. More rapid subduction in the earlier stages of Cascades subduction could have cooled the mantle wedge. This could result in freezing of CAB type magmas or /and formation of hydrated lithospheric mantle containing modal amphibole-phlogopite within parts of the shallow mantle. Then, if subsequent reheating occurred due to rising HAOT melts or decompression you could produce 'second-stage' basaltic magmas having a CAB signature with signs of mixing and differentiation among magma batches (Leeman et al., 2005). CAB lavas are thought to be derived from subduction modified mantle at depths near the base of the crust (Figure 7; Righter, 2000).

1.2.1.3 Intraplate Basalts

Intraplate or Within-Plate (WIP) basalts are not common within the Modern Cascades arc, but they are found in the Basin and Range province to the east (Farmer et al., 1995). The Mojave Cima volcanic field, just east of the town of Baker in the Mojave Desert in southern California is a good example of an intraplate basalt field. The Cima basalts are 3-5 Ma old with trace element patterns similar to OIB's that were erupted from scoria cones (Bacon et al., 1997; Farmer et al., 1995). The lava flows are primarily alkali basalts and hawaiites that straddle the boundary between hypersthene and nepheline normative compositions (Farmer et al., 1995). Mantle derived peridotite xenoliths are common (Farmer et al., 1995). The Mojave basalts have high εNd values (+7.6-+9.3), low $^{87}Sr/^{86}Sr$ (0.7028 to 0.7040), and Pb isotopic compositions generally plot close to MORB (Farmer et al., 1995). Basalts erupted in within-plate settings are enriched in most incompatible elements and LILE; they do not have a Nb-Ta anomaly and have a REE pattern decreasing from light to heavy when compared with primitive mantle (Pearce, 1983; Schmidt et al., 2008). Higher Nb concentrations in subduction components are necessary to produce Cascade intraplate-like compositions. A strongly incompatible element-depleted peridotite (i.e. MORB source) cannot generate intraplate-like lavas.

Cima basalts were likely derived from LREE-enriched portions of the Pacific asthenosphere which rose from a slab window beneath the southwestern U.S.A. during the late Cenozoic transition from convergent to a transform plate margin. The high εNd do not suggest that LREE enriched lithospheric mantle as the primary source of the basalts and instead suggests a mantle source with a long term LREE depletion, most likely young Cenozoic lithospheric mantle or asthenospheric mantle. The εNd values overlap Pacific MORB values, which is striking since MORB basalts within the eastern Pacific are inferred to be derived from upwelling

asthenospheric mantle (Farmer et al., 1995). This also suggests that the Mojave basalts did not interact with old continental lithosphere. The only problem with this assessment, which Farmer et al., (1995) conceded, is that small degrees of partial melting of a garnet lherzolite source is required to produce the observed LREE enrichment would create an extremely silica under-saturated magma (i.e. basanite) which are not observed (Farmer et al., 1995). Alkali basalt magmatism above slab windows is a commonly accepted product of passive upwelling of asthenospheric mantle. This type of magmatism is small in volume, often long-lived and is not usually accompanied by extensional tectonism (Farmer et al., 1995). The most accepted explanation for the origin intraplate lavas is decompression melting of depleted and/or enriched asthenosphere, respectively (Figure 7; Righter, 2000).

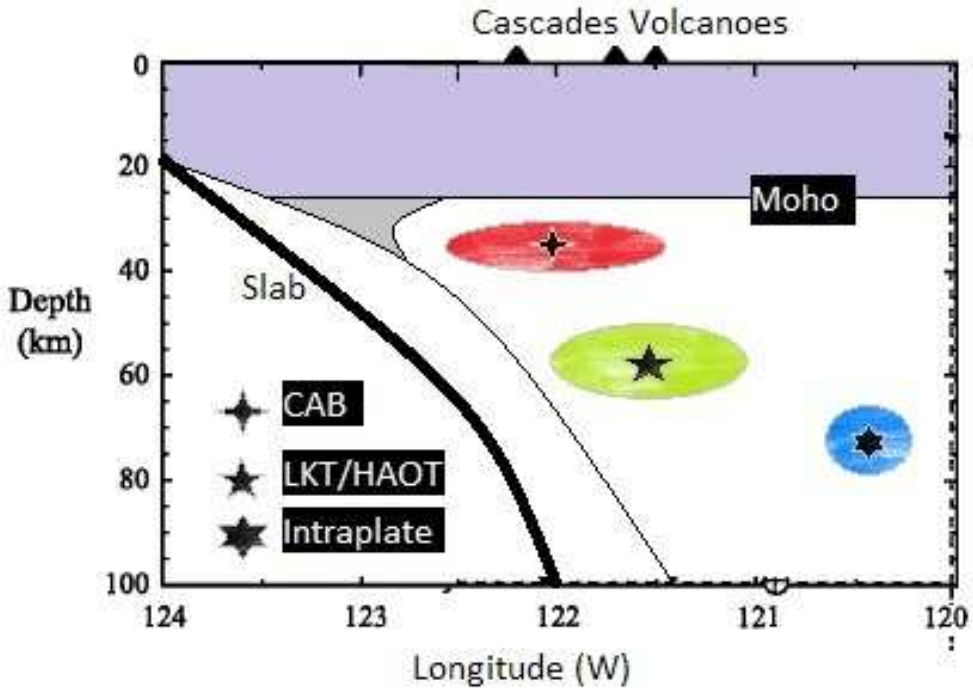

Figure 7: Representative diagram of the relative locations of the three main lava types in the Cascades. CAB lavas are derived from relatively shallow depths (low T & P) along the subducting slab while HAOTs are derived from deeper sources along the slab. Intraplate lavas are not necessarily influenced by subducting slab and are produced more from convective fluxing of deep mantle under the continental plate. Modified from Leeman, (2005).

1.3.2 Geology of the Modern Cascades

The Modern Cascades arc extends from northern California to southern British Columbia; the southernmost Modern Cascade center is the Lassen Volcanic Center (LVC). About twenty active composite centers compose the Modern Cascades with eruptive products ranging from basalts to high silica rhyolites (Borg et al., 2002). The easterly dipping Juan de Fuca, Gorda and Explorer plates are the main driving force for arc volcanism within the Modern Cascades. The present mantle wedge is thought to be derived from sub-oceanic mantle due to the presence of an accreted block of oceanic lithosphere beneath portions of the arc. Convergence rates have progressively decreased since the initiation of the arc from ~16 cm/yr to ~4 cm/yr (Riddihough, 1984; Verplanck and Duncan, 1987) and with increasingly oblique convergence (Leeman et al., 2005).

The Cascades convergent margin is typified by slow subduction of the relatively young Juan de Fuca and Gorda plates beneath North America results in unusually warm conditions within the subduction zone. The Wadati-Benioff zone seismicity is limited to relatively shallow depths (<100 km; Weaver and Baker, 1988), below which the slab descends aseismically to at least ~300 km depth (Benz et al., 1992). Seismic data show the Juan de Fuca plate is subducting at 45-60° underneath Washington resulting in the arc being ~100 km above the subducted slab (Righter, 2000). The forearc is also undergoing northward compression while south of the Columbia River there has been significant late Cenozoic east-west extension (Leeman et al., 2005). The flux of subduction components (fluids and/or melts) to arc melts is smaller in the Cascades than in more typical, cooler subduction zones. Regional variations within the Cascades show a greater varying influence and instead fluid release is more common in the forearc arc than in the arc due to the early dehydration of the slab (Leeman et al., 2005).

Cascades stratovolcanoes produce a variety of andesitic to dacitic magmas, while late Cenozoic (<5 Ma) diffusely distributed monogenetic and shield vents produce basaltic and basaltic andesite lavas. During the Oligocene to Early Miocene, rhyolite and dacite common eruptive products, and in the Mid-Miocene andesite was the dominant eruptive product. Basaltic rock types have dominated since that time (McBirney, 1978). The common occurrence of basaltic magmas reflects a significant input of heat or mantle upwelling beneath the region (Leeman et al., 2005).

1.3.2.1 Lassen

Lassen is the closest modern Cascades volcanic centre to the SVC field area. The currently active Lassen Peak stratovolcano is the most recent of several long-lived volcanic centres in the southernmost Cascades Range. Brokeoff Volcano, an 80 km^3 andesitic stratocone within the LVC, produced two episodes of silicic volcanism between 0.60 and 0.40 Ma, to form a dacite dome field totaling 30–50 km^3(Clynne, 1990). Between 0.3 and 0.2 Ma, two dacite domes composed of pyroxene–hornblende were also erupted (Clynne, 1990). Since 0.1 Ma, hornblende–biotite dacite compositional domes, lava flows and pyroclastic flows have been emplaced (Clynne, 1990; Clynne, 1999). Also, since 0.3 Ma, about 10 km^3 of andesite consisting of thoroughly mixed mafic and silicic magma has intermittently erupted from the margins of the dacite dome field (Clynne, 1990).

The LVC has produced eruptive products ranging from basalt to andesite. The LVC (Brokeoff Volcano) is similar to medium K_2O, calc-alkaline volcanic rocks emplaced in moderately thick continental crust (Clynne, 1990). The FeO/MgO ratio of most LVC rocks

remains constant with increasing SiO_2, while MgO, Al_2O_3, FeO, CaO, TiO_2 and P_2O_5 decrease and K_2O & Na_2O increase with increasing SiO_2 (Clynne, 1990). The LVC shows progressive enrichments of Sr and LILE which infers there is increasing contributions of slab derived fluids towards the forearc west of Lassen (Leeman et al., 2005). At Lassen Peak, Sr/P_{pmn} (pmn = primitive normalized mantle) is interpreted to reflect variable slab-derived fluid addition to the mantle wedge: lavas with low Sr/P_{pmn} were interpreted as melts of unmodified mantle wedge peridotite, whereas lavas with high Sr/P_{pmn} imply melting of hydrous, Sr-enriched, metasomatized mantle peridotite (Borg et al., 1997). Sr/P_{pmn} also correlates with trace element ratios, such as Ba/Nb, that are also sensitive to fluid addition from the subducting slab. At Lassen, lavas with low $^{87}Sr/^{86}Sr$ have high Sr/P_{pmn}, suggesting that slab-derived fluids have mid-ocean ridge basalt (MORB)-like Sr isotope ratios, whereas lavas with high $^{87}Sr/^{86}Sr$ have low Sr/P_{pmn}, consistent with melts from an enriched, Paleozoic lithospheric mantle source (Cousens et al, 2008).

Clynne, (1990) outlines three stages to the evolution of the LVC. Stage 1 & 2 include the growth of the Brokeoff volcano with dominantly andesitic lavas, and Stage 3 is dominant silicic volcanism along the northward flank of the Brokeoff volcano. Stage 1 magmas were produced in small independent batches that mixed together producing heterogeneous products such as olivine-augite basaltic andesites and olivine-hypersthene-augite andesites (Clynne, 1990). The lithologic units display high degrees of variations in phenocryst assemblages and abundances. Stage 2 magmas are generally more homogeneous in compatible major elements but trace element and isotopic data shows that they were also formed in independent batches (Clynne, 1990). The stage 2 lithology consists of porphyritic augite-hypersthene silicic andesite which has homogenous phenocryst assemblages and abundances (Clynne, 1990). Stage 3 magmas do not

appear to be directly related to previous lavas and consists of a silicic dome with adjacent hybrid andesites to dacites (Clynne, 1990). Partial melting of young mafic crust is inferred to be the origin of the silicic magmas in the LVC (Clynne, 1990). Hybrid andesites and abundant quenched inclusions of resorbed sialic phenocrysts in dacites are the main arguments for interactions between mafic and silicic magmas (Clynne, 1990).

1.4.3 Geology of the Ancestral Cascades

Paleo-reconstruction of the subducting Juan de Fuca slab indicates that a continental volcanic arc should have been present along the northern Sierra Nevada in the Miocene and Pliocene (Dickinson, 1997). Dickinson (1997, 2006) referred to this volcanic activity as the Ancestral Cascades arc that extended from British Columbia south to the California-Nevada-Arizona state boundary intersection at 15 Ma. Modeling of the movement of the trailing edge of the Juan de Fuca plate relative to North America shows that it has moved progressively northward over the past 20 Ma, leaving a slab window in its wake (Figure 8; Atwater & Stock, 1998). The south edge of the subducting Juan de Fuca slab reached the latitude of Lake Tahoe at ca. 6 Ma and is now (presently) stalled just north of the lake at ~39.5°N (Benz et al., 1992).

Late Tertiary volcaniclastic and volcanic rocks of the ACA blanket a large area of the Sierra Nevada of north-eastern California and the adjacent western Nevada (Cousens et al., 2008; Dickinson, 1997). The southern Ancestral Cascades Arc extends southward from Lassen Peak (the southernmost volcano in the Modern Cascades Arc) along the eastern side of the Sierra Nevada Batholith into the western and southern portions of Nevada (Dickinson, 1997; Guffanti et al., 1990). The volcano-tectonic history of the Northern Sierra includes several overlapping volcanic settings such as subduction/arc volcanism of the Farallon (Juan de Fuca) plate, Basin and Range extension, and hotspot magmatism from the Columbia River flood basalts (Cousens et

al., 2008; Garrison et al., 2008 Henry, 2001). Ultimately, the end of the southern Ancestral Cascades as an active arc occurred at ca. 3 Ma when the Mendocino Triple Junction moved northward to its present location at Lassen (Atwater & Stock, 1998).

The mineralogy of the volcanic rocks of the Ancestral Cascades Arc is commonly highly porphyritic, including abundant plagioclase with clinopyroxene, amphibole, and rare biotite (Cousens et al., 2008). The rocks range in composition from basaltic andesite to dacite to less common poorly phyric, olivine- and clinopyroxene-bearing basalts and basaltic andesites (Cousens et al., 2008). Porphyritic lavas dominate composite volcanic centers, whereas the poorly phyric lavas form isolated cinder cone and lava flow complexes which are common in the Lake Tahoe-Reno area (Cousens et al., 2008; Dickinson, 1997). In previous works, the porphyritic volcanic rocks are generally termed the Kate Peak Formation while the less phyric, olivine-clinopyroxene units are termed the Lousetown Formation (e.g., Birkeland, 1963).

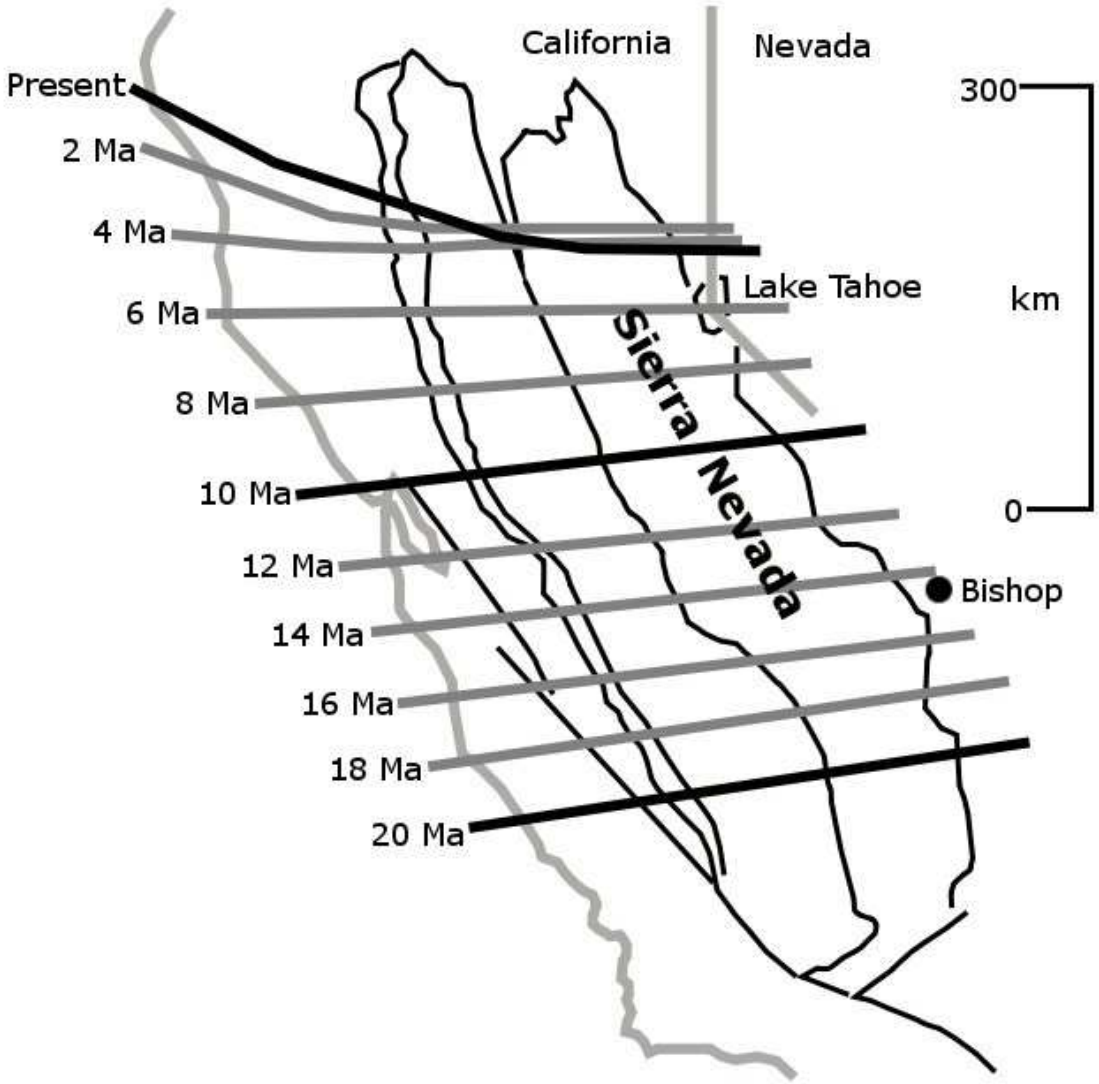

Figure 8: Northward migration of the southern edge of the Farallon plate beneath California and eastern Nevada. The Farallon plate would have been under Lake Tahoe around the time of volcanism within the SVC. The relative position of the Farallon plate at the time of SVC volcanism is equivalent to the current position of the Farallon plate under Lassen. Figure modified from Atwater & Stock, 1998.

1.4.3.1 Tahoe-Truckee Area Arc & Post-Arc Volcanism

Volcanism near Lake Tahoe occurred from 28 Ma to 1 Ma, with major pulses at 16 Ma, 12 Ma, 10 Ma, 8–6 Ma, 5–3 Ma, and 2.6–1 Ma (Cousens et al., 2008). The 28 Ma pulse is based on isolated pyroxene andesite lavas erupted on the Carson Range (CR: Figure 9), the 16 Ma pulse is composed of voluminous basaltic and andesitic lavas emplaced around Babbit Peak (BP: Figure 9) (Cousens et al., 2008). The next major pulse of volcanism occurred at ca. 12 Ma which resulted in the development of an andesitic stratovolcano on the north end of the Carson Range; there was also a coeval period of extension along the eastern margin of the Sierra Nevada (Cousens et al., 2008). At ca. 10 Ma a major emplacement of basaltic andesites occurred along the Verdi Range (VR: Figure 9) and towards Reno. Volcanism between ca. 8-6 Ma resulted in two possible andesite stratovolcanoes, one centred on Martis Peak and the other near Mount Lincoln (Figure 9: MP, ML; Cousens et al., 2008). From 5-3 Ma, voluminous volcanism occurred around the Twin Peaks and Squaw Peak (Figure 9: TP, SP) composed of andesite and basalt lavas which are strikingly similar in terms of relative proportion and absolute volume to the Lassen area of the Cascade Arc (Cousens et al., 2008). The last pulse of volcanism took place less than 2.6 Myrs ago and was highly constrained volumetrically and geographically along an east-west trend from the north shore of Lake Tahoe to the Carson Sink, and was predominantly mafic and slightly alkalic; this pulse is not considered to be part of Miocene-Pliocene arc suite as it is post-dates the passage of the southern edge of the Juan de Fuca plate and is chemically and petrographically distinct (Cousens et al., 2008).

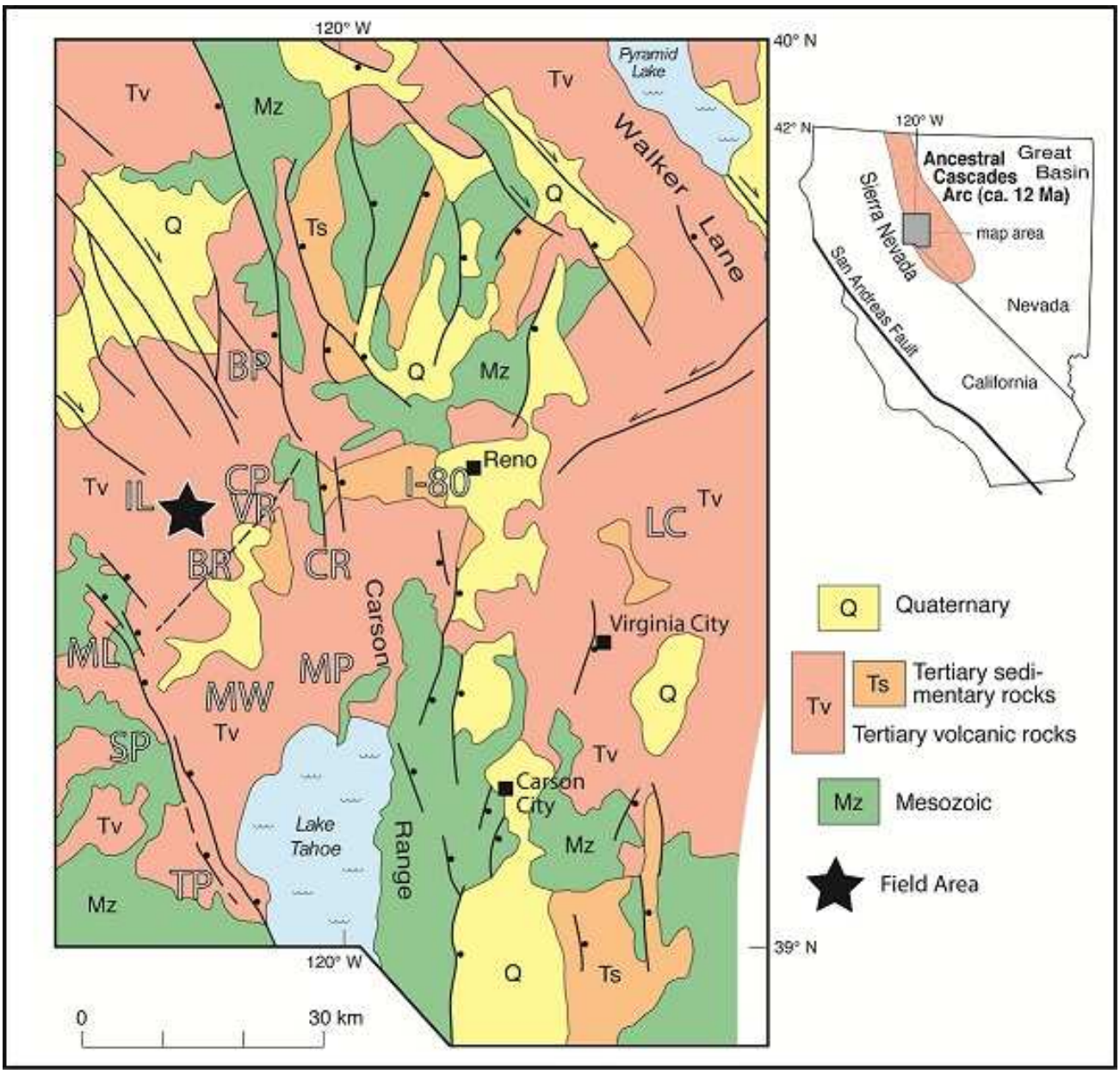

Figure 9: Geology of the Ancestral Cascades, Lake Tahoe Region. The Star represents the location of Sagehen. TP—Twin Peaks; SP—Squaw Peak; ML—Mount Lincoln; MW—Mount Watson; MP—Mount Pluto; BR—Boca Reservoir; VR—Verdi Range; CR—north Carson Range; CP—Crystal Peak; BP—Babbitt Peak; I-80—I-80 suite area; LC—Lousetown–Clark Mountain. Modified from Cousens et. al., 2008:

1.4.3.2 Sagehen

The SVC lies within the centre of the Ancestral Cascades immediately north of the town of Truckee. The major landmarks within the SVC are Independence Lake and Carpenter Ridge.

Very little geological work has been done in this area except for a 1:25,000 scale map produced by Sylvester and Raines in 2007 (Figure 10). The Sagehen property owned by University of California Berkeley, and the surrounding State of California Parkland is a major aquifer for the Truckee/Reno area and outcrops are generally at high relative topographies due to thick overburden with a high water table (pers comm. Jeff Brown; Sagehen administrator). The Sylvester and Raines (2007) map outlines a ~4-6 Ma Miocene-Pliocene suite of volcanic rocks which overlies a Cretaceous plutonic basement and Oligocene rhyolitic tuffs and is overlain by Quaternary alluvium and glacial till (Figure 10; Sylvester & Raines, 2007). The Miocene-Pliocene volcanics are variable facies of andesitic and basaltic lava flows. The mapped suite of andesites range in composition from andesite to basaltic andesite with variable facies of porphyritic plagioclase, pyroxene and hornblende and non-porphyritic rock units. The basalts and andesites appear to be topographically and fault controlled. The basalts have been dated at 4.41±0.21 Ma while porphyritic pyroxene andesite flows are dated at 5.65±0.21 Ma and the pyroclastic deposits at 6.25±0.26 Ma (Table 1). The SVC marks one of the last areas of arc related volcanism before the south edge of the Farallon/Juan de Fuca subducting slab moved north through the Truckee area towards its present location at Cape Mendocino. There are a number of faults within the SVC believed to be related to incursion and extension of the Basin and Range province (Sylvester & Raines, 2007).

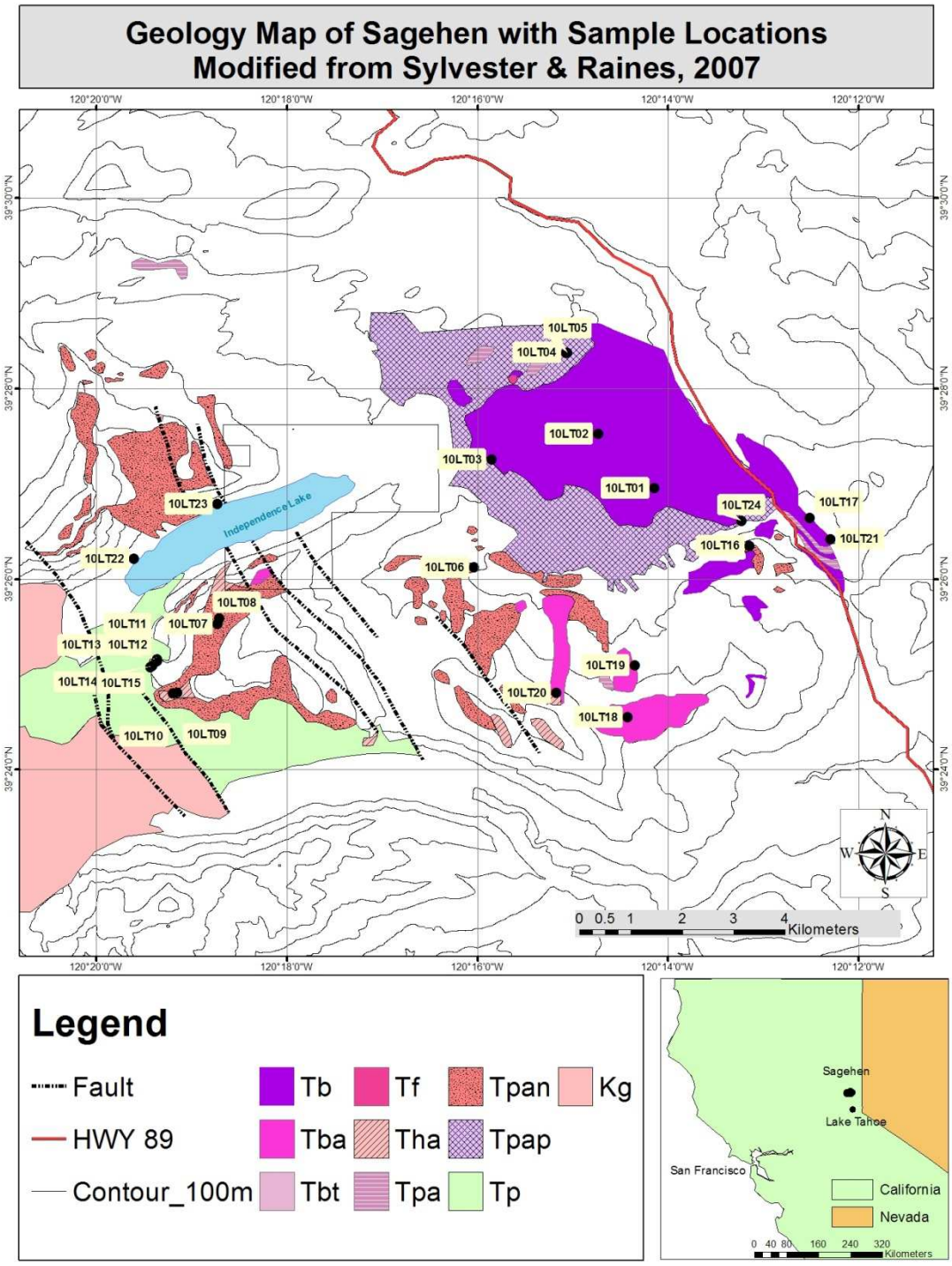

Figure 10: A geology map of the SVC showing sample locations for this study (Redrafted from Sylvester & Raines, 2007). Tb=Basalt Flows, Tba=Basaltic Andesite Flows, Tbt=Basaltic Tephra, Tf=Felsite, Tha=Hornblende Andesite Flows, Tpa=Pyroxene Andesite Flows: undivided, Tpan=Pyroxene Andesite Flows: nonporphyritic, Tpap=Pyroxene Andesite Flows: porphyritic, Tp=Pyroclastic Flows, Kg=Granodiorite. From SW to NE the stratigraphy progresses from Cretaceous granitic basement, to tertiary rhyolitic tuffs, andesites, and basalts with Quaternary glacial/alluvial sediments.

TABLE 1. $^{40}Ar/^{39}Ar$ AGES SAGEHEN FIELD STATION AREA.

						Ages (Ma)[2]										
Sample[1]	rock type	Location	Latitude	Longitude	material	plateau	±2σ	%^{39}Ar[3]	steps	isochror	±2σ	$^{40}Ar/^{36}Ar_i$	±2σ	MSWD	total gas	±2σ
H07-135	pyroxene andesite lava (Tba)	Sagehen Creek	39.439	-120.228	matrix	**5.65**	0.21	89.1	5/10	**5.5**	0.5	320	70	2.6	6.8	2.6
H07-139	dacite debris-flow breccia (Tvc)	Carpenter Ridge	39.418	-120.323	plagioclase	**6.25**	0.26	67.2	7/10	**6.2**	0.3	270	100	1.2	7.2	0.6
H07-140	basalt lava (Tb)	Sagehen Hills, north	39.456	-120.242	matrix	**4.41**	0.21	72.1	5/10	**4.3**	0.2	300	70	1.1	5.3	2.3

[1] All analyses at the New Mexico Geochronological Research Laboratory (methodology in McIntosh et al., 2003); Neutron flux monitor Fish Canyon Tuff sanidine (FC-1).

Decay constants and isotopic abundances after Steiger and Jäger (1977); $\lambda_b = 4.963 \times 10^{-10}\ yr^{-1}$; $\lambda_{ec'} = 0.581 \times 10^{-10}\ yr^{-1}$; $^{40}K/K = 1.167 \times 10^{-4}$

[2] ages in bold are best estimates of eruption age.

[3] %^{39}Ar = percentage of ^{39}Ar used to define plateau age.

Table 1: Previous age dates of SVC rock units from Chris Henry (Nevada Bureau of Mines and Geology). 1: All analyses were performed at the New Mexico Geochronological Research Laboratory (methodology in McIntosh et al., 2003); Neutron flux monitor is Fish Canyon Tuff.

1.5 Research Goals

The primary goal of this study is to provide a broad overview of the geochemical landscape within the recently mapped Sagehen Volcanic Centre (SVC). This overview includes a study of the mapped rock units as defined by the Sylvester and Raines (2007) map and evaluates them based on their chemical characteristics which include whole rock: major elements, trace elements and Pb, Sr, & Nd isotopes. Thin section optical techniques and SEM micro-probing were made use of, but were not the primary focus of the study: instead, they were used to ascertain if the mapped rock units displayed mineralogical variability. The whole rock geochemistry was used to classify the SVC map units geochemically (mineralogical identifiers were used when the need arose), identify a potential source for SVC lavas, determine if there is crustal contamination within SVC map units and compare SVC map units to the existing volcanic suites. Comparisons have been made to the Ancestral Cascades such as the surrounding arc and post-arc rock suites described in Cousens et al., (2008) and Cousens et al., (2011), respectively, and the nearest Modern Cascades volcanic centre: Lassen. Geochemical analytical techniques are based on the recent work by Brian Cousens (Carleton University) in the Tahoe-Truckee region.

2. Methods

Samples of SVC Miocene–Pliocene lavas and volcaniclastic rocks were collected in July of 2010, primarily near Forest Service roads and hiking trails while hiking on foot or being transported in a four wheel drive vehicle. All samples were precisely located using a Garmin handheld global positioning system (GPS) unit. Sample locations are shown in Figure 2, and GPS coordinates are listed in Appendix 1.

Electron microprobe analyses of phenocrysts, and groundmass minerals were performed using the Camebax MBX at Carleton University. A beam current of 20 nA and an accelerating potential of 15 kV was used for silicates and oxides. Peak counting times for each element were 15–40 s, and backgrounds were collected on both sides of the peak. Raw X-ray data was converted to element weight percent by the Cameca PAP matrix correction software.

Rock samples were slabbed, crushed in a Bico Chipmunk jaw crusher, and ground to a fine powder in a ceramic ring mill. Whole-rock major and trace element contents were determined by fused-disc X-ray fluorescence spectrometry (University of Ottawa) and solution-mode inductively coupled plasma–mass spectrometry (Ontario Geological Survey). The precisions of the data, based on replicate analyses of samples and blind standards, are listed in Appendix 2. Some samples were analyzed for Pb, Sr, and Nd isotopic ratios at the Carleton University TIMS lab (Appendix 3; techniques of Cousens, 1996). All Pb mass spectrometer runs are corrected for fractionation using NIST SRM981. The average ratios measured for SRM981 are $^{206}Pb/^{204}Pb = 16.888 \pm 0.006$, $^{207}Pb/^{204}Pb = 15.425 \pm 0.008$, and $^{208}Pb/^{204Pb} = 36.490 \pm 0.028$. The Pb fractionation correction is based on the values of Todt et al., (1984). Sr isotope ratios are normalized to $^{86}Sr/^{88}Sr = 0.11940$. Two Sr standards are run at Carleton, NIST SRM987 ($^{87}Sr/^{86}Sr = 0.710238 \pm 13$) and the Eimer and Amend (E&A) $SrCO_3$ ($^{87}Sr/^{86}Sr = 0.708037 \pm 30$).

Nd isotope ratios are normalized to $^{146}Nd/^{144}Nd = 0.72190$ (Richard et al., 1976, Stieger & Jager, 1977). Analyses of the U.S. Geological Survey standard BCR-1 yield $^{143}Nd/^{144}Nd = 0.512668 \pm 0.000020$ (n = 4), and 54 runs of the in-house Nd standard average $^{143}Nd/^{144}Nd = 0.511820 \pm 0.000010$ equivalent to LaJolla $^{143}Nd/^{144}Nd = 0.511850 \pm 0.000010$. All quoted uncertainties are 2σ standard deviations of the mean and presented in Appendix 2. The formula for εNd, εSr, CHUR and UR are from Farmer & DePaolo, (1983) as well as their assumptions for decay constants with $\lambda_{147Sm}=6.5 \times 10^{-12}a^{-1}$ and $\lambda_{87Rb}=1.42 \times 10^{-11}a^{-1}$. Chemical analyses are presented in Appendix 3.

Computer programs used to analyse the resultant data were: Microsoft Excel 2007™, Delta Graph 6™ (for Windows™), Isoplot version 3.72, and ArcGIS™ version 9 and 10. GIS interpolations were made using the ArcGIS™ software toolset which included the use of Inverse Distance Weighted (IDW) and Kriging functions. DEM overlays and maps were also downloaded from the USGS Data Centre and the Sagehen Research Institute.

3. Results

3.1 Petrography

3.1.1 Pyroclastic Flow

Tbt- Basaltic tephra

Tbt is a polymict pyroclastic flow. Hand samples of Tbt are dark grey to black along fresh and weathered surfaces. Clasts are round to subangular glassy basalts, hornblende andesites, scoria, and pyroxene andesites. There is only one outcrop of Tbt which is 20 m high and displays facies changes in its stratigraphy. The bottom section of the outcrop is a poorly sorted, framework dominated, pebble to boulder sized volcaniclastic flow with an aphanitic basaltic matrix (the matrix was not chemically analyzed). The upper section is matrix supported and better sorted.

In thin section, samples of Tbt, texturally, are a random assortment in terms of size and sorting of fractured mineral grains. Plagioclase (50%) is sieve textured, fractured and angular to sub angular and ranges in size from a <20 µm groundmass to phenocryst sizes of 5 mm. Pyroxene (30%) is subround to round and ranges in size from a <20 µm groundmass to phenocryst sizes (5 mm). Glass is also a major component of the groundmass (20%).

3.1.2 Andesite

Tpan-Pyroxene andesite, non-porphyritic

Hand samples of Tpan are light grey to dark grey depending on the amount of weathering. Weathered surfaces contain vesicles of eroded phenocrysts that have secondary mineralizations of rounded feldspar (5 mm) in one outcrop. Samples are non-porphyritic (<5%) with an aphanitic groundmass of acicular-euhedral plagioclase (<1 mm). Phenocrysts of plagioclase (3-5 mm) and pyroxene (3 mm) are also present. In some outcrops plagioclase is the

major phenocrystic phase while in other outcrops it is pyroxene. It should be noted that Tpan is very similar petrographically to Tpap; phenocryst abundances are not consistent throughout each outcrop. Tpan and Tpap may simply be one unit with different facies.

In thin section, samples of Tpan texturally are primarily a glassy/aphanitic matrix that is 50% abundant (grains are not easily visible under 10x). Small (<50 µm) acicular grains of plagioclase are visible within the groundmass. Grains of sub-angular plagioclase (15%) 100-200 µm in size are also present while some appear to be fragments of larger grains. Phenocrysts of plagioclase (5%) are oscillatory zoned and have sieve textured zones. Sub-angular to sub-round pyroxene (200 µm, 15%) grains are also present. Some grains of pyroxene have surface pitting with plagioclase inclusions. Rare phenocrysts of pyroxene also have orthopyroxene cores which zone outwards to clinopyroxene rims.

Tpap-Pyroxene andesite flows, porphyritic

Hand samples of Tpap are grey to black depending on the amount of weathering. Samples exhibit a fine grain groundmass of euhedral plagioclase with euhedral phenocrysts of pyroxene (3-4 mm) and plagioclase (5 mm). There is also weak a foliation in the outcrop.

In thin section, samples of Tpap are primarily (60%) interlocking, weakly foliated equant euhedral plagioclase grains ~50 µm in size. Plagioclase phenocrysts (200 µm-5 mm, 15% abundant) are also present and are either oscillatory zoned or have a sieve texture. Olivine grains (<5%) are generally ~100-200 µm in size and sub-angular. The plagioclase groundmass forms a trachytic texture around the olivine. Sub-angular to sub-round zoned grains of pyroxene with orthopyroxene cores and clinopyroxene rims (15%) are also present, some grains have sieve textures (<5%) and opaque minerals (<5%).

Tba-Basaltic andesite flows

Hand samples of unit Tba are light grey to black depending on the amount of weathering. Texturally, Tba is mildly porphyritic with subround olivine and plagioclase visible under hand lens. Flow banding is visible in some outcrops and follows topography.

In thin section, samples of unit Tba are primarily (60%) interlocking foliated equant euhedral plagioclase grains ~50 µm in size. Larger plagioclase grains (100-200 µm, 10% abundant) are also present and are either oscillatory zoned or have a sieve texture. Olivine grains (<5%) are generally ~100-200 µm in size and sub-angular. Pyroxene is also present with sub-angular grains (10%) ~100-200 µm. Opaque minerals (10%) <100 µm in size form part of the matrix as well.

Tha-Hornblende andesite flows

Hand samples of Tha are light grey to grey depending on the amount of weathering. Samples are dominantly aphanitic with flows bands (1-1.5 cm) and are fissile. Hornblende appears as bladed or radial phenocrysts (2 mm-3 cm) though larger grains are rare (10%) and abundances and sizes vary dramatically between outcrops. Plagioclase appears rarely as a phenocryst (3-4 mm) and is euhedral. One outcrop of Tha in the southeast is highly magnetic to the point of rendering magnetic compasses useless in that area. This outcrop also has a mauve coloured alteration pattern on some of its surfaces.

In thin section, samples of Tha are primarily (60%) interlocking weakly foliated equant euhedral-acicular plagioclase grains ~50 µm in size. Hornblende grains (200 µm 15%) are heavily altered with a fine grained (recrystallized?) amphibole groundmass surrounding a Fe altered (pleochroic) core; the groundmass defines a relict hornblende grain boundary. The boundary is sharp and clearly defines a hexagonal crystal habit Plagioclase phenocrysts (200 µm-

4 mm, 5% abundant) are also present and are either oscillatory zoned or have a sieve texture. Sub-angular to sub-round pyroxene (5%) is also present, some grains have sieve textures (<5%). Fe oxide minerals (<50 µm) are also present (10%).

3.1.3 Dykes

Hand samples of two separate mafic dykes were taken. The first dyke (10LT15) is near the Tbt outcrop and is heavily thermally oxidized along its surface. Texturally, the dyke is aphanitic with no discernible minerals under hand lens. The second dyke (10LT22) was sampled along the shore of Independence Lake. This dyke has variable Fe alteration along its surface and fresh surfaces are black with metallic speckles. Texturally the dyke is aphanitic with blocky fractures.

In thin section, samples of the dykes are identical to each other. The groundmass is glass rich with foliated plagioclase grains. Phenocrysts of plagioclase are present and are euhedral and tabular with either fresh grains (non-zoned) or sieve textured (20%). Pyroxene phenocrysts are sub angular and 0.5-3 mm in size.

3.1.4 Basalt

Hand samples of unit Tb are light grey to black depending on the amount of weathering. Texturally Tb has an aphanitic matrix with subround olivine and plagioclase phenocrysts visible under hand lens (<1 mm) and foliated vuggs 1-8 cm in length. Flow foliation is visible in some outcrops and follows topography.

In thin section samples of unit Tb are primarily (60%) interlocking foliated equant euhedral plagioclase grains ~50 µm in size. Larger plagioclase grains (100-200 µm, 10% abundant) are also present and are either oscillatory zoned or have a sieve texture. Olivine grains

(10%) are generally ~100-200 µm in size and sub-angular. The plagioclase-rich groundmass forms a trachytic texture around the olivine. Minor amounts of sub-angular pyroxene (<5%) are also present and opaque minerals (10%).

3.2 Mineral Chemistry

3.2.1 Olivine

Olivine is most abundant within the basaltic unit, Tb, but it is also present in lesser amounts in the andesites, pyroclastics (Tbt) and dykes. The olivines are fresh and do not have reaction rims surrounding them in thin section and microprobing shows that they are generally the same composition and are forsteritic (Figure 11, Figure 12). Some of the olivine grains have inclusions along the grain's rim such as 10LT-01 (unit Tb, Figure 13) that contain Fe, Ti magnetites. Also the surface of the olivine grain is sieve textured in 10LT-01. Olivine is present within the Tpap andesites (10LT-03, Tpap, Figure 14) only as inclusions within pyroxene grains; olivine was not identified in the other andesite map units. Microprobe analysis reveals that the cores of the olivine grains are forsteritic while the outer zones of the grains are forsteritic but contain a greater amount of fayalite (Figure 15).

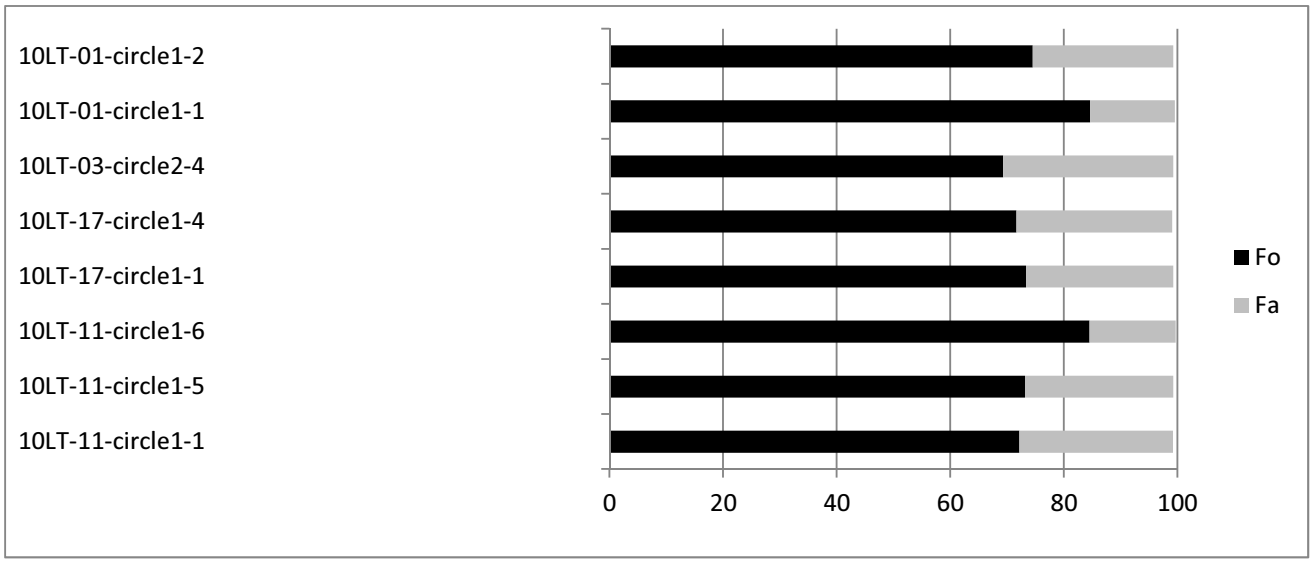

Figure 11: Samples 10LT-01 and 10LT-17 are Tb map units. Sample 10LT-03 is a Tpap map unit. Sample 10LT-11 is a Tpan map unit.

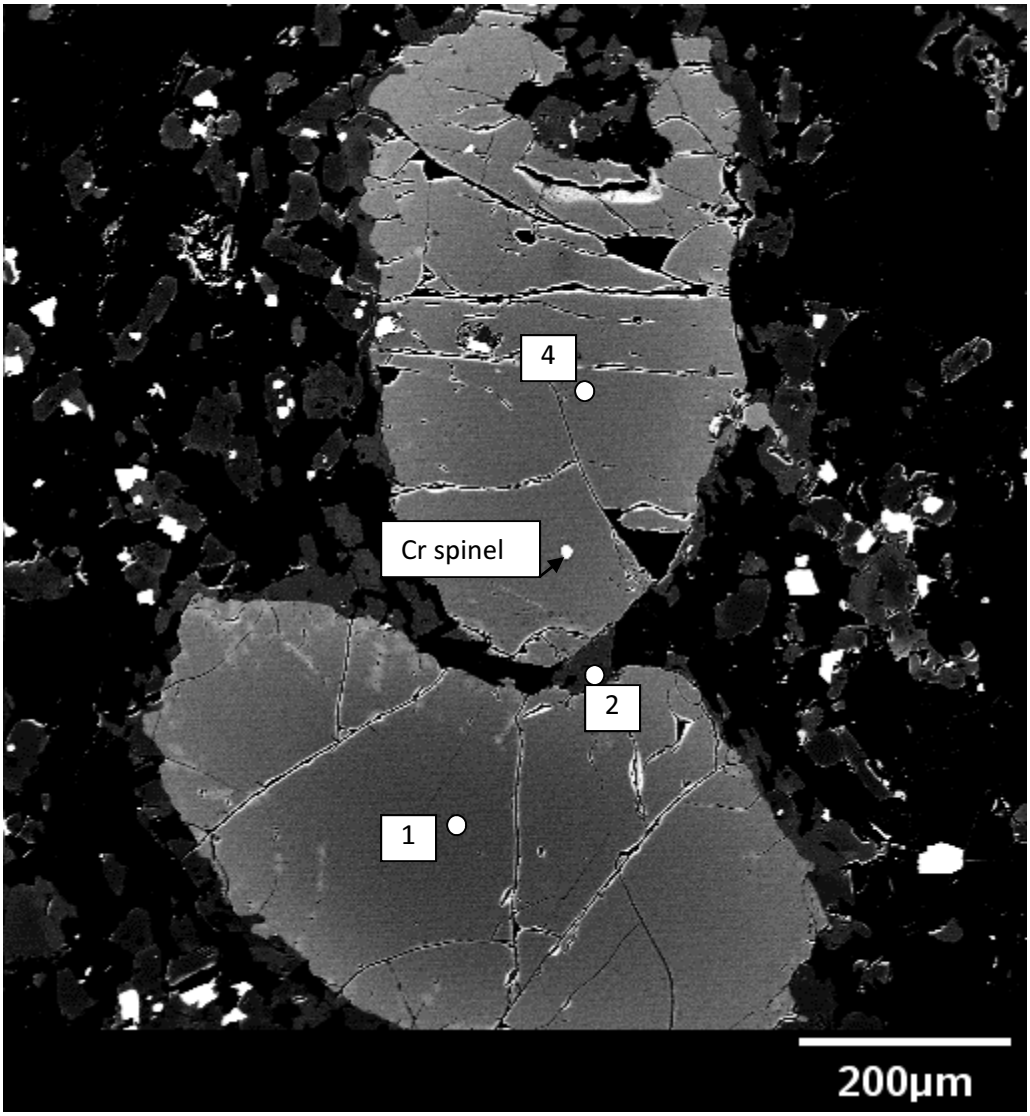

Figure 12: 10LT-17, Tb unit, SEM BSE image of two olivine grains. This is what the majority of olivine grains look like.

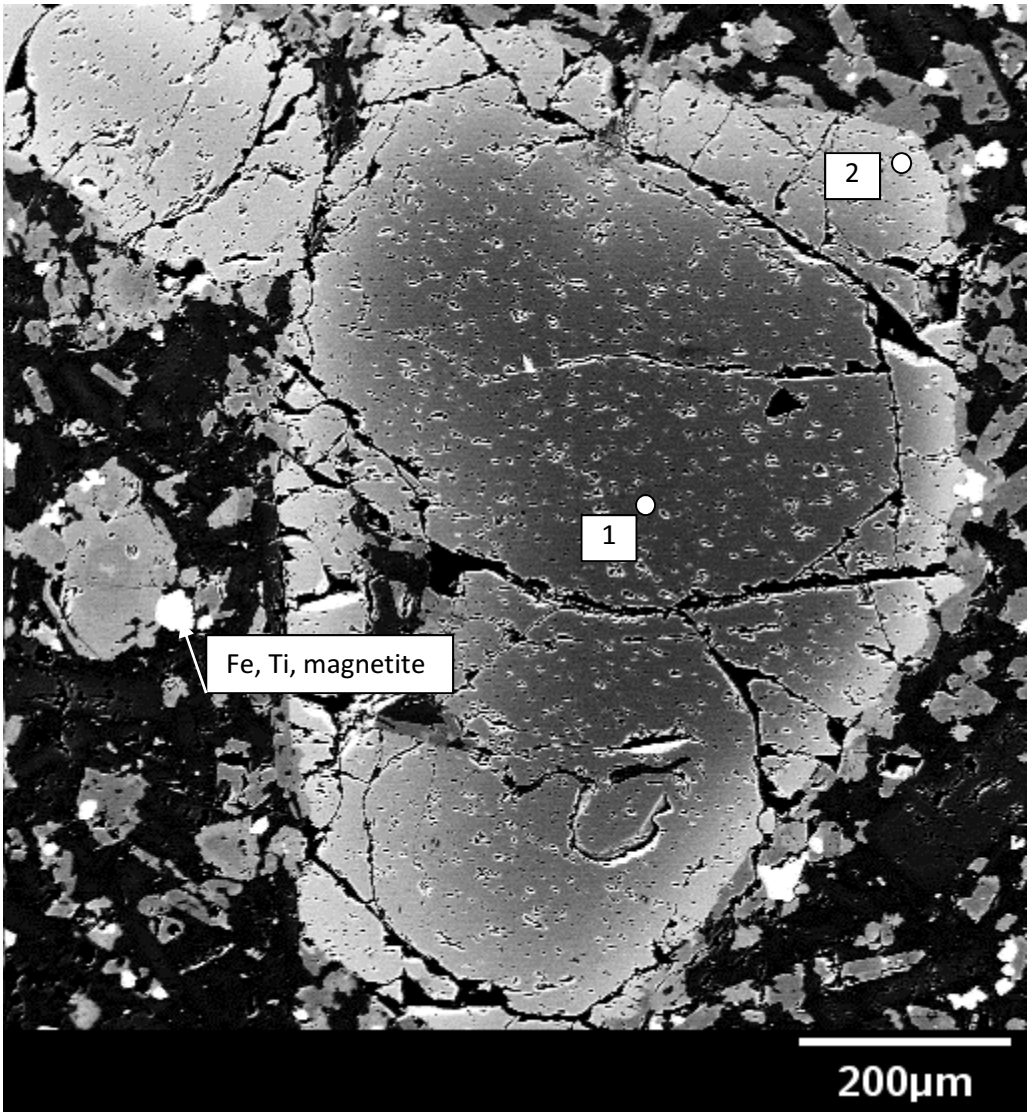

Figure 13: 10LT-01, SEM BSE image of olivine from unit Tb with sieve textures.

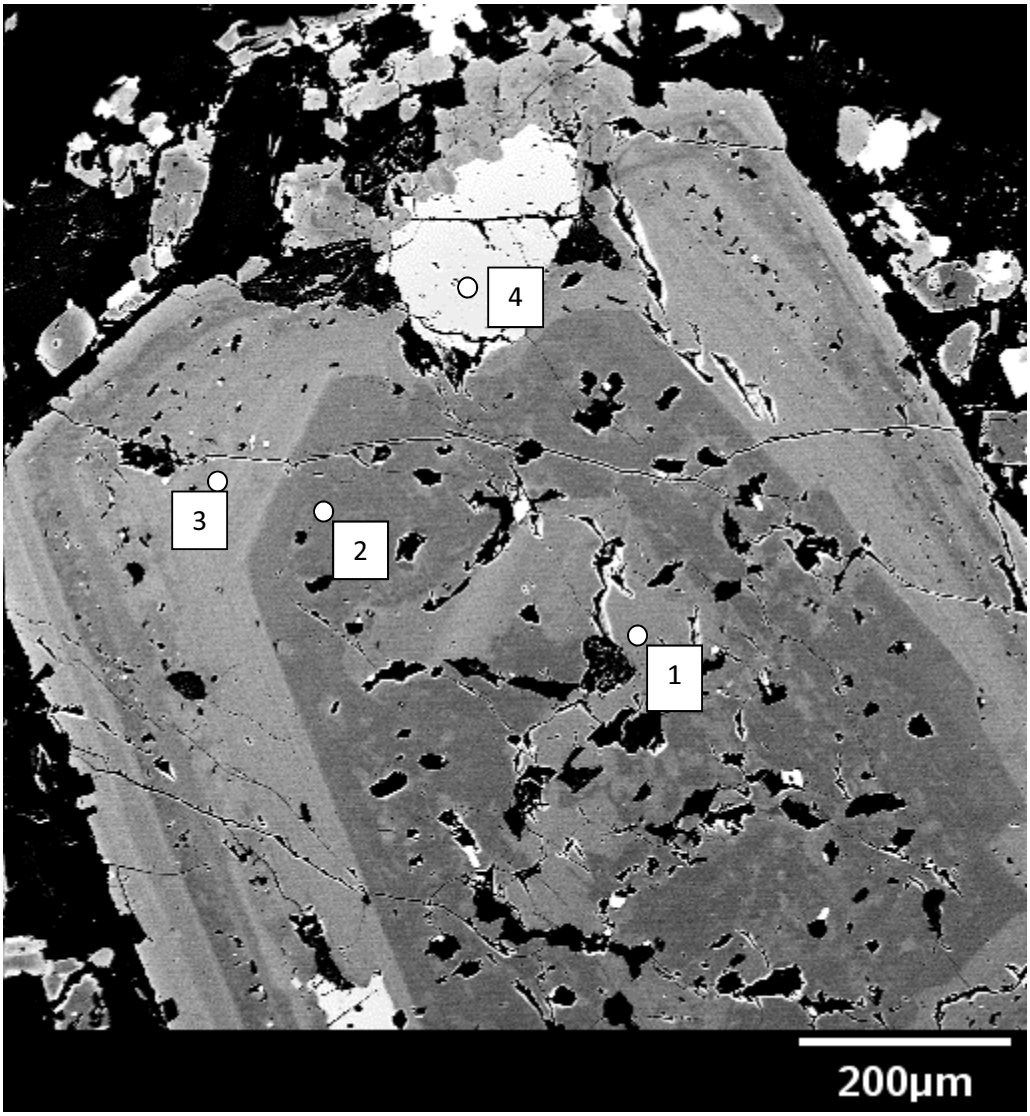

Figure 14: 10LT-03, Tpap, SEM BSE image of olivine inclusion (spot 4) in a zoned augite.

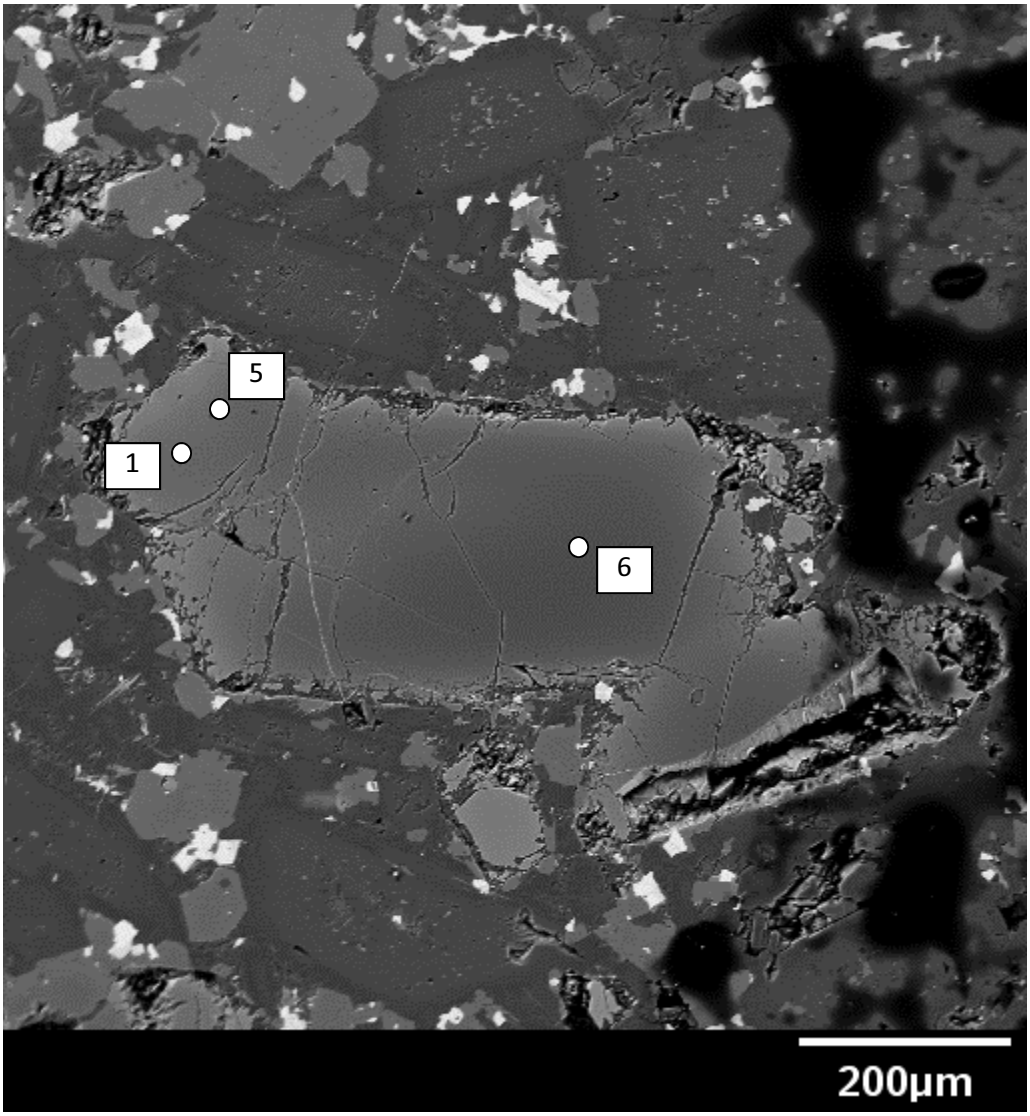

Figure 15: 10LT-11, SEM BSE image of olivine from the basaltic portion of the Tbt unit.

3.2.2 Plagioclase

The plagioclase is composed of two morphologies common to all extrusive rock units in the SVC. The first morphology is fresh, unaltered, variably thick-thin albite twinned plagioclase with oscillatory zoning which can be part of the groundmass or as large phenocrysts (Figure 16, Figure 17, Figure 18, Figure 19). The second morphology is variably sieve-textured plagioclase which can also have the remnants of zoning as well (Figure 16, Figure 20). The morphologies of

plagioclase are similar to those described in Stewart & Fowler (2001). In thin section, the Michel-Levy method reveals most plagioclase to be labradorite or bytownite under cross-polars and microprobing of grains in the SEM also show this trend (Figure 16). Plagioclase grains (both fresh and sieve textured) vary in size and shape from an acicular groundmass to euhedral phenocrysts in a consistent (prograding) manner; some grains appear to be fractured into fragments, especially within the Tbt samples. Microprobe analysis reveals the zoning in the plagioclase can be normal and reverse zoned that alternates between labradorite and bytownite end-members confirming thin section observations. The oscillatory zoning is of variable thickness in unaltered or sieve textured grains and is not necessarily tied to Anorthite (An) content (i.e. two rims side-by-side can be the same composition even though visually they look different in terms of thickness and brightness in SEM). Rims can be thick (>20 µm) or thin (<20 µm) with individual rims varying in thickness as well (Figure 20) and can be angular or rounded (Plate 1a). The rims can either have smooth or sieve/dissolution growth zones (Plate 1b). Furthermore, An content is generally higher than 75% which is anomalously high for basaltic and andesitic arc rocks which should be An_{49-54} (Stewart & Fowler, 2001).

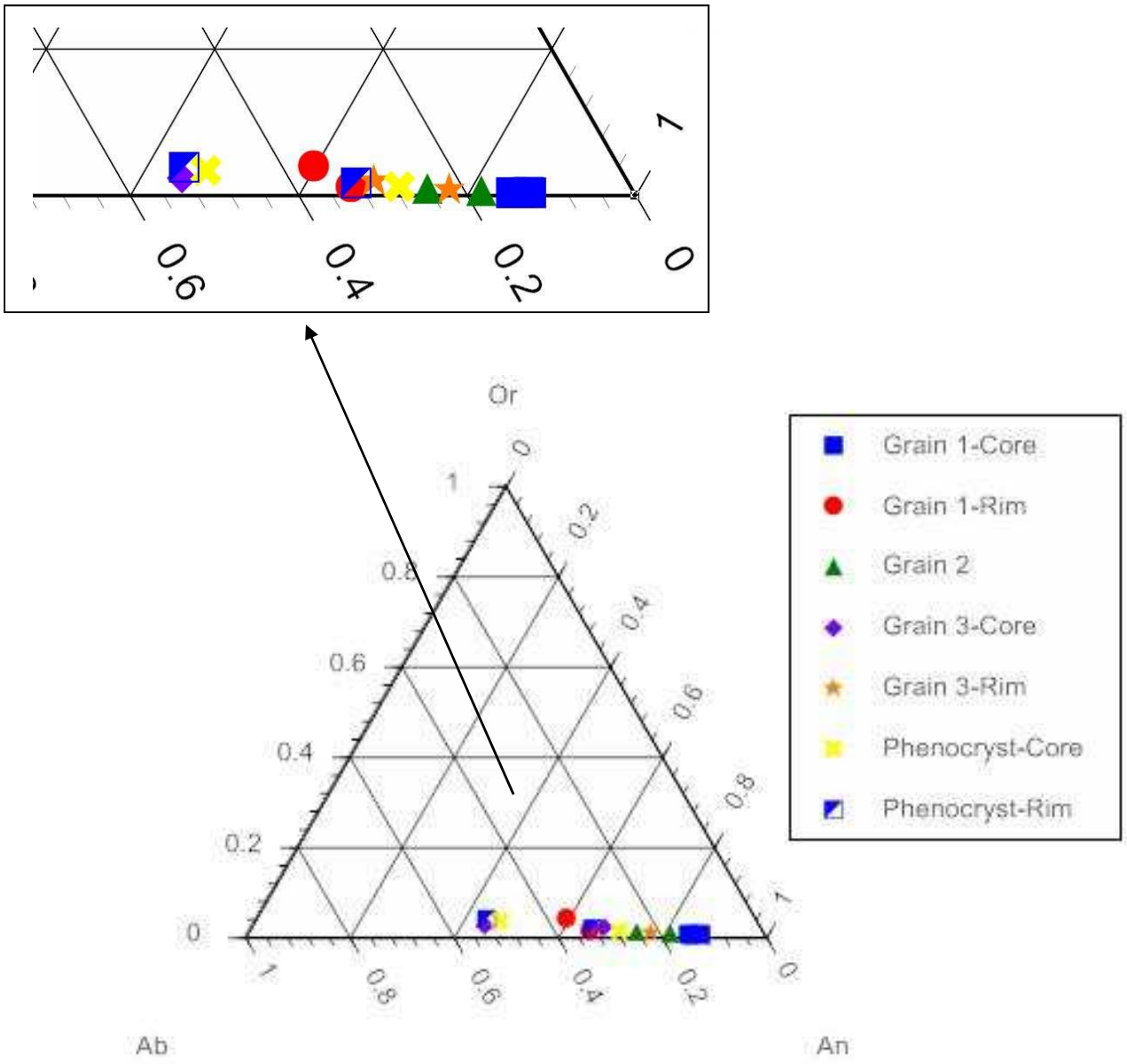

Figure 16: Microprobe results of plagioclase. Or=Orthoclase, Ab=Albite, An=Anorthite. Icon sizes are approximately similar to uncertainty. From 10LT-02 (Tb, basalt): Grains 1 (Fig. 9) and 2 (Fig. 10) are typical groundmass plagioclase while grain 3 (Fig. 11) is a phenocryst. From 10LT-06 (Tpan, andesite): a phenocryst with reverse zoning (Fig. 12).

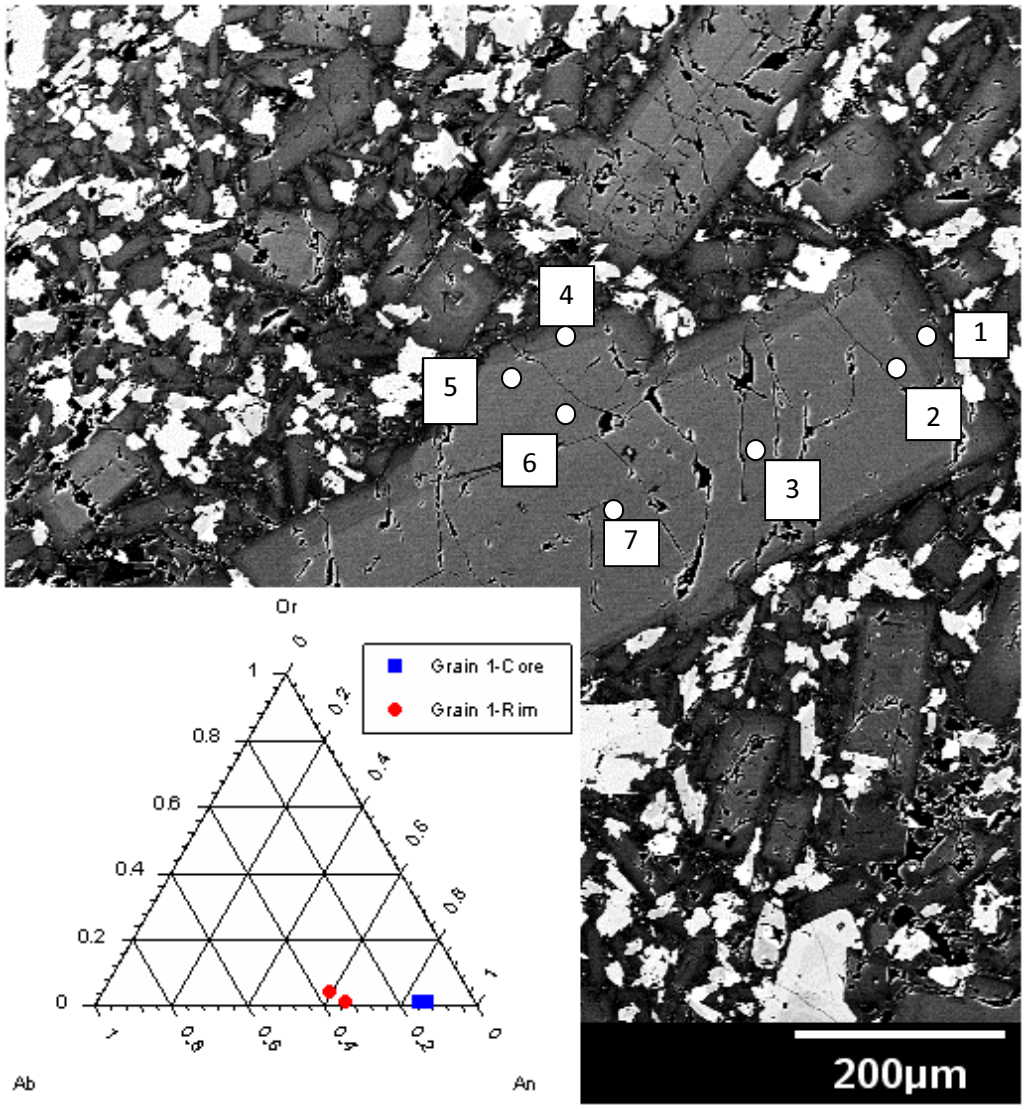

Figure 17: 10LT-02 (Tb), SEM BSE image of Grain 1 with normal zoning.

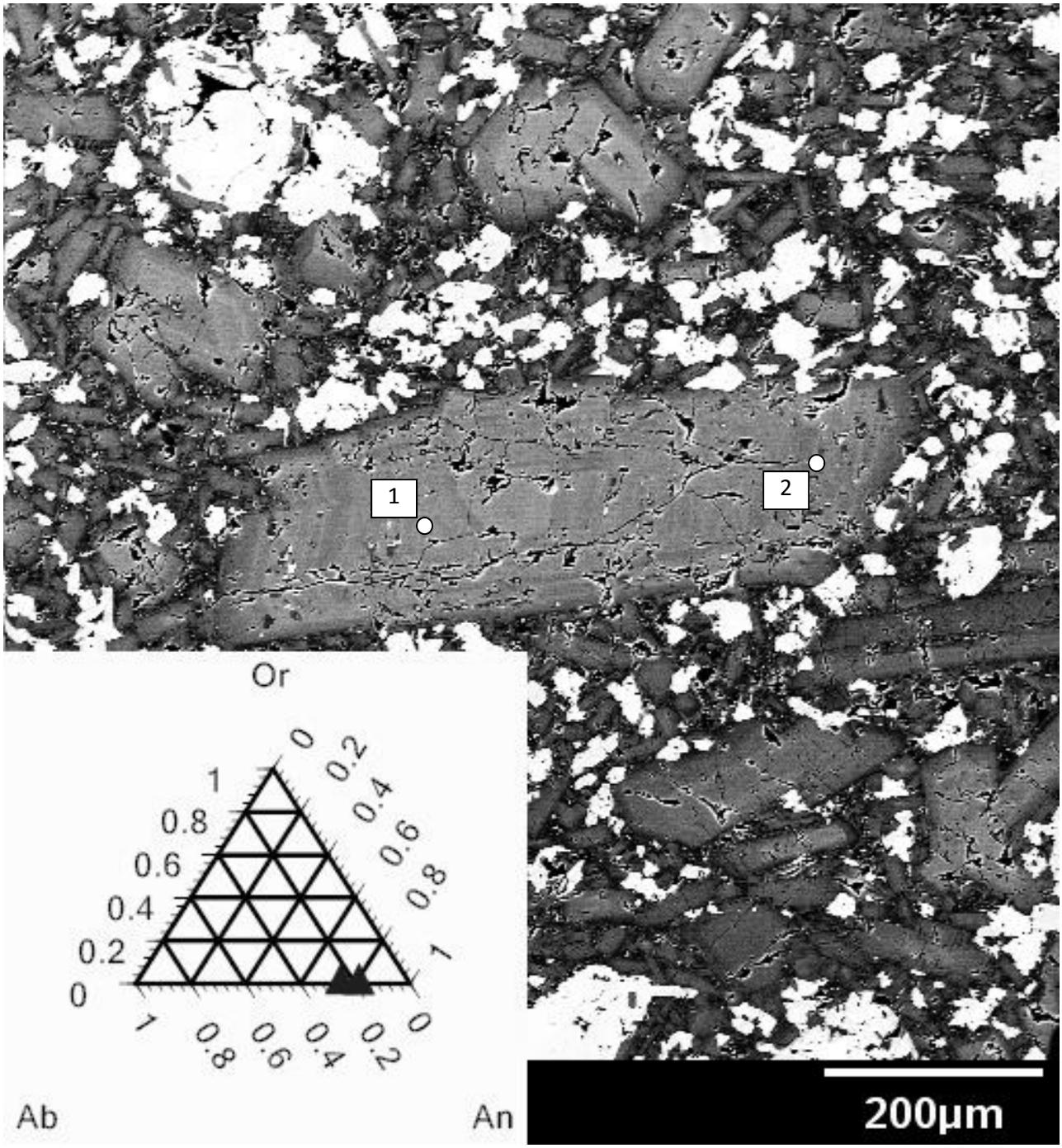

Figure 18: SEM BSE image of 10LT-02 (Tb), Grain 2.

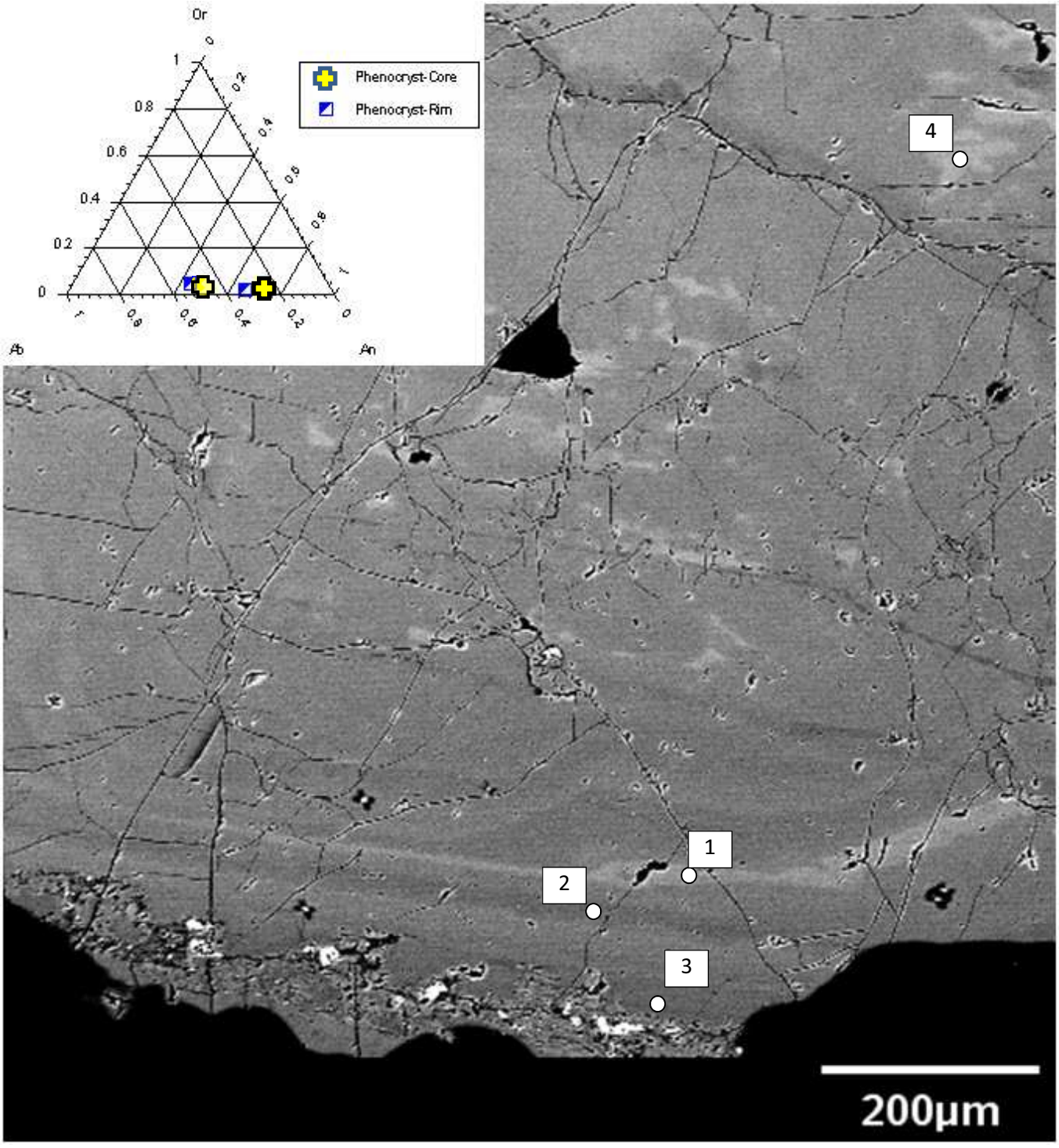

Figure 19: SEM BSE image of 10LT-06, Tpan, plagioclase phenocryst.

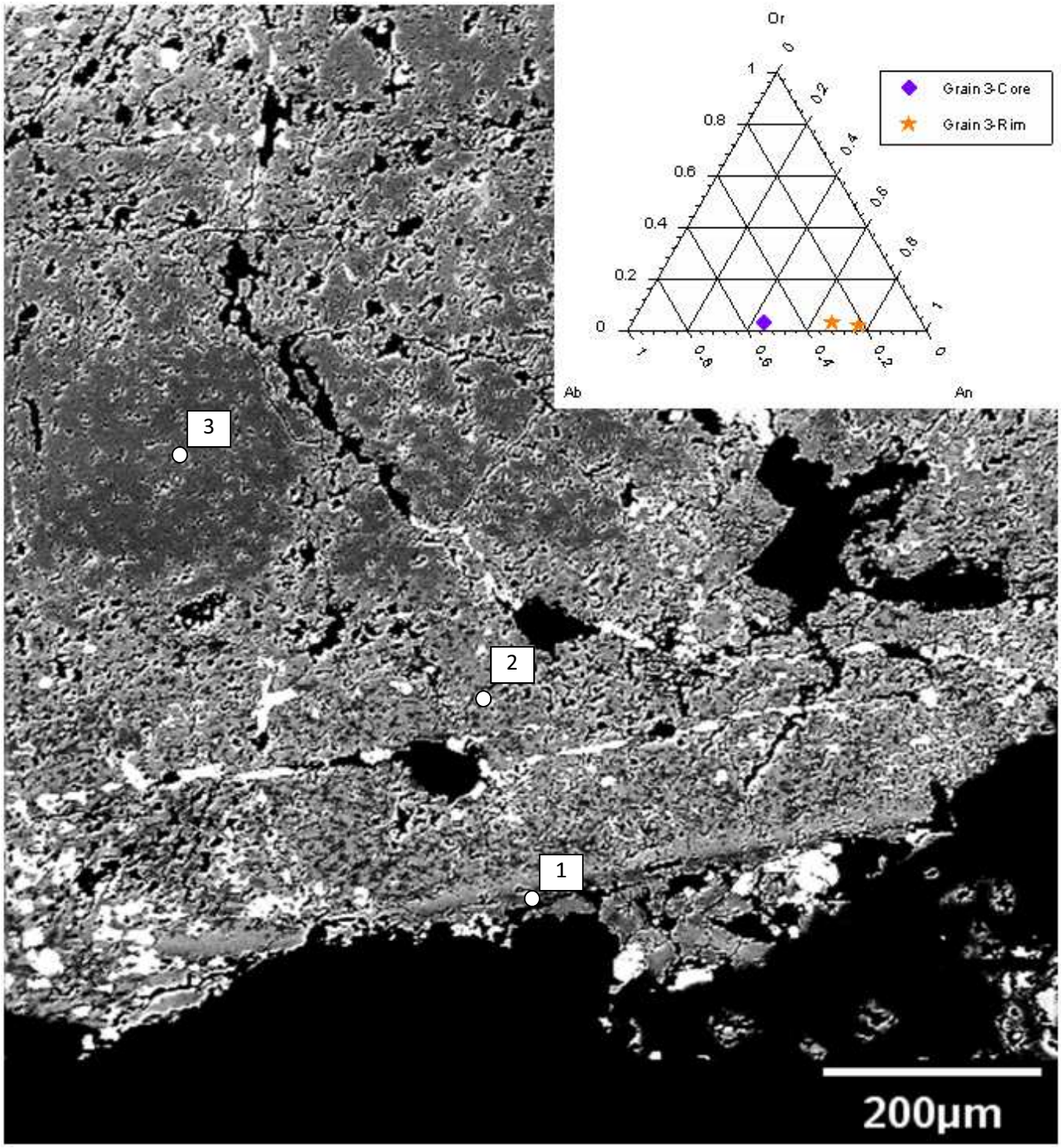

Figure 20: SEM BSE image of 10LT-02, Grain 3, plagioclase with heavy sieve texturing and reverse zoning.

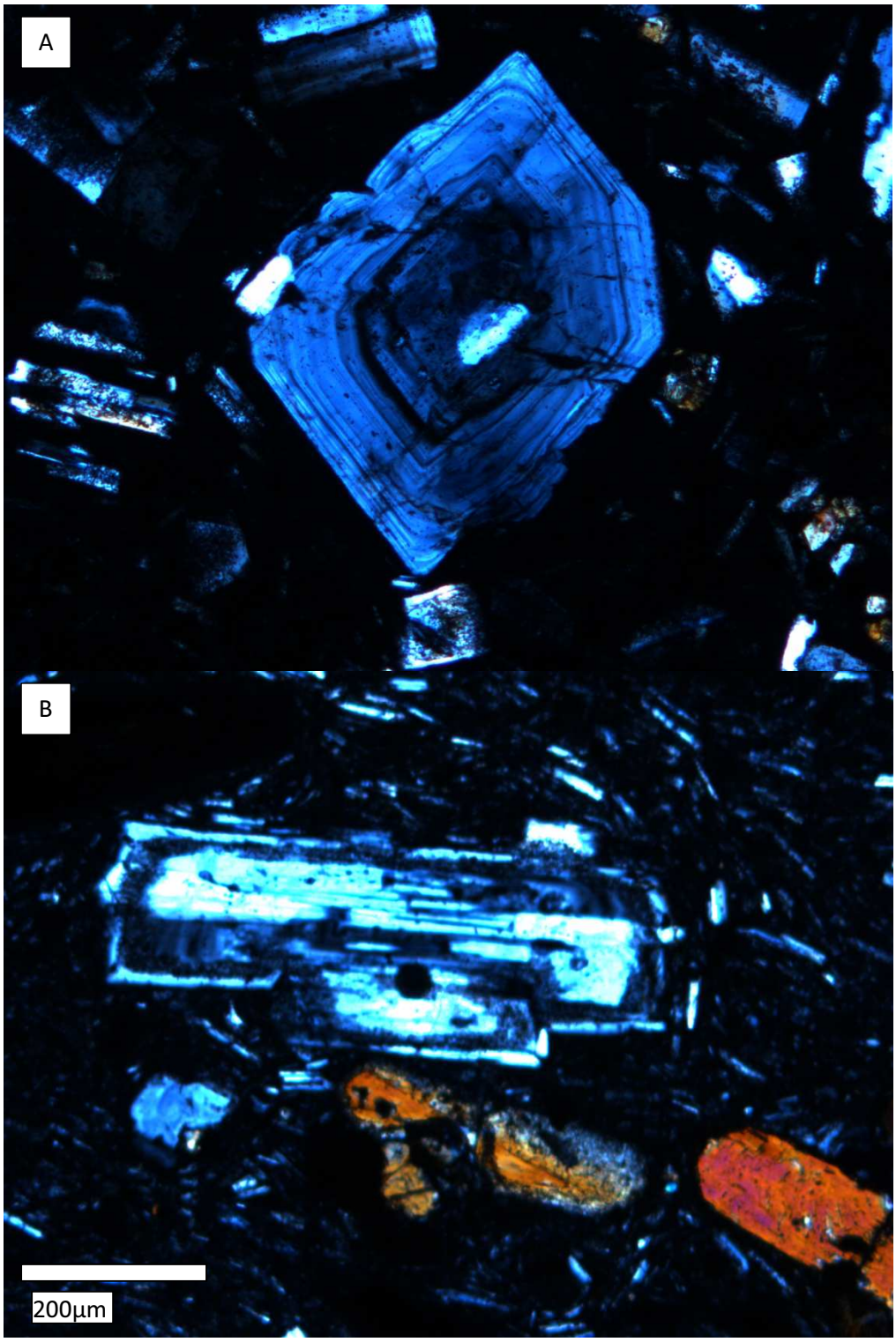

Plate 1: Thin section cross-polar photos of plagioclase grains. A: 10LT-18, Tba with distinct oscillatory zones with intact margins between zones. Zones are angular or rounded. B: 10LT-08, Tpan with a sieve/dissolved rim.

3.2.3 Pyroxene

The pyroxene within the rock units is dominantly augite. Banding was observed in SEM within many phenocrysts of pyroxene but microprobe analysis reveals that the light and dark banding is cpx of roughly the same composition (Figure 21). The bands are angular and distinct with variable thickness under the SEM. The map unit Tpan does have rare individual euhedral grains of opx which often have inclusions of magnetite (Figure 22, Figure 23). There are also some rare grains within some of the andesite units (Tpan and Tpap) which have cores of opx with variable amounts of enstatite that intermix and appear to have solidified ‘in-situ’ with each other but are surrounded by a thick cpx rim (Figure 24).

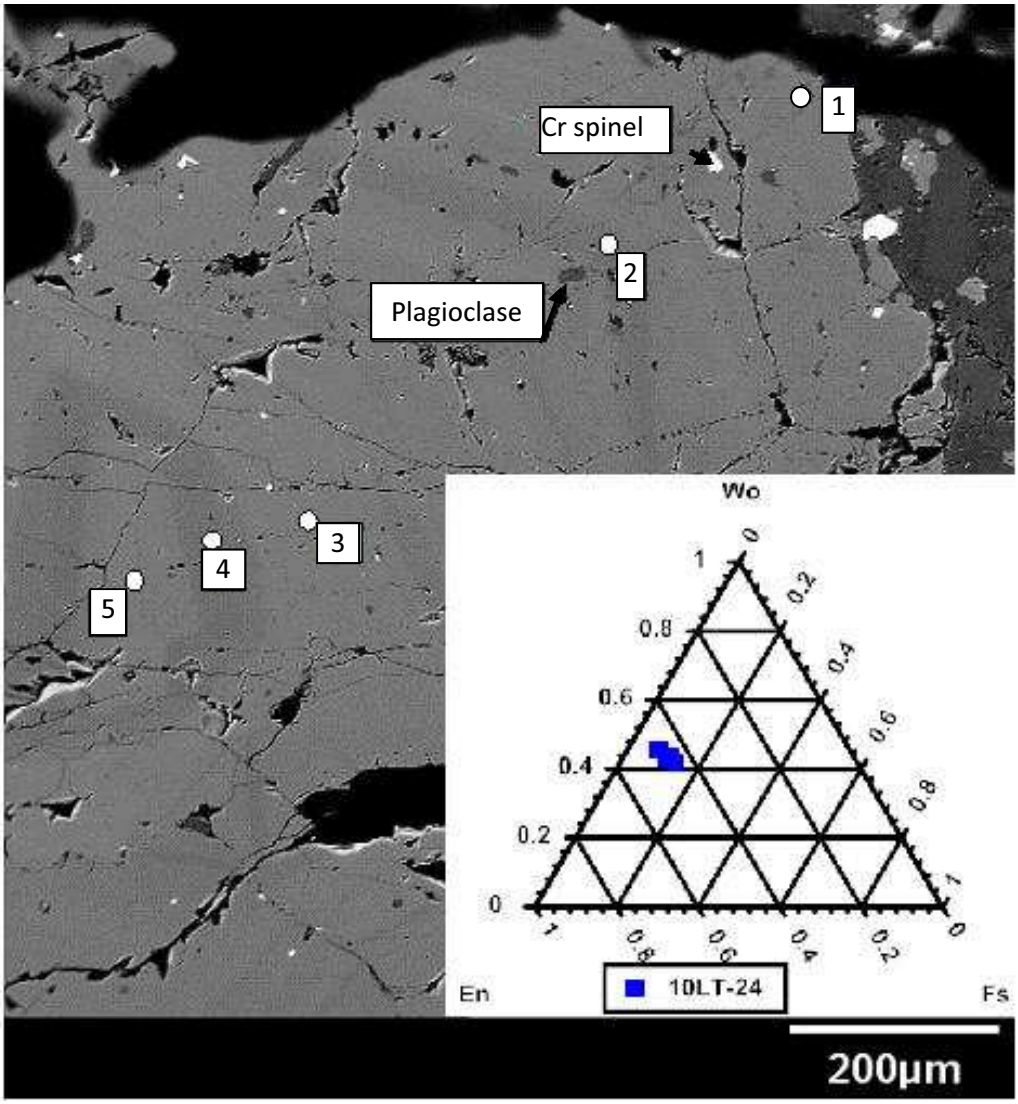

Figure 21: Microprobe results of pyroxene in sample 10LT-24, Tpap alongside a SEM BSE image of the pyroxene grain showing where the analysis was performed.

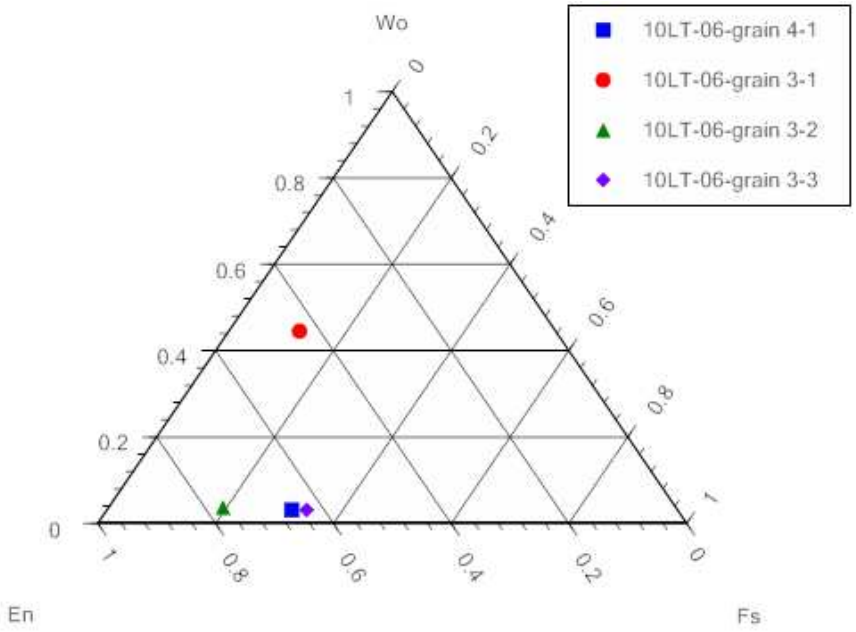

Figure 22: Microprobe results of pyroxene in sample 10LT-06, Tpan (Fig 15, 16). Low Wo (wollastonite) samples: grain 4-1, grain 3-2 & grain 3-3 are orthopyroxene while grain 3-1 is clinopyroxene (Wo 45%).

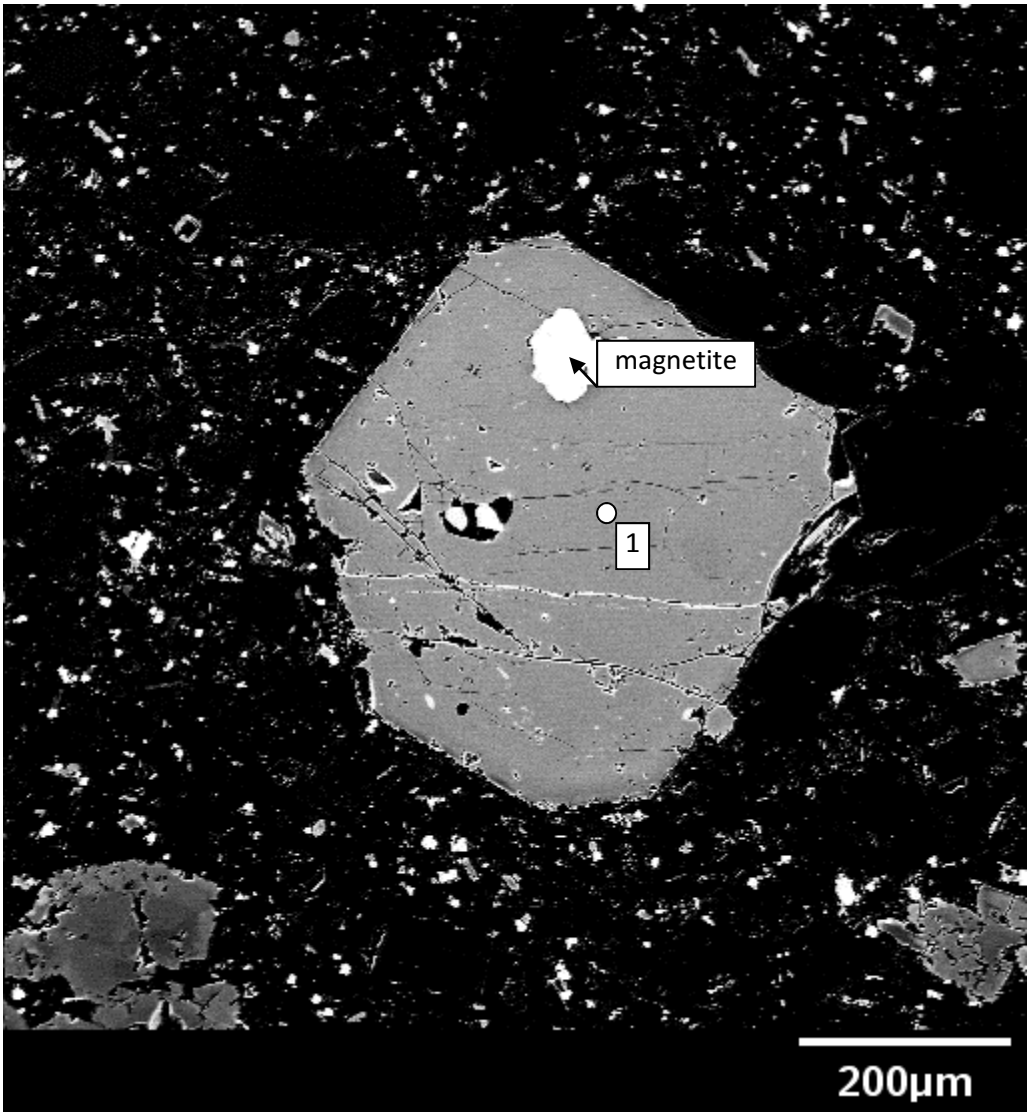

Figure 23: SEM BSE image of Tpan 10LT-06, opx grain 4.

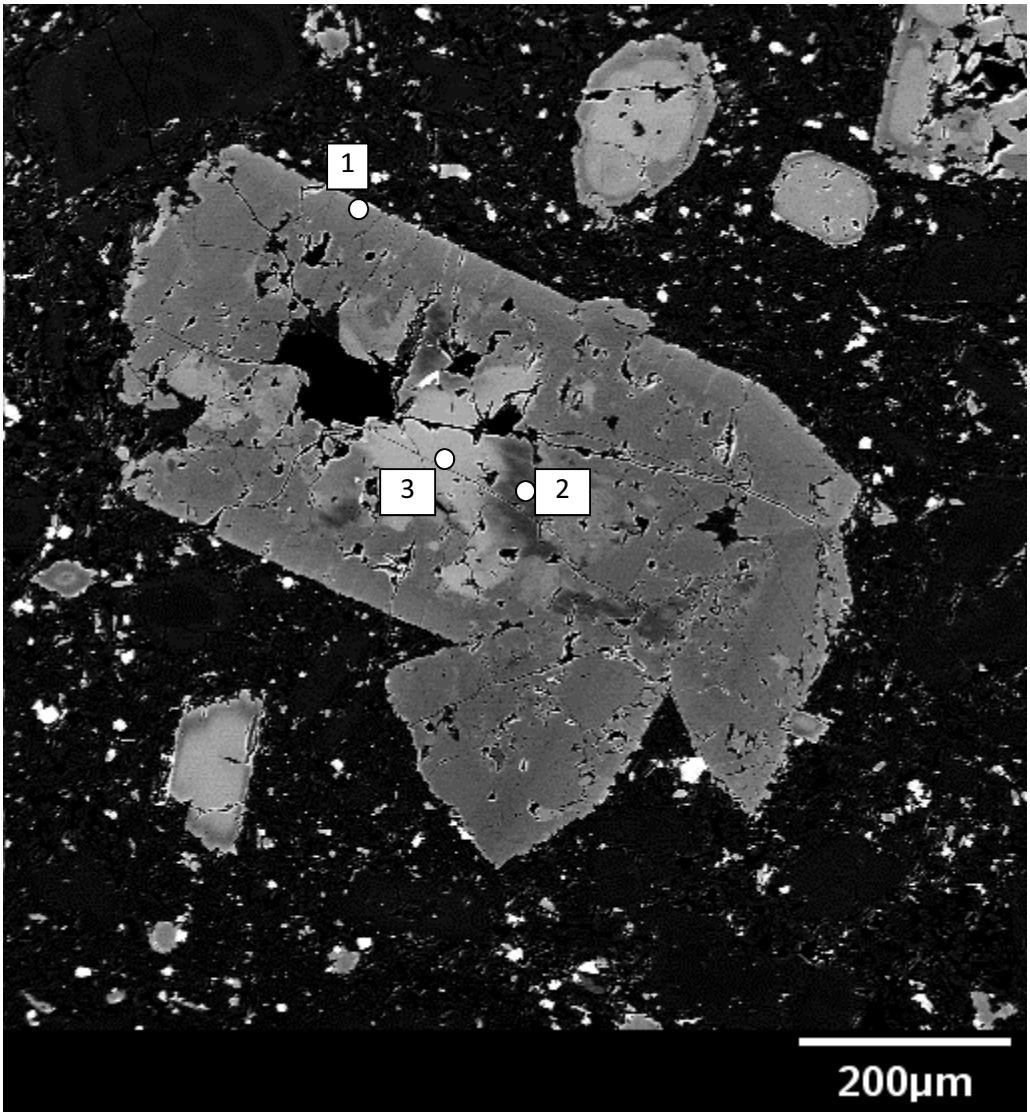

Figure 24: SEM BSE image of 10LT-06, Tpan grain 3 with an opx core and a cpx rim.

3.2.4 Amphibole

Amphiboles are present only in the Tha and Tpan units. Both sets of amphiboles appear heavily altered when first observed, but further study reveals this to not be the case. Within the Tpan unit only relict grains are visible and in the Tha unit there is a thick ~100 µm rim of fine grained amphibole denoting a relict amphibole grain shape which surrounds a Fe altered amphibole core (Figure 25, Figure 26). Microprobe scans indicate that the both 'phases' of the

amphibole grain are Fe-rich hornblende (Table 2). There are also inclusions of plagioclase within the altered zone of the hornblende in the Tha samples (Figure 25, Figure 26). Rutherford & Hill (1993) describes a possible origin for this type of amphibole petrogenesis, by describing two types of amphibole rims: a black (plagioclase is absent in the rim) rim and a gabbroic rim (plagioclase is present in the rim). The black rim type is produced from oxidation and dehydrogenation during/after extrusion while gabbroic rims are produced from fH_2O decrease within the magma reservoir (gabbroic rims can also be indicative of magma mixing; Rutherford & Hill, 1993). The amphibole breaks down into rims when not in contact or surrounded by crystalline phases; it only occurs when in contact with the melt (Rutherford & Hill, 1993). Amphiboles react with the melt as a result of the reduction of the dissolved water content of the melt. Rim growth beginning at the outside of the grain and moving inward towards the amphibole's core as the magma ascends to the surface with pressure decreasing while temperature remains relatively constant (Rutherford & Hill, 1993). Thicker rimmed amphiboles (>10 µm) represent magma(s) which spent more than ten days travelling from the deep storage region of the volcano to the surface (Rutherford & Hill, 1993). For the Mt. St. Helen's amphiboles, several models were proposed: at 8 km depth an amphibole would need 15 days to grow a rim 25 µm in thickness, at 6.5 km depth an amphibole would need 11 days to grow a rim 50 µm in thickness and at 3.5 km depth an amphibole would need 22 days to grow a rim 100 µm in thickness (assuming a 900°C annealing temperature and starting at 220 MPa and dropping to 2 MPa; Rutherford & Hill, 1993). The SVC amphibole rims are ~100 µm so if we use the Rutherford & Hill, (1993) model: at 8 km depth we would need 45 days, at 6.5 km depth we would need 22 days and at 3.5 km we would need 22 days.

Table 2: Amphibole Microprobe Data. All values are in percent.

Descrip.	10LT-10-circle1-1 (Rim)	10LT-10-circle1-2 (Core)	10LT-10-circle1-3 (plagioclase inclusion)
SiO_2	42.19	43.38	46.58
TiO_2	2.14	2.09	Below detectable limit
Al_2O_3	10.73761	10.67	33.14
FeO	16.19	12.31	0.64
MnO	0.30	0.21	Below detectable limit
MgO	13.79	14.71	Below detectable limit
CaO	11.31	11.28	17.12
Na_2O	1.75	2.20	1.83
K_2O	0.23	0.50	0.06

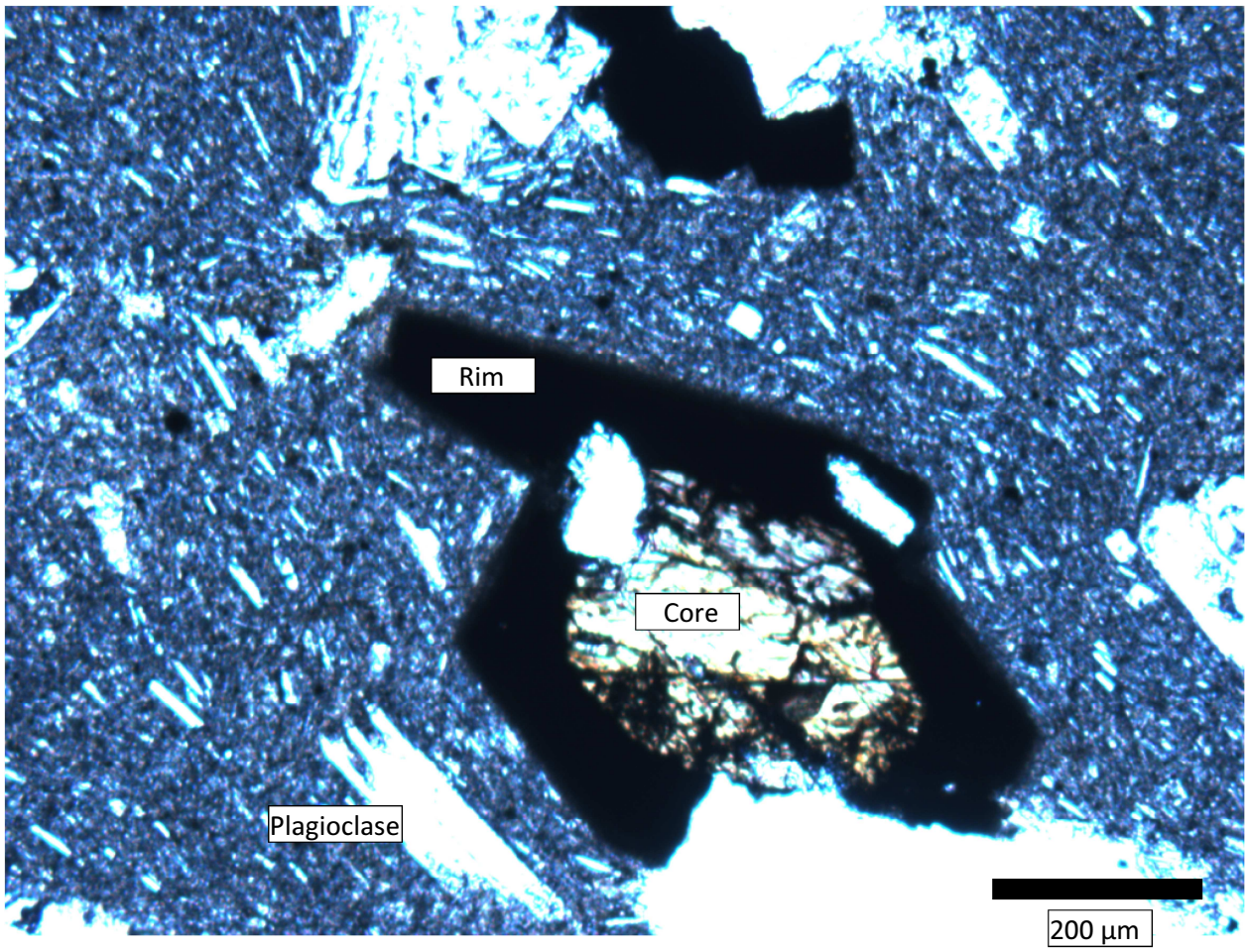

Figure 25: Transmitted light thin section image of 10LT-10 under 5x mag. Hornblende with a Fe-rich core surrounded by a recrystallized hornblende rim containing plagioclase inclusions and a matrix with a trachytic texture.

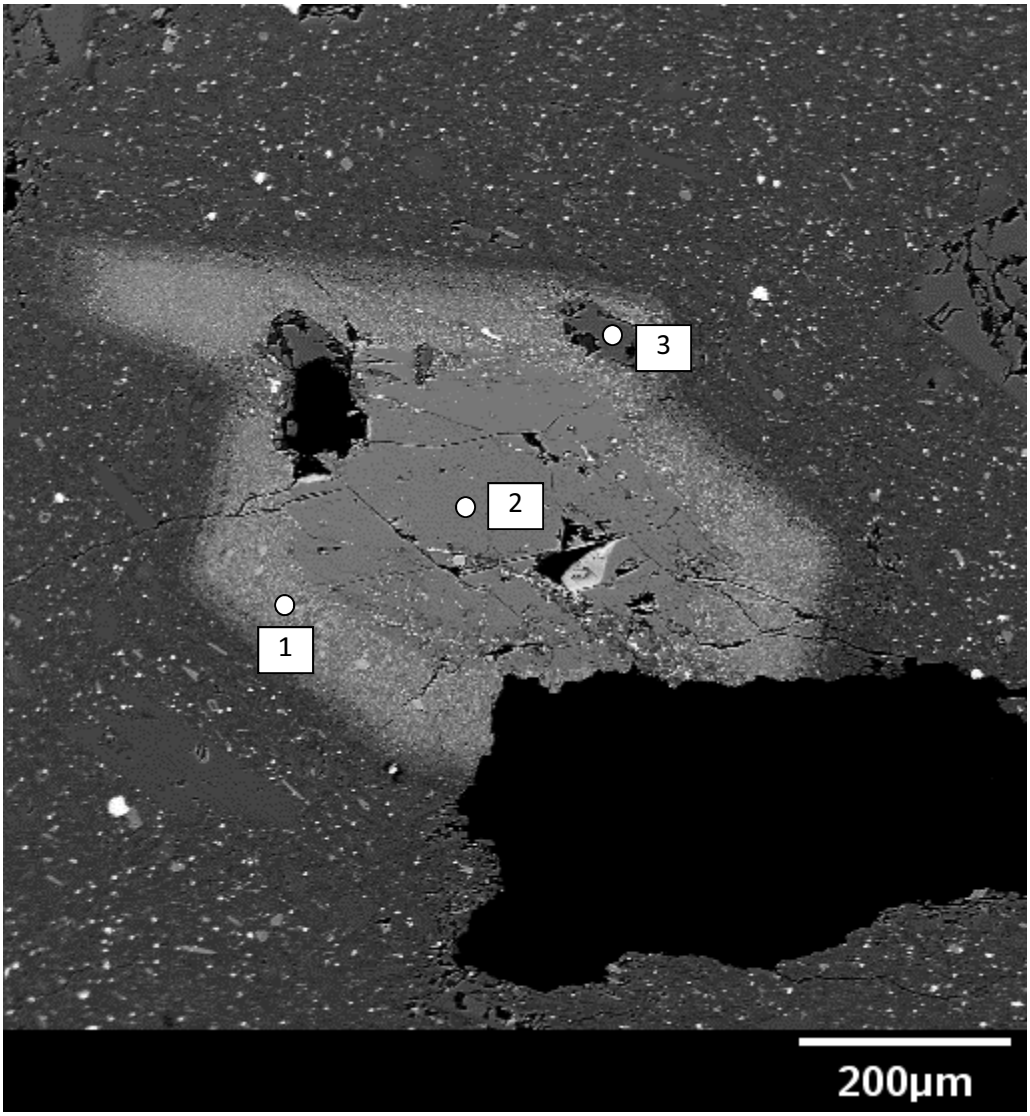

Figure 26: SEM BSE image of 10LT-10, Tha. SEM image of amphibole in Figure 20, site 3 is a plagioclase inclusion.

3.3 Geochemistry: Major Element, Trace Element & Isotopic Element Results

Twenty-four samples were analysed for major and trace elements (Appendix 2), of the twenty-four samples seventeen (representing each map unit) were also analysed for Pb, Sr and Nd isotopes (Appendix 3). According to the Total Alkali Silica (TAS) diagram (Figure 27) the sample set is composed of eight basalts (one is alkali), ten basaltic-andesites and five andesites. Overall the sample series defines a calc-alkaline trend and is primarily basaltic-andesite.

The TAS diagram is a result of the International Union of Geological Sciences (IUGS) trying to create a workable classification scheme for igneous rock nomenclature namely the quartz-alkali feldspar-plagioclase-feldspathoid (QAPF) diagram. The QAPF diagram cannot make easy distinctions between andesite and basalt (a color index is used but it is highly subjective since it involves looking at a hand specimen), the essential point being that volcanic rocks like basalt and andesite are typically aphanitic and therefore one cannot visually discern the minerals even if they are well developed. Because of this, the IUGS recommends the use of the TAS developed be LeBas et al., (1986) which uses geochemical data to provide a more reliable classification. The TAS is a simple Harker style diagram comparing total alkalis (Na_2O+K_2O) versus silica normalized to a non-volatile basis and is divided into 15 fields defining various aphanitic volcanic rocks. According to the Total Alkali Silica (TAS) diagram (Figure 27) the Sagehen sample set is composed of eight basalts (one is alkali), ten basaltic-andesites and five andesites. Silica values range from 47.92 to 60.71 wt% and total alkalis range from 3.33 to 5.68 wt% this forms a roughly linear trend with a positive slope of 0.2 along the plot. The Tpan (Tpan = non-porphyritic andesite) map units plot more within the basaltic-andesite field than in the andesite field and the Tba (Tba = basaltic-andesite) samples plot within

the andesite field; The Tb (Tb = olivine basalt) samples cluster around each other and fall along the basalt and basaltic-andesite boundary and the Tpap map unit (Tpap = porphyritic andesite) plots well within the basalt field. Basaltic tephra (Tbt) samples display a wide variation in silica and alkalis and this is more a reflection of the samples coming from different areas of the flows (the basalt rich volcaniclastics plot in the basalt field while the more andesite rich volcaniclastics plot in the basaltic-andesite field). The scoria sample (from map unit Tpap) plots as an alkaline basalt; the hornblende andesite is the only map unit that consistently plots within its corresponding field (andesite).

The Alkali-Iron-Magnesium (Alkalis: Na_2O+K_2O, Iron FeO $+Fe_20_3$, Magnesium: MgO) diagram or AFM diagram is one of the most common triangular variation diagrams used by igneous petrologists. An AFM diagram is plotted using a wt% or using only the cations; the relative proportions of Na and K are believed to not affect each other and that the total alkali content is more important than the individual cations (Irvine & Barager, 1971). For most mafic minerals Mg/Fe abundances are higher in the solid phase than in the coexisting melt, so removal of solidified mafic minerals from the melt will increase the relative iron contents in the AFM. Parental magmas will be closer to the MgO corner while more evolved magmas will plot near the Alkali apex. This is because alkalis are generally more enriched in fluids and so will enter the solid phase later in later stages of crystallization (remember water content lowers the melting point). Suites of samples that plot with high iron are considered to be tholeiitic while lower iron contents are considered calc-alkaline. Overall the sample set is calc-alkaline when plotted according to the AFM diagram (Figure 28) with the only exception being the scoria sample. The basalts plot near the MgO corner while the basaltic andesites and andesites trend towards the alkali corner.

A good method of evaluating chemical trends within a rock series are bivariate diagrams, notably, Harker diagrams named after Alfred Harker (1909). A Harker diagram is a simple x-y plot which plots silica along the x-axis while a major oxide or trace element or a ratio of major oxides or trace elements is plotted along the y-axis. Because silica content generally indicates magmatic evolution, a plot comparing silica content can suggest which samples/rocks are derived from parental magmas or are evolved. Samples with low silica are considered to be parental magmas while samples with high silica experienced some sort of chemical differentiation are considered to be evolved. Decreases in CaO with respect to silica can indicate that CaO was removed from the melt by either a calcic plagioclase and/or clinopyroxene. A typical Al_2O_3 Harker diagram for a volcanic rock suite will at first increase but then decreases, this can be reconciled by assuming olivine is removed early followed by plagioclase removing both Ca and Al. A plot of SiO_2 versus CaO/Al_2O_3 can therefore be used to exclusively distinguish pyroxene fractionation from plagioclase from the melt (Figure 29). Figure 29 shows two distinct groups, with samples classified as basalt in the TAS diagram forming one clustered group which follows a flat trend, whereas the basaltic-andesite and andesite samples classified in the TAS diagram from a different group which follows a flat to shallowly dipping negative linear trend. The CaO/Al_2O_3 ratio values range from 0.309 to 0.662 with the basaltic units having the higher values while the andesites have the lower values; the two groups of samples both follow a general slope of-0.0066 but the basalt group and the basaltic-andesite and plot along the same line but two separate lines with the same slope. The plot of P_2O_5 versus SiO_2 used to observe potential apatite fractionation follows a generally flat trend (Figure 30) and ranges in values from 0.14 wt% to 0.32 wt%. The plot of TiO_2 versus SiO_2 follows a shallowly dipping negative linear trend and indicates the level of fractionation of titanomagnetite and opaque mineral phases

(Figure 31). Values of TiO_2 range from 0.527 to 1.037 wt% with the andesites having the lower TiO_2 values and the basalts having the higher TiO_2 values.

Distinctions between tholeiites and calc-alkaline magma series can be difficult, there are several classification diagrams each with their own boundaries for tholeiite/calc-alkaline rocks (TAS, AFM) making classifications of tholeiites and calc-alkaline lava series based on one diagram spurious. Also, originally calc-alkaline series were considered to be exclusive to subduction zones while tholeiites were considered to be part of established continental volcanic provinces but this is not always the case. Gill (1981) further complicates this by defining andesite suites along K_2O vs. SiO_2; because K_2O is considered separately from Na_2O, this classification cannot use tholeiite or calc-alkaline as a descriptor alone. Gill (1981) defines four broad categories for andesites based on K_2O vs. SiO_2 Low-K, Med-K, High-K and Shoshonites (Higher-K). Low-K type rocks are dominantly tholeiitic (island arc tholeiites) while Med-K rocks are primarily calc-alkaline (convergent margin), High-K corresponds to mixtures of both tholeiites and calc-alkaline rocks. Values of K_2O in Sagehen samples range from 0.84 to 1.69 wt% and follow a positive linear slope of 0.13. When the samples were plotted on a K_2O vs. SiO_2 graph the majority of the samples plotted in the med-K field which is a strong indicator of calc-alkaline lava sources (Figure 32).

Compatible trace element abundances plotted against silica give a good window into fractionation phases within the rock sample. Compatible elements will readily concentrate into solid phase quickly while incompatible elements will prefer to concentrate in the melt (liquid). The incompatible elements are subdivided into two groups: 1) *High field strength elements* (REE, Th, U, Ce, Pb^{4+}, Zr, Hf, Ti, Nb and Ta) which are smaller and more highly charged and 2)

Light ion lithophile elements (K, Rb, Cs, Ba, Pb^{2+}, Sr, Eu^{2+}) which have high ionic radii and are more mobile, especially in fluid phases. Ni, Sc and Cr are highly compatible elements with Ni concentrated in olivine, Sc in clinopyroxene and Cr in spinel and clinopyroxene. High concentrations of these elements indicate a mantle source, limited fractionation and/or crystal accumulation. The Ni abundances in the Sagehen samples range from 5 to 48 ppm and follow a general negative linear trend with a slope of -0.38 ppm/wt% with the basaltic samples generally having higher abundances of Ni relative to the andesites. The Cr abundances in the Sagehen samples range from <24 (below detection limit) to 287 ppm the basaltic samples follow a positive linear trend with a slope of 22.4 ppm/wt% while the andesitic samples have a flat slope along the lower limit of the detection range. The Sc abundances in the Sagehen samples range from 12.6 to 47.5 ppm and follow a general linear trend with a slope of -2.51 ppm/wt% with the basaltic samples having the higher Sc abundances while the andesites are have the lower values. The relative decreases in abundances of Ni and Sc versus increasing silica indicate olivine and clinopyroxene are being fractionated out of the melt (Figure 33). Incompatible trace element plots versus silica of La, Ba, Nb and Th versus $SiO_{2\ also}$ show consistent trends (Figure 34). Lanthanum is a REE, specifically, is a light rare earth element (LREE) therefore it does not partition strongly into most minerals, it is also mobile in fluids. Lanthanum abundances range from 9.98 to 34.96 ppm with a slope of 2.29 ppm/wt%. Barium is an incompatible element that substitutes for K in hornblende. Barium abundances range from 150.1 to 1168.9 ppm and follow a positive linear trend with a slope of 88.89 ppm/wt%. Niobium is a HFSE and is strongly influenced by rutile, ilmenite or sphene mineral phases. Niobium abundances range from 2.11 to 6.98 ppm and follow a positive linear trend with a slope of 0.40 ppm/wt%. Thorium is a highly immobile element and is highly insoluble in water/fluids, it is generally found in K-feldspar rich granites,

pegmatites and syenites. Thorium abundances range from 1.58 to 6.67 ppm and follow a positive linear trend with a slope of 0.40 ppm/wt%. The elements La, Ba, Nb and Th all increase with increasing silica and show generally positive linear trends with basaltic members belonging to the lower end of the trend and andesitic members belonging to the higher end of the trend.

Trace element abundances were normalized to primitive mantle after Sun and McDonough (1989). Within the sample set, Ba, Pb, and Sr are enriched relative to La; Zr and Hf are enriched relative to Sm; Nb is depleted relative to La and Ti is depleted relative to Gd. The REE patterns follow a concave-up trend for LREE and is flat along the HREE (Figure 35 a, b, c, d, e, f, g). The samples can be subdivided into two main groups based on Zr and Hf abundances. The first group is composed of samples that are classified as basalt in the TAS (Figure 27); these samples will have a Zr-Hf concave-up pattern and will be relatively more enriched in Sr relative to Pb. The second group is composed of the basaltic-andesites and andesites from the TAS (Figure 27); these samples have a Zr-Hf concave-down pattern. The basaltic-andesites can be subdivided within this group since their relative abundances of Zr and Hf are lower than the andesites. Also, the andesite sub-group will be relatively more enriched in Pb relative to Sr.

Because the parent isotopes to Sr, Nd & Pb isotopes are unstable (and therefore decay; e.g. ^{87}Rb to ^{87}Sr, ^{238}U to ^{206}Pb, ^{235}U to ^{207}Pb, ^{232}Th to ^{208}Pb, and ^{147}Sm to ^{143}Nd) they can easily show us if the map units (and by extension the melts) were modified or contaminated by crustal assimilation or modified by fluids from the subducting slab. The samples analyzed can enable us to better compare the SVC to previously studied areas within the Cascades so that we can evaluate if they are from the same source. Crustal sources will have relatively more isotopic Sr and relatively less isotopic Nd compared to more mafic (basaltic) sources and furthermore,

basaltic samples modified by fluids from the slab will have higher isotopic Nd than basalts not modified by the slab. At the same time, isotopic Sr and Pb are elements that are concentrated in hydrous fluids coming from the slab, as well as in pelagic sediments or upper continental crust, relative to the mantle. Fluids and crustal sources also have isotopic compositions different from mantle rocks, such that isotope systematics are fingerprints of fluid or slab additions to the mantle wedge, or to crustal contamination as melts move up through the crust.

Isotope values of the Sagehen samples define a consistent trend of values for isotopic Pb, Sr and Nd and also show a distinct grouping of basalt relative to andesite. Overall the $^{87}Sr/^{86}Sr$ ratio sample values range from 0.70340 to 0.70516 while $^{143}Nd/^{144}Nd$ ranges from 0.51281 to 0.51254. The $^{143}Nd/^{144}Nd$ v. $^{87}Sr/^{86}Sr$ plot (Figure 36 A) shows a roughly negative linear trend and two distinct groups each with their own subgroups. The basalts form two sub-groups based along the map units Tb and Tpap, whereas the basaltic-andesites and andesites form their own main group with two sub-groups based along basaltic-andesite and andesite (the andesites have the higher Sr isotopic ratio). The range of $^{207}Pb/^{204}Pb$ is 15.595 to 15.662 while $^{208}Pb/^{204}Pb$ ranges from 38.458 to 38.801 and $^{206}Pb/^{204}Pb$ ranges from 18.837 to 19.012. Plots of $^{208}Pb/^{204}Pb$ versus $^{207}Pb/^{204}Pb$ and $^{207}Pb/^{204}Pb$ versus $^{206}Pb/^{204}Pb$ (Figure 36B, C) show positive linear trends, where low isotopic Pb values are basaltic while andesitic samples have higher isotopic Pb. The εNd vs. εSr plot after Farmer & DePaolo, (1983) shows that basaltic samples plot within the depleted mantle field while the andesite rich units plot within enriched mantle/crustal lithosphere fields (Figure 36 D).

Radioactive (parent) and radiogenic (daughter) elements can be fractionated from each other by partial melting and crystal fractionation and have ratios that vary with time; radiogenic

isotopes will form from the isotopic decay of radioactive isotopes leading to the term *parent-daughter*. Plots of parent versus daughter isotopes or if need be plotting one isotope ratio versus a corresponding non-isotopic parent-daughter ratio (ex: Rb/Sr_{pmn} v. $^{87}Sr/^{86}Sr$) can indicate if there is more than one parent i.e. two melts each with their own parent (but it is the same element). Parent-daughter plots also can be used to compare to existing sources outside of the SVC to determine if the melts came from a 'old' or 'young' source. Both types of source, if they have the same initial ratio can reach the same final ratio, the mitigating factor is time. Relatively young (~10 Ma) low percentage partial melts from the mantle will have $^{87}Rb/^{86}Sr$ ratios that will rapidly increase from an initial ratio with respect to time. While relatively old (Proterozoic) high percentage partial melts that are from the lithosphere will have $^{87}Rb/^{86}Sr$ ratios that slowly increase from an initial ratio with respect to time. This can be seen in the relative compatibility of Rb to Sr; Rb is more incompatible compared to Sr meaning older lithospheric sources, which incorporate Sr, will have a lower rate of increase compared to younger mantle sources. The Rb/Sr ratio, therefore, can indicate the degree of crustal assimilation while the $^{87}Sr/^{86}Sr$ ratio indicates the relative age. Parent-daughter plots of Rb/Sr_{pmn} v. $^{87}Sr/^{86}Sr$ (Figure 37A) and Sm/Nd v. $^{143}Nd/^{144}Nd$ (Figure 37 B) show similar patterns. The Rb/Sr_{pmn} v. $^{87}Sr/^{86}Sr$ (Figure 37A) plot shows clustered basalt samples progressing to a scattered basaltic-andesites and andesites with increasing Rb/Sr and $^{87}Sr/^{86}Sr$. The Sm/Nd_{pmn} v. $^{143}Nd/^{144}Nd$ plot is the inverse of Rb/Sr_{pmn} v. $^{87}Sr/^{86}Sr$ with a vertical basaltic group and then more scattered basaltic-andesite and andesite samples of lower Sm/Nd and $^{143}Nd/^{144}Nd$.

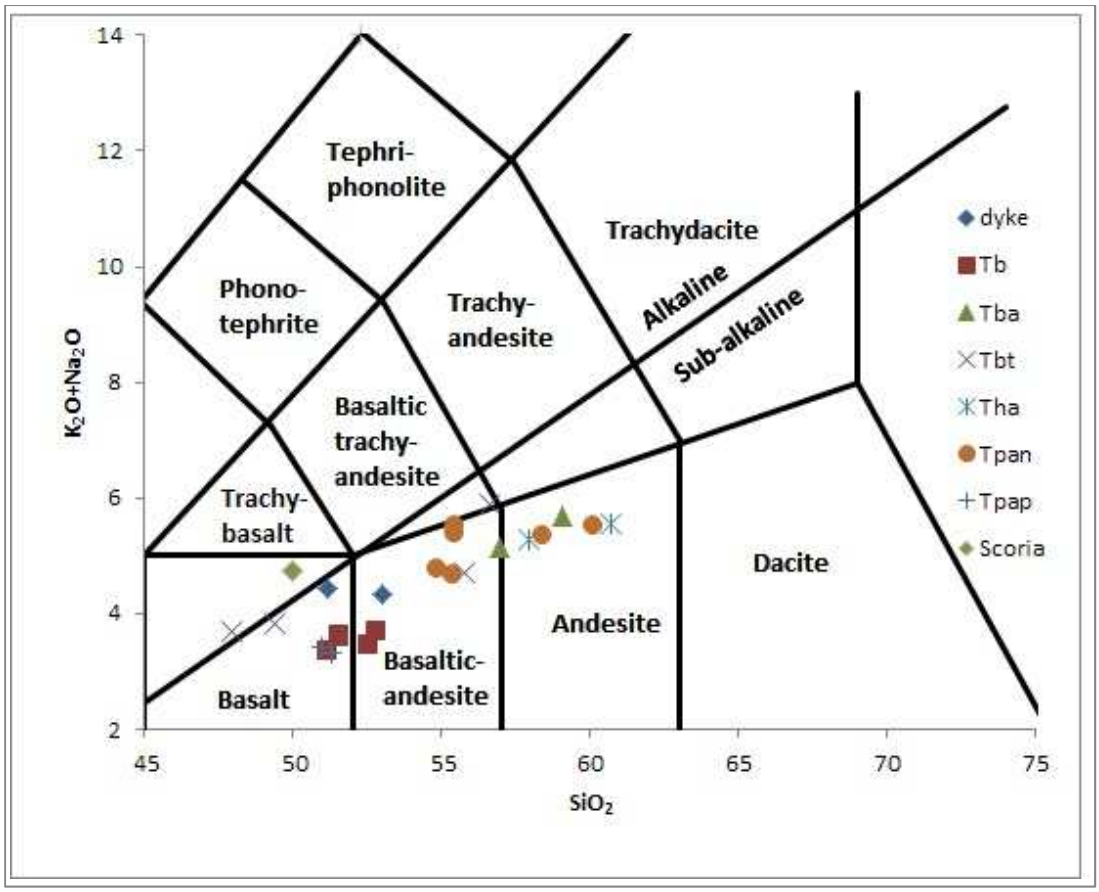

Figure 27: Total Alkali silica plot of SVC samples after LeBas et al., 1986.

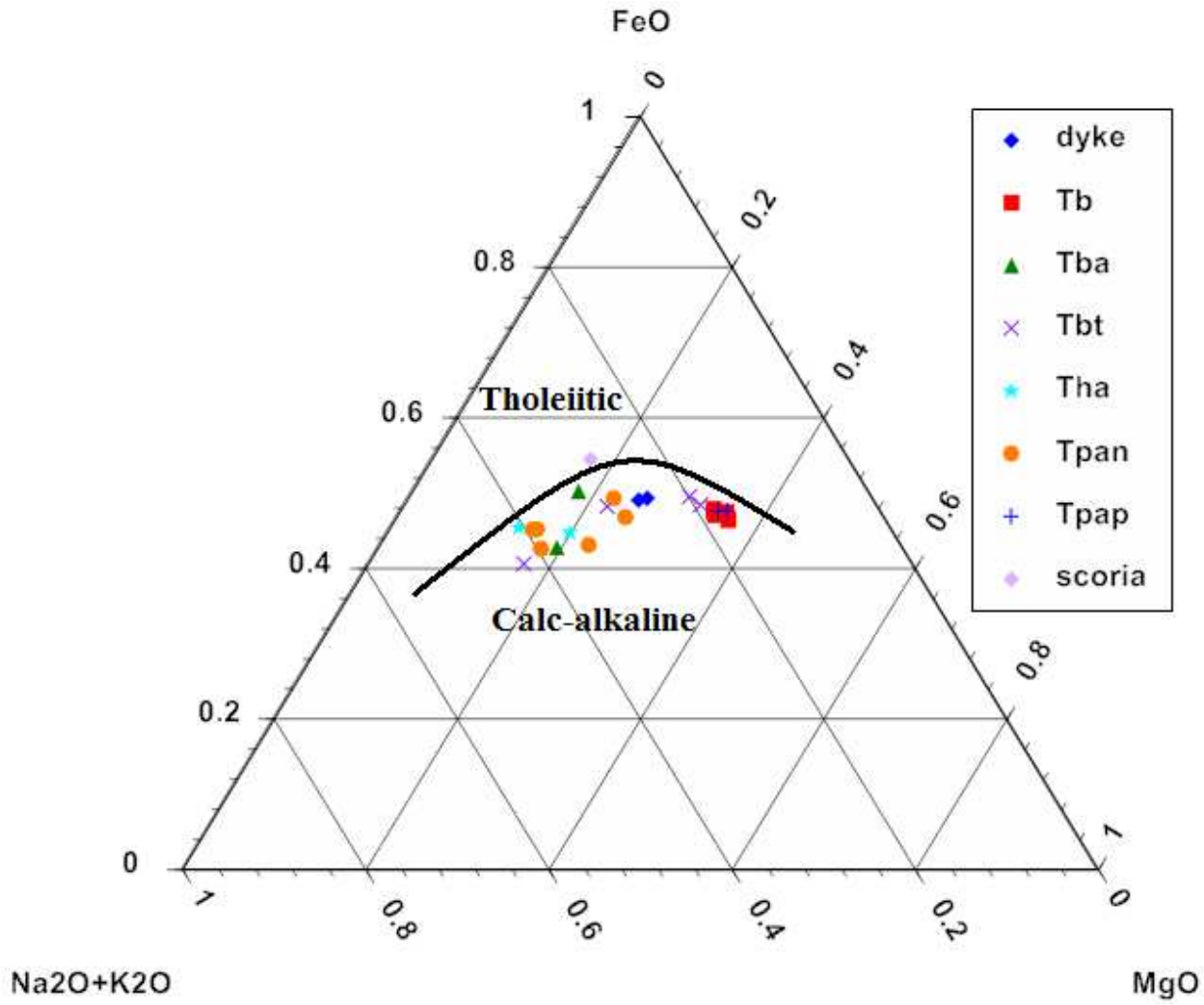

Figure 28: AFM diagram of SVC samples showing a primarily enriched calc-alkaline character, values are in percent after Irvine & Barager, 1971.

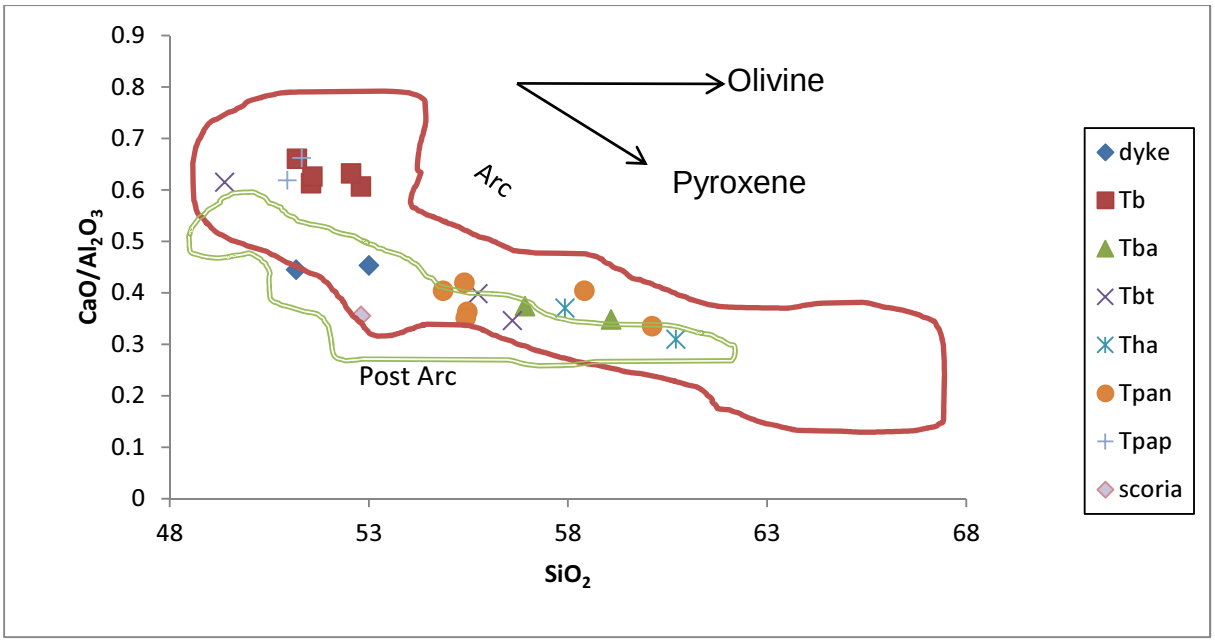

Figure 29: A plot of CaO/Al_2O_3 versus SiO_2 for the SVC samples showing pyroxene fractionation. The solid (Arc) line denotes the extent of previous Ancestral Cascades Arc chemical analyses (compiled in Cousens et al., 2008). The double line denotes post-arc chemical analyses (compiled in Cousens et al., 2011). SVC samples trend in a shallow negative linear slope indicating the fractionation of pyroxene in the high silica andesites.

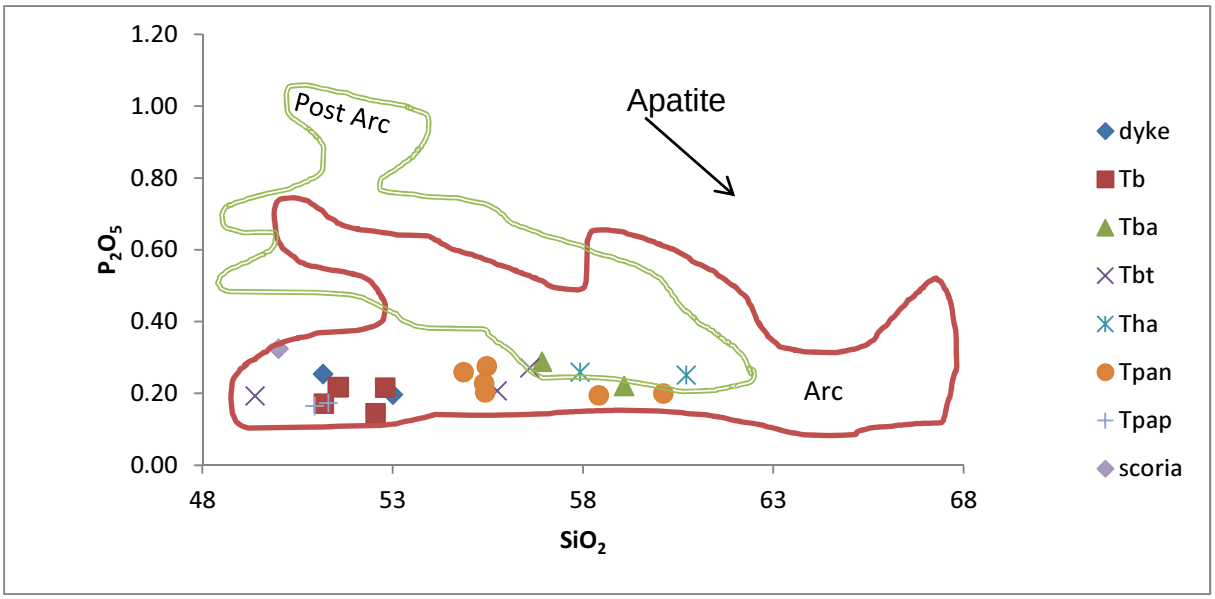

Figure 30: Plot of P_2O_5 versus SiO_2 which can be used to indicate apatite fractionation: apatite indicates an alkaline setting. The solid (Arc) line denotes the extent of previous Ancestral Cascades Arc chemical analyses (compiled in Cousens et al., 2008). The double line denotes post-arc chemical analyses (compiled in Cousens et al., 2011). SVC samples show a flat P_2O_5 pattern indicating apatite is not a major fractionating mineral phase and that the samples are sub-alkaline.

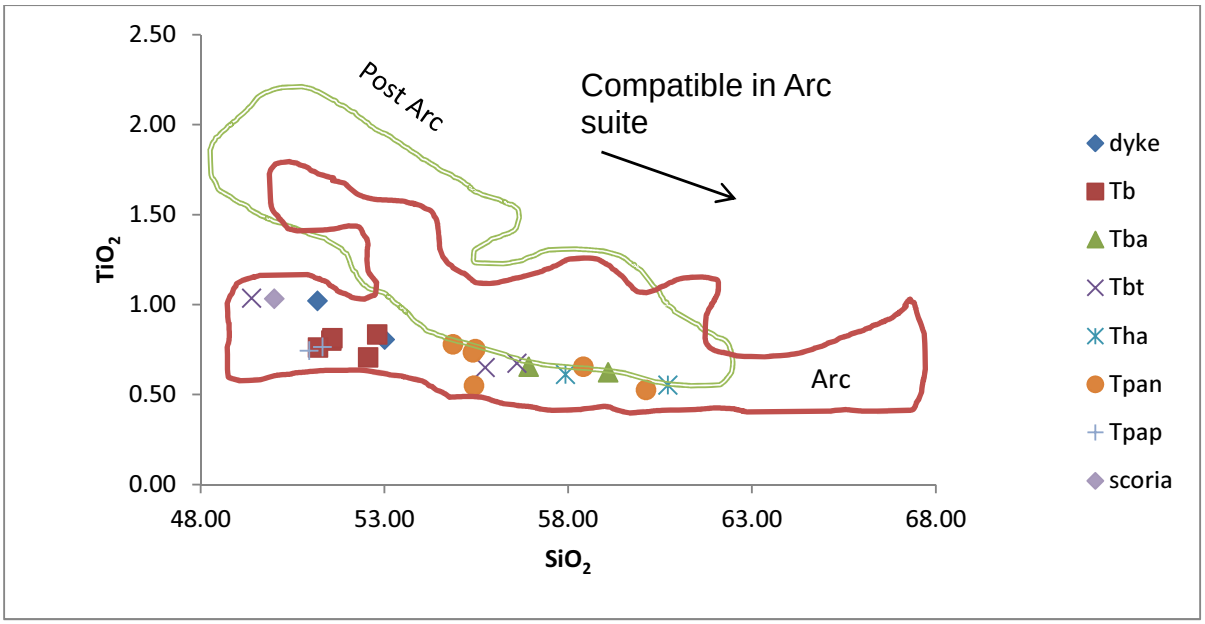

Figure 31: Plot of TiO_2 versus SiO_2 which is used here to show compatibility if Ti within the arc and if titanomagnetite is crystallizing from the melt. The solid (Arc) line denotes the extent of previous Ancestral Cascades Arc chemical analyses (compiled in Cousens et al., 2008). The double line denotes post-arc chemical analyses (compiled in Cousens et al., 2011). Sagehen follows the Arc trend

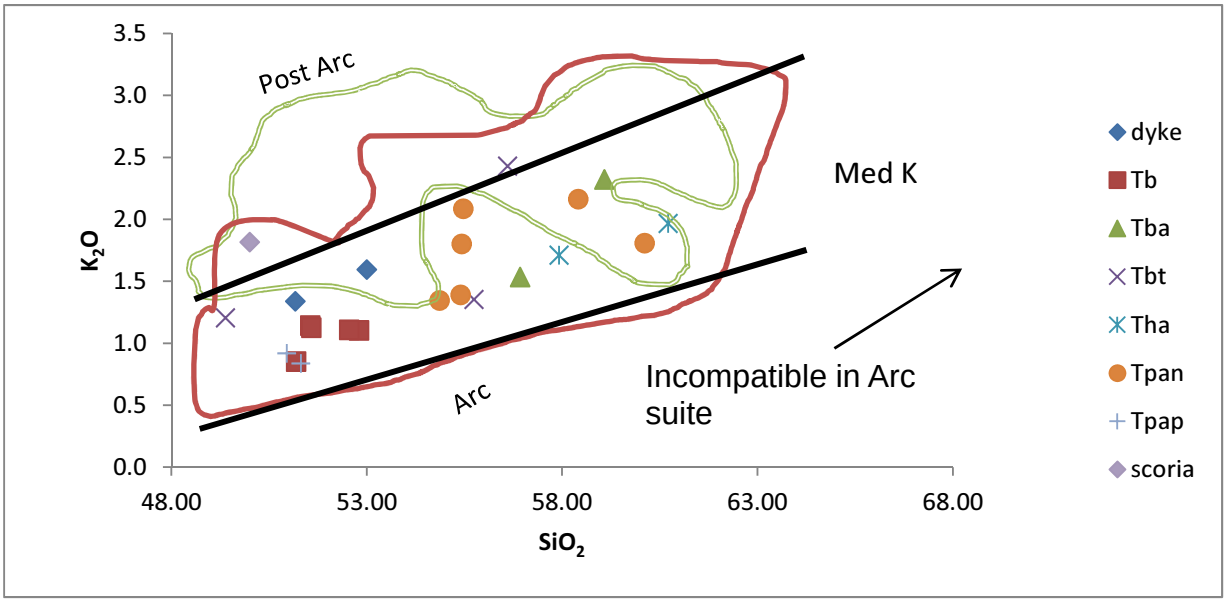

Figure 32: A plot of K_2O versus SiO_2 of SVC samples used to infer crustal thickness. The solid (Arc) line denotes the extent of previous Ancestral Cascades Arc chemical analyses (compiled in Cousens et al., 2008). The double line (Post-Arc) denotes post-arc chemical analyses (compiled in Cousens et al., 2008). SVC samples follow a med-K trend, which is comparable to most Ancestral Cascades arc rocks and calc-alkaline magmas. Increases in K_2O relative to SiO_2 are typical of continental arc rocks passing through and assimilating crust. The alkali scoria is more K-rich than all other basalts.

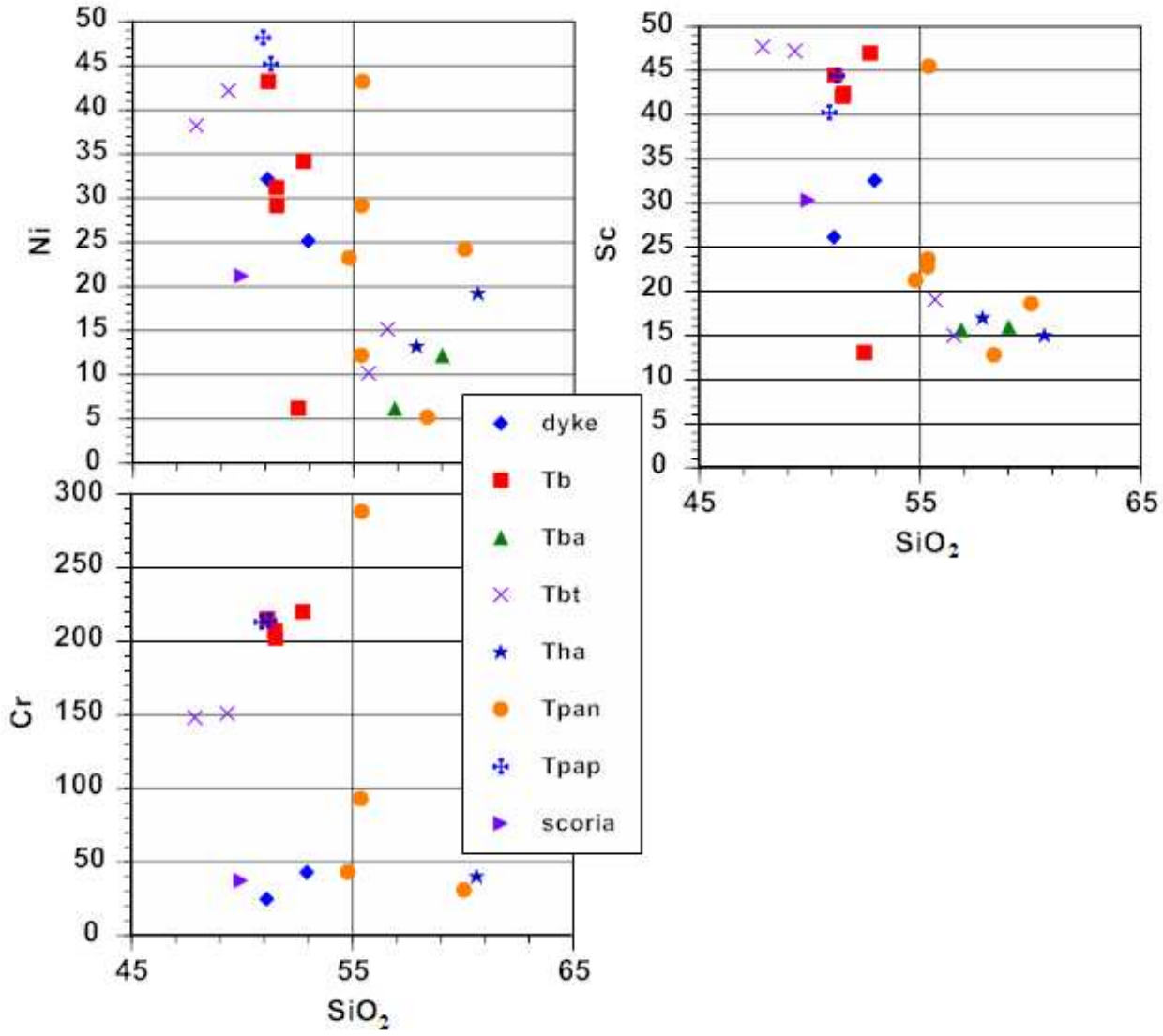

Figure 33: Compatible trace elements (ppm) versus silica showing fractionation patterns. The element Ni represents olivine, the element Cr represents Cr-spinel, and the element Sc represents clinopyroxene. Nickel levels decrease with increasing silica (basalt to andesite) and Sc levels decrease with increasing silica. Chromium levels are split into two different groups with the basalts forming a positive linear trend while the andesites and mafic dykes define a flat trend with lower relative abundances. Note: all lavas are low in compatible elements; therefore, fractionation of olivine, Cr-spinel & clinopyroxene should be present.

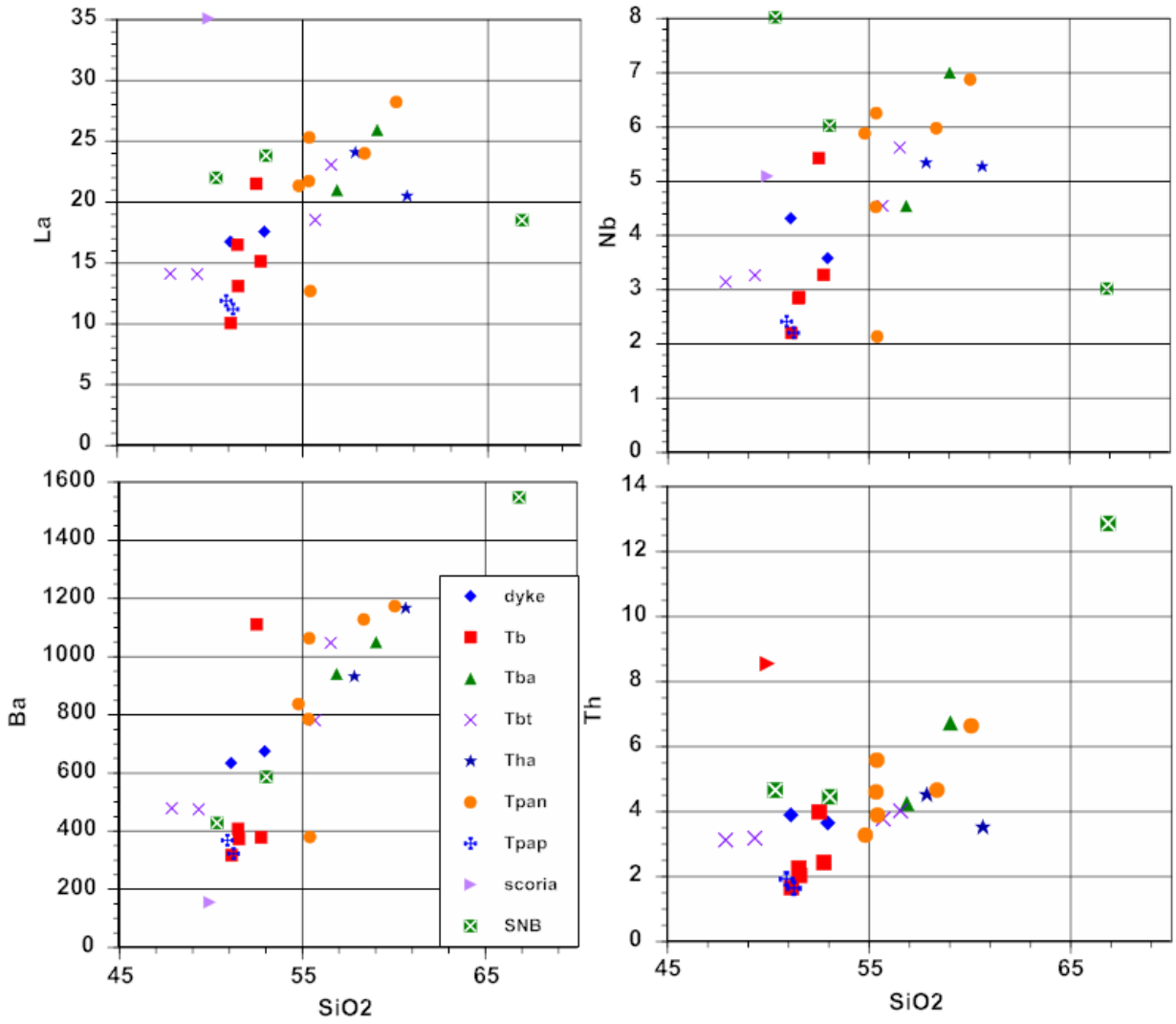

Figure 34: Incompatible trace elements (ppm) versus silica within the SVC. La levels increase in a positive linear trend versus silica (from basalt to andesite abundances increase 3x). Ba levels increase in a positive linear trend versus silica with the basalts somewhat shifted relative to the andesites and mafic dykes (from basalt to andesite abundances increase 3x). Nb levels increase in a positive linear trend versus silica (from basalt to andesite abundances increase 2-3x). Thorium levels increase in a positive linear trend versus silica and represents crustal assimilation levels (from basalt to andesite abundances increase 3x). All the elements in the samples are behaving the same from basalt to andesite except for the scoria. The scoria could therefore be part of a different parental magma and/or fractionation history.

Figure 35: Primitive Mantle Normalized Trace element data of the SVC map units. A; Tbt, B:Tpan, C: Tpap, D: Tba, E: Tha, F: dyke, G: Tb. All plots are use the normalizing factors of Sun & McDonough (1986).

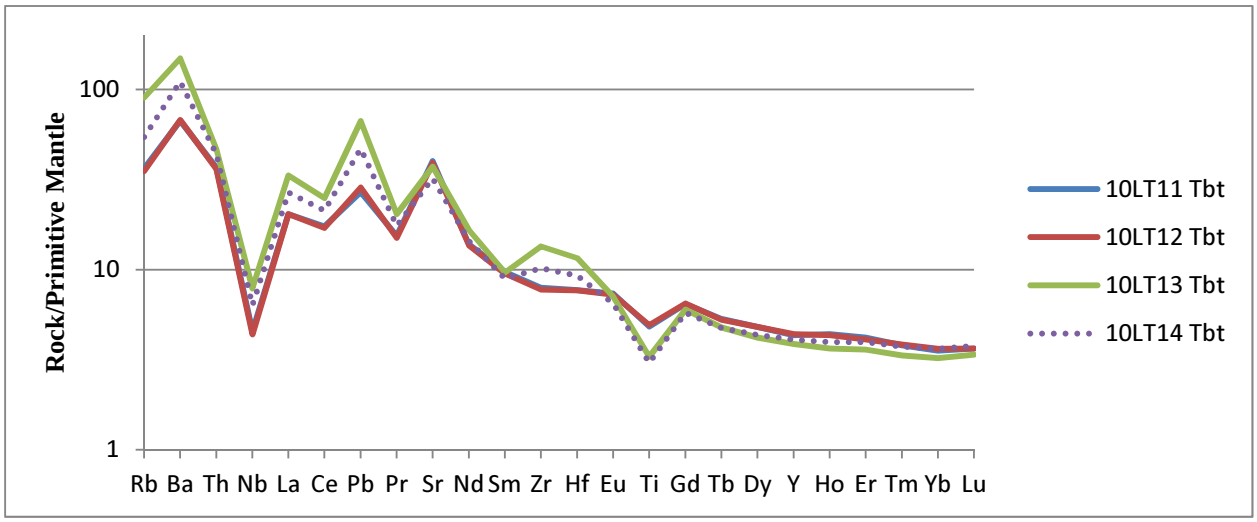

35A: Primitive Mantle Normalized incompatible element diagram of Tbt map unit samples (normalized in ppm). Samples 10LT14 and 10LT13 (andesite-rich clasts) follow a trend similar to SVC andesite trends (Zr, Hf enriched) while the lower units 10LT11 and 10LT12 follow a more SVC basaltic trend (Zr, Hf depleted).

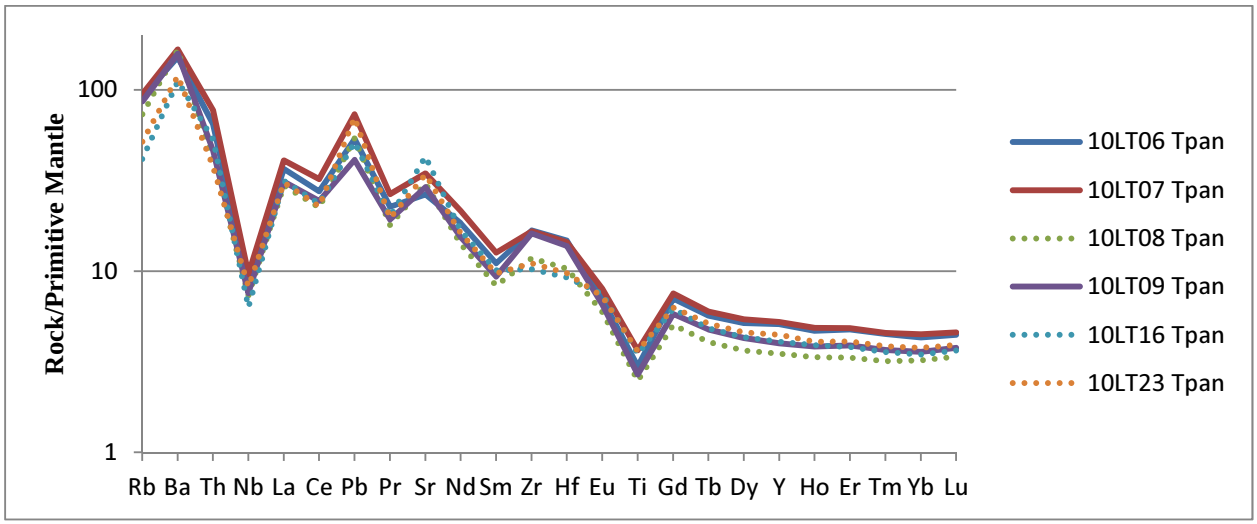

35B: Primitive Mantle Normalized incompatible element diagram of Tpan map unit samples. Dotted lines are basaltic-andesites, solid lines are andesites. The Tpan samples can be split by SiO_2 content in that the andesite and basaltic andesite units are distinguishable namely by the relative enrichment of Zr and Hf. Samples 10LT06 and 10LT09 plot as andesites in the total alkali silica plot and they have higher relative abundances of Zr and Hf than the samples that plot as basaltic andesites. Sample 10LT07 is the exception to this pattern and overlaps 10LT06 and 10LT09.

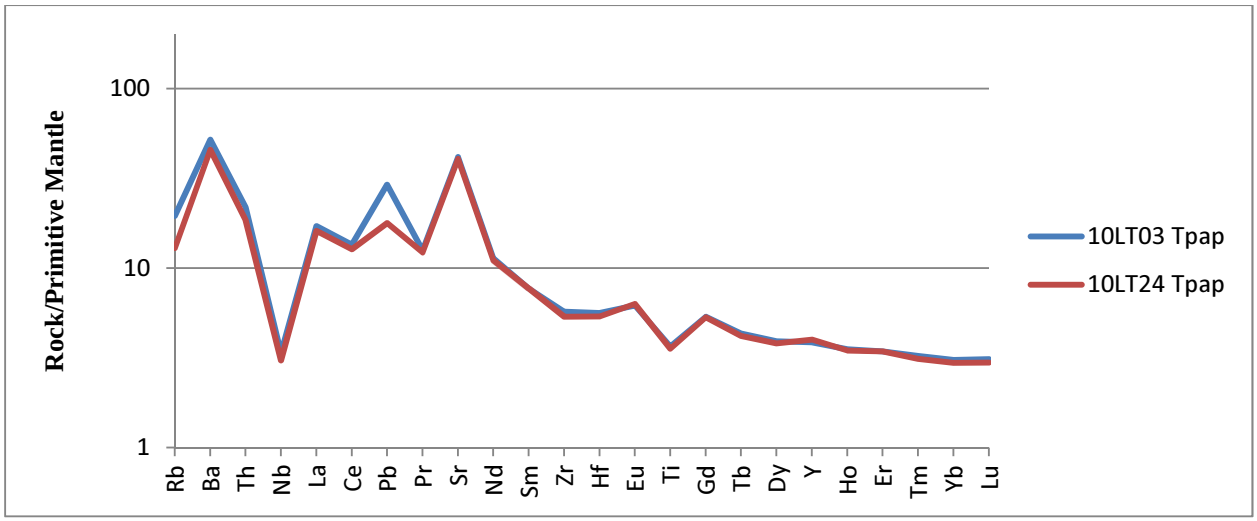

35C: Primitive Mantle Normalized incompatible element diagram of Tpap map unit samples. Tpap samples have trace element abundances more similar to Tb (basalt) samples than any other andesitic map unit in the SVC. Tpap has depletions of Zr and Hf and Sr is relatively more enriched that Pb. Similarly Rb and Ba abundances are smaller than other andesite units which are >100; Tpap's relative Rb and Ba abundances are more similar to Tb samples.

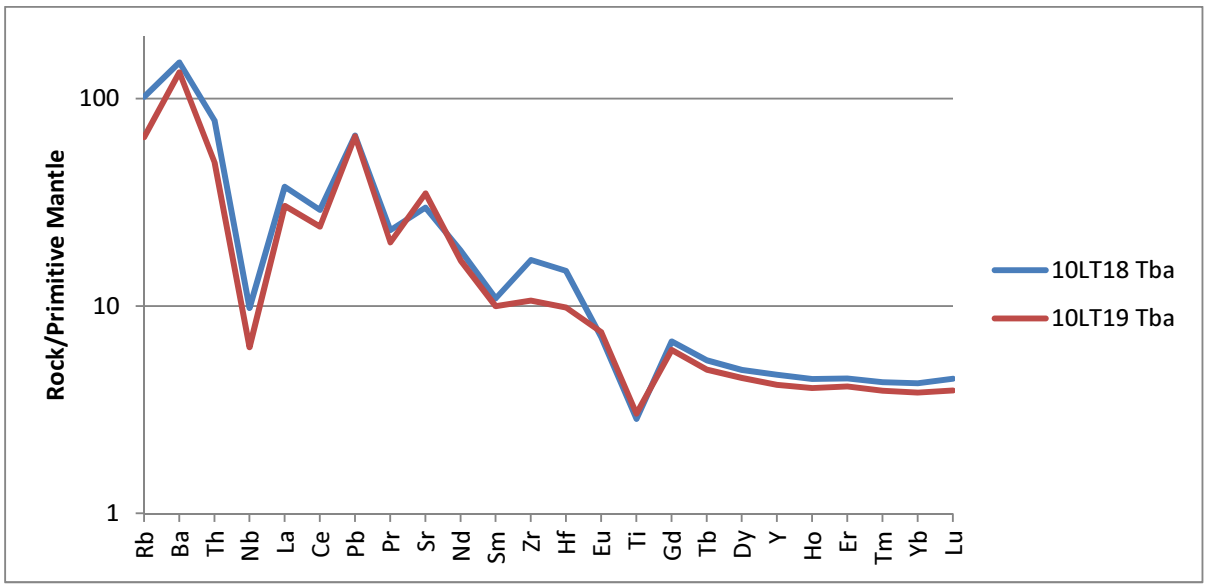

35D: Primitive Mantle Normalized incompatible element diagram of Tba map unit samples (normalized in ppm). The Tba samples have markedly different relative enrichments of Zr and Hf and both plot as andesites not basaltic andesites. The relative difference in Zr and Hf enrichment could be a function of silica content, since 10LT19 has lower SiO_2. The high Zr and Hf abundances in 10LT18 are similar to andesite samples.

35E: Primitive Mantle Normalized incompatible element diagram of Tha map unit samples. The Tha samples overlap each other relatively well and they are part of the andesite field in the total alkali silica plot showing relative enrichments of Zr and Hf and greater relative abundances of Pb over Sr.

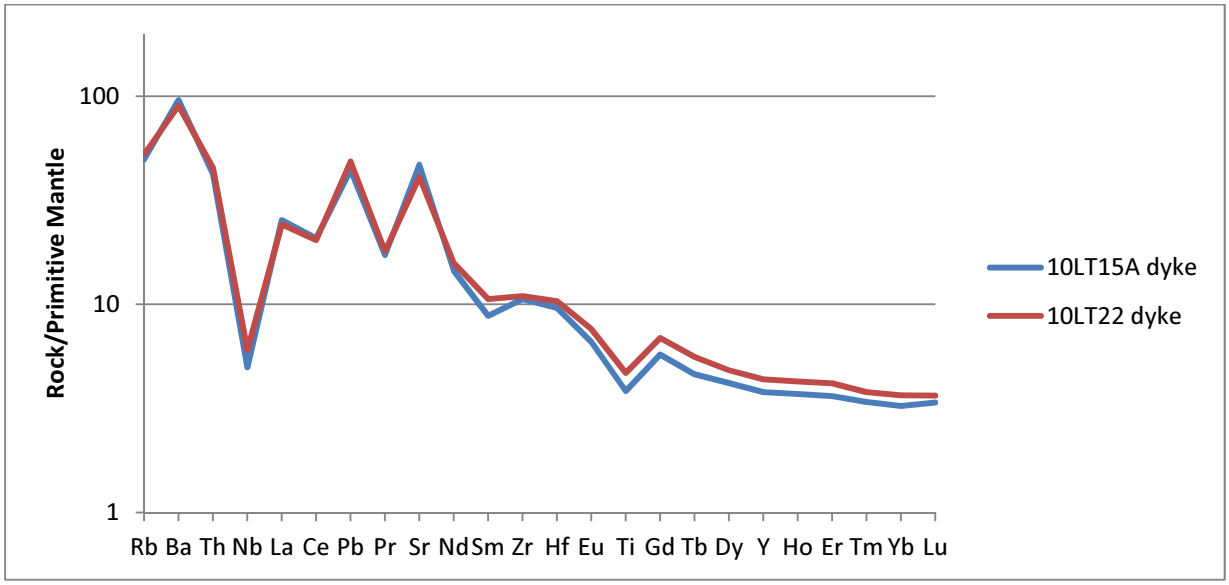

35F: Primitive Mantle Normalized incompatible element diagram of dyke samples. The dykes while plotting more closely to the basaltic field in the total alkali silica plot leading one to assume a strong basaltic character in the trace element patterns. This is not the case. There appears to be a strong hybridization of basaltic and andesitic characteristics. Namely Rb and Ba relative abundances are low (similar to SVC basalts) and Zr and Hf relative abundances are enriched relative to the adjacent REE (similar to SVC andesites) but Pb and Sr relative abundances almost even.

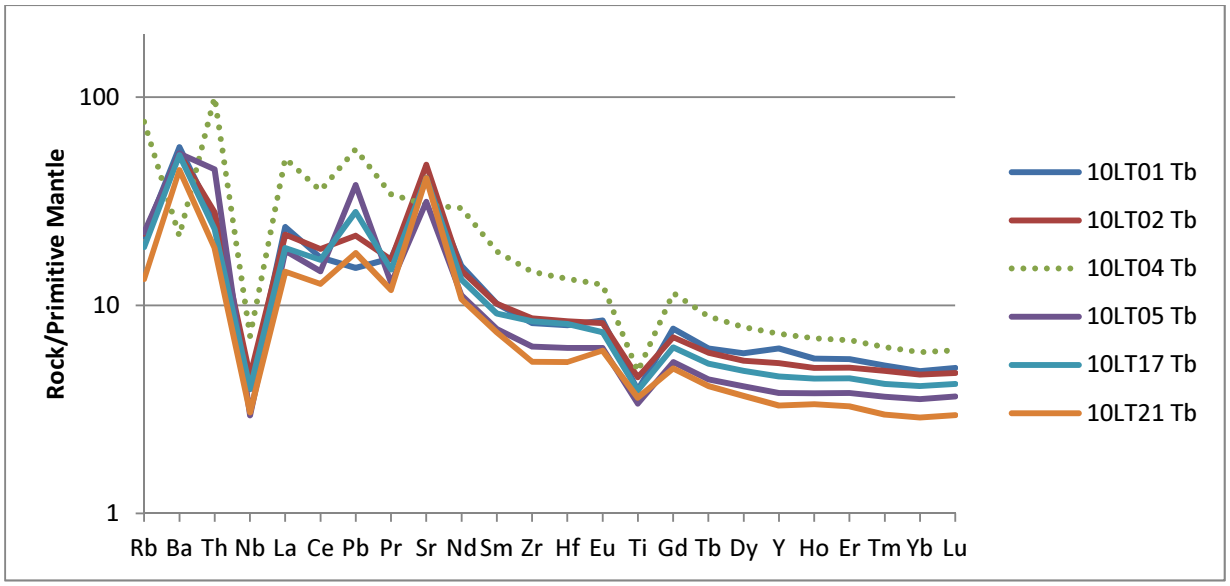

35G: Primitive Mantle Normalized incompatible element diagram of Tb map unit samples. The Tb trace element patterns are the least uniform of the SVC samples with relative abundances varying to a good degree but relative enrichments and depletions remain generally the same (except for 10LT04 - the scoria). Samples are generally enriched in Rb and Ba (but have lower relative abundances compared to SVC andesites), Sr is relatively more abundant than Pb and Zr and Hf are depleted relative to the middle REE. The sample 10LT04 is a scoria and bears no resemblance to the other SVC samples both basaltic and andesitic.

Figure 36: Isotope Plots of SVC map units. A: $^{143}Nd/^{144}Nd$ versus $^{87}Sr/^{86}Sr$, B: $^{208}Pb/^{204}Pb$ versus $^{207}Pb/^{204}Pb$, C: $^{206}Pb/^{204}Pb$ versus $^{207}Pb/^{204}Pb$, D: εSr versus εNd

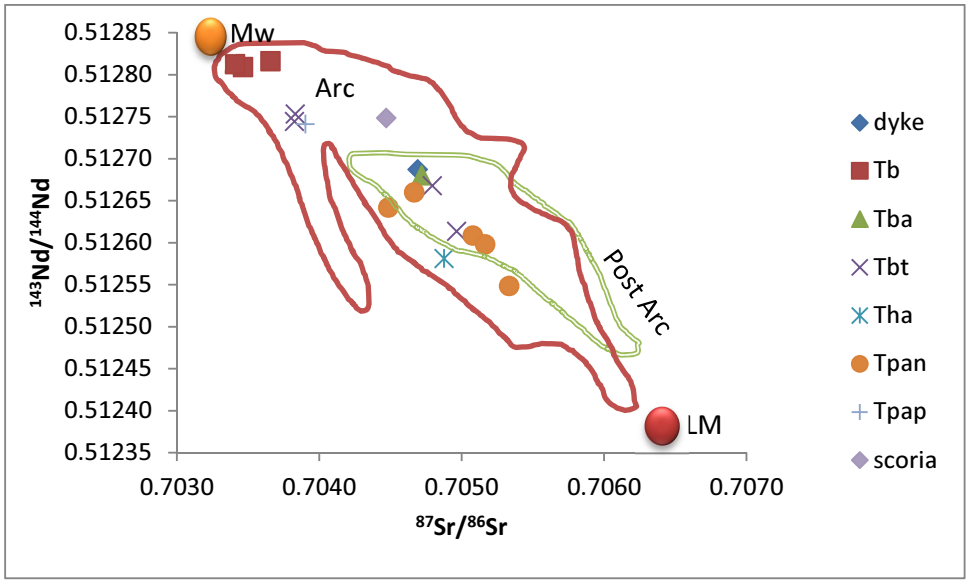

36A: $^{143}Nd/^{144}Nd$ versus $^{87}Sr/^{86}Sr$ plot of SVC samples. The solid (Arc) line denotes the extent of previous Ancestral Cascades Arc chemical analyses (compiled in Cousens et al., 2008). The double line denotes post-arc chemical analyses (compiled in Cousens et al., 2011). The SVC samples follow a relatively linear trend that potentially denotes a two-part mixing line between a lithospheric end-member (LM) and a mantle wedge end-member (Mw) similar to that of Cousens et al. (2008).

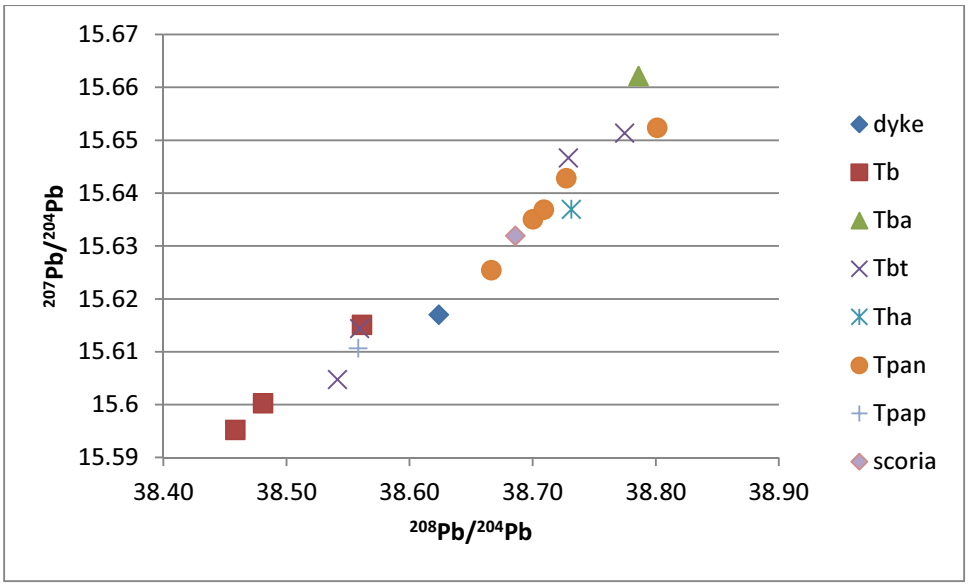

36B: $^{208}Pb/^{204}Pb$ versus $^{207}Pb/^{204}Pb$ plot of SVC samples. The SVC samples define a strong linear trend moving from basaltic samples to more andesitic samples.

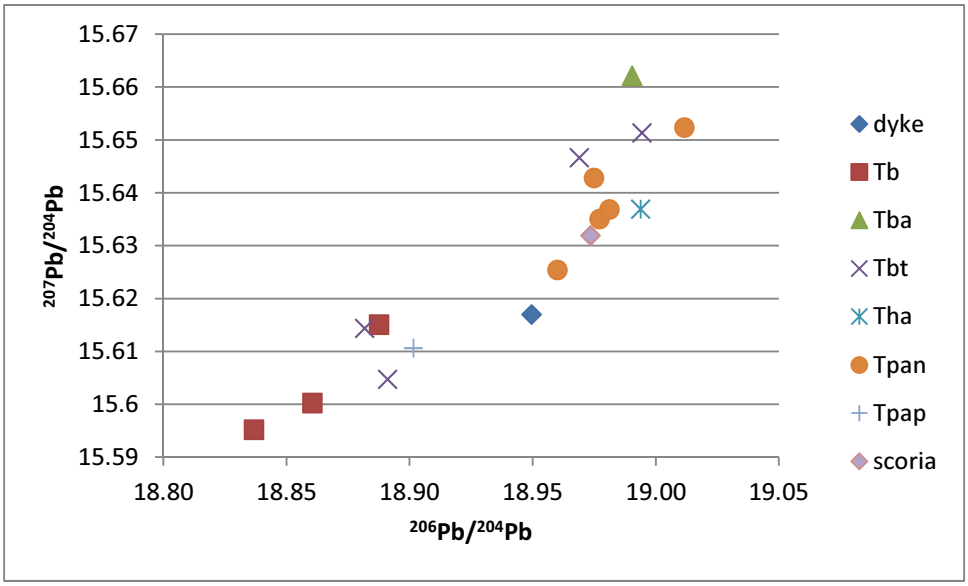

36C: $^{206}Pb/^{204}Pb$ versus $^{207}Pb/^{204}Pb$ of SVC samples. The SVC samples define a relatively linear relationship but there is a distinct separation between basaltic and andesitic samples.

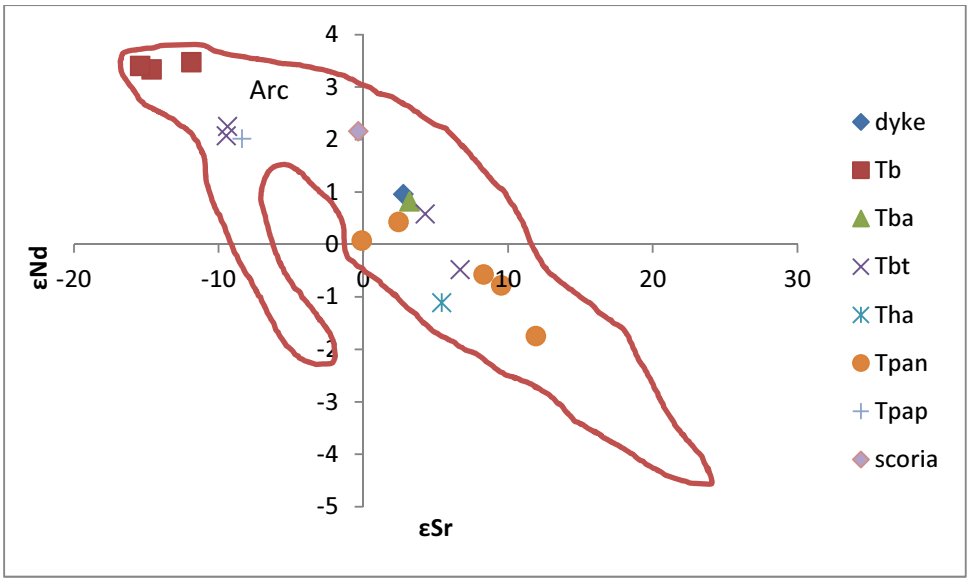

36D: εSr versus εNd of SVC samples. The solid (Arc) line denotes the extent of previous Ancestral Cascades Arc chemical analyses (compiled in Cousens et al., 2008). The basaltic samples fall within the depleted mantle/OIB field while the Tha andesites and Tpan basaltic-andesites fall within the enriched crustal field, the Tpan andesites and Tba andesites occupy the transition zone between depleted mantle and enriched crust.

Figure 37: Parent/daughter isotope relationships of SVC samples. A: Rb/Sr_{pmn} versus $^{87}Sr/^{86}Sr$, B: Sm/Nd_{pmn} versus $^{143}Nd/^{144}Nd$

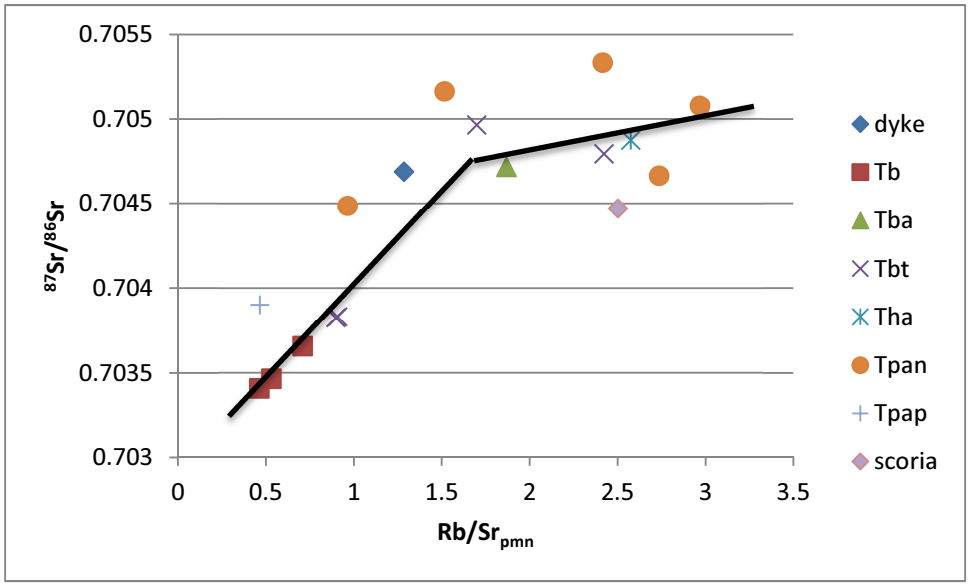

37A: Rb/Sr_{pmn} versus $^{87}Sr/^{86}Sr$ of SVC samples showing the relative relationship of parent/daughter isotopes. The basaltic samples define a positive linear trend but the andesite samples follow sub-horizontal a trend.

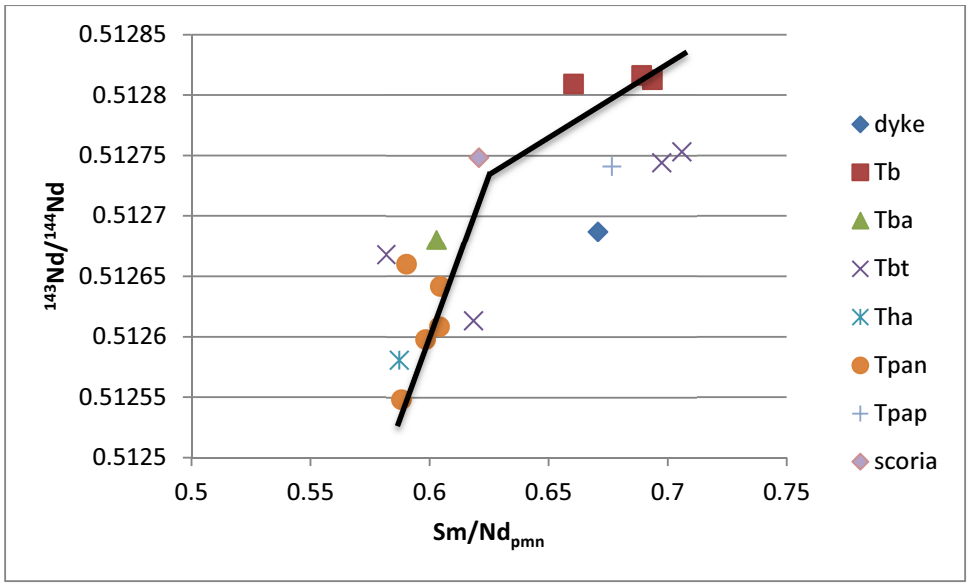

37B: Sm/Nd_{pmn} versus $^{143}Nd/^{144}Nd$ SVC samples showing the relative relationship of parent/daughter isotopes. The samples define a nonlinear trend and there is a distinct separation between basalts and andesites.

4. Discussion

4.1 Development of the Sagehen Volcanic Centre

The development of the SVC will entail us to move from the bottom to the top of the system. We shall first classify the source/type of melt, second define the lava-type (parental magma), third determine if crustal components (contamination) is present and fourth define the rock samples based on their petrography and geochemistry and attempt to define a physical model for the emplacement of our samples (i.e. type of volcanic setting).

4.1.1 Basaltic Sources of Melt

Let us first evaluate the possible source of partial melts that could potentially generate the basalts observed in the SVC. Given the young ^{40}Ar-^{39}Ar age dates of the andesite and basalt, a Cascade-type source for mafic arc lavas should be the primary cause for the basalt's characteristics. This is primarily because of the association with subduction of the southern Juan de Fuca plate beneath the continental margin during the Miocene–Pliocene which is equivalent to the modern south Cascades. However, the relative enrichment in incompatible elements (Ba, Th, Sr, Pb) and the distinctive Sr and Nd isotopic compositions compared to modern south Cascade arc lavas do not support this. Several other possibilities for a lava source have been proposed with regard to the ACA:

(1) Ancient enriched domains in the subcontinental lithospheric mantle beneath the Western Great Basin of the eastern Sierra Nevada and east of the modern Cascade arc (Cousens, 1996; Omerod et al., 1991).

(2) Enriched intraplate mantle sources, commonly interpreted to be small to medium degree melts of enriched components (blobs, veins) in the asthenospheric upper mantle or lowermost lithospheric mantle. Examples include the Mojave Desert and central Basin and Range of

Western and offshore California, and in the arc and back-arc of the modern Cascades (Dickinson, 1997; Laventhal et al., 1995).

(3) A mantle plume, such as the Columbia River–Yellowstone hotspot (Garrison et al., 2008; Graham et al., 2009).

(4) Subduction modified (fluid) spinel peridotites of the mantle wedge (Leeman et al., 2005; Reiners et al., 2000; Righter et al., 2000).

4.1.2.1 Option 1: Western Great Basin enriched lithospheric melts

The Western Great Basin (WGB) to the south of the study area could potentially account for the differences in the $^{143}Nd/^{144}Nd$ versus $^{87}Sr/^{86}Sr$ plot between modern Cascade and SVC basalts. WGB basalts are associated with late Proterozoic and younger lithosphere west of the 0.706 Sr isotope line and approach $^{87}Sr/^{86}Sr$ isotopic compositions similar to many ocean island basalts (Reid & Ramos et al., 1996). The WGB also has a distinctive mantle source composition thought to be the result of partial melting of the Sierra Nevada subcontinental lithospheric mantle (Omerod et al., 1991). This lithospheric mantle was metasomatized by earlier subduction episodes beneath the western margin of the south-western U.S. (Omerod et al., 1991). This means WGB incompatible element patterns include subduction signatures. However, due to the great age of enrichment, WGB mantle sources have much lower $^{143}Nd/^{144}Nd$ and much higher $^{87}Sr/^{86}Sr$ than modern south Cascades and SVC lavas. If enriched lithospheric melts were the source magma for the SVC they would have to undergo severe depletion of isotopic ^{87}Sr which is unlikely since you cannot fractionate radiogenic isotopes (Figure 38; Cousens et al., 1996). Furthermore, the subalkaline composition of SVC samples, the abundance of highly porphyritic volcanic rocks typical of continental arcs, and the evidence for larger volcanic edifices with

dome collapse and debris flow deposits such as the Tbt map unit indicate that the SVC does not conform to WGB magmatic or geological characteristics (Menzies et al., 1983; Omerod et al., 1991).

4.1.2.2 Option 2: Intraplate Magmas

The basaltic units (Tb, Tpap) display characteristics that suggest they were stalled at depth as part of an intraplate magma. The characteristics that led us to initially suspect this was the presence of sieve textures (which are a disequilibrium texture) in both units, and the abundant pyroxene phenocrysts in the Tpap unit. Basalts erupted in intraplate settings are enriched in most incompatible elements and LILE; they do not have a Nb-Ta anomaly and have a REE pattern decreasing from light to heavy when compared with primitive mantle (Pearce, 1983; Schmidt et al., 2008). The SVC basalts display a Nb-Ta anomaly but their incompatible element patterns are not similar to Mojave basalts. Isotopic values of εNd for SVC basalt samples are +3.5 to +2 with εSr values ranging -15.5 to -8.5; these values fall under the OIB field/depleted mantle field of Farmer & DePaolo (1983) and could suggest 'OIB-like sources' (Figure 36). However, the Mojave basalts plot higher (high Nd and low Sr isotope ratios) than SVC samples in $^{143}Nd/^{144}Nd$ versus $^{87}Sr/^{86}Sr$ plot (Farmer et al., 1995) indicating that the Mojave basalts are not isotopically similar to Miocene–Pliocene basalts from the SVC region (Figure 38). This therefore makes an intraplate (Mojave Desert) source incredibly unlikely for the SVC basalts.

4.1.2.3 Option 3: Hotspot

The Lovejoy basalts of eastern California have been proposed to represent an off-shoot of the Miocene Columbia River basalts and therefore the Yellowstone hotspot provides a potential source of hotspot magmatism under the Sierran Cascades (Garrison et al., 2008). The Lovejoy basalts have higher HREE abundances compared to all SVC samples, ACA basalts from the

Tahoe-Reno region and modern Cascade calc-alkaline basalts, and thus do not correspond to Lovejoy basalts. Isotopically, $^{87}Sr/^{86}Sr$ versus Sr/P_{pmn} (Figure 39) plots Lovejoy basalts well outside the field of South Cascades basalts where SVC basalts plot. Furthermore, Lovejoy basalts plot higher (high Nd and low Sr isotope ratios) than SVC samples in $^{143}Nd/^{144}Nd$ versus $^{87}Sr/^{86}Sr$ scatter plots indicating that the Lovejoy basalts are not an isotopically enriched component in Miocene–Pliocene basalts from the SVC region (Figure 38). Therefore we cannot conclude that hotspot magmatism, such as the Columbia River event, was a primary source for SVC lavas.

4.1.2.4 Option 4: Subduction (Fluid) Modified Spinel Peridotites

From previous studies fluid metasomatized peridotites of the mantle wedge have been proposed to be the main sources of Cascades melts such as those at Lassen (Clynne, 1990), Sceptor Creek (e.g. Western Cascades; Ducea & Saleeby, 1998) and in the Ancestral Cascades Arc (Cousens et al., 2008).

Borg et al., (1997, 2002) showed that Lassen region calc-alkaline basalts can be defined by the degree of Sr enrichment over incompatible elements. Sr/P_{pmn} can be used in place of LILE/LREEs to show the relative enrichment of Sr over middle REE in arc rocks which is due to Sr addition via fluids from the subducting slab (Borg et al., 1997). Variations in Sr and P are not simply due to fractional crystallization of plagioclase and apatite which can be seen by the lack of Eu anomalies and the relative constant abundances of P_2O_5 in SVC samples. In the Tahoe-Reno region, Miocene-Pliocene basalts cover the same range of Sr/P_{pmn} as the south Cascades, but at much higher $^{87}Sr/^{86}Sr$ values. None of the lavas have MORB-like Sr isotopic compositions, although they trend toward the same low $^{87}Sr/^{86}Sr$ ratios (~0.7030) at the high Sr/P_{pmn} end of the south Cascade field (Borg et al., 1997). Borg et al., (1997) infers that this trend

indicates a source from late Phanerozoic lithospheric mantle (low Sr/P) and mantle wedge (high Sr/P); basaltic samples that plot within the WGB field are inferred to de derived from a 1 Ga lithospheric mantle (Fig 36). However, the conclusions reached by Borg et al. (2002) for the Lassen area also apply to the Tahoe-Reno lavas: the high $^{87}Sr/^{86}Sr$, low Sr/P component is not a fluid component, and must either be an enriched component in the mantle wedge or a lithospheric mantle component. In the case of Lassen this is inferred to be a mantle wedge peridotite. The basaltic samples of the SVC overlie the Southern Cascades range of $^{87}Sr/^{86}Sr$ versus Sr/P_{pmn} and do not intersect the OIB-like mantle component of the Mojave Desert (Figure 39). High Sr isotopic ratios are characteristic of granites in the southern Sierra Nevada and are not thought to be a product of two-component mixing of melt in the basalts; the batholiths themselves are thought to have lithospheric mantle melts as one of their source (Farmer & DePaolo, 1983).

A study of He isotopes of basalts from the Newberry volcano (a back-arc volcano in the Modern Cascades Figure 2) in Graham et al. (2009), have slightly lower $^{3}He/^{4}He$ (7.6 to 8.3 R_A ; R_A = ratio to asthenosphere), and overlap the range for basalts from the Cascades volcanic arc (7.0 to 8.4 R_A). Graham et al. (2009) argues that these results suggest that helium in the mantle source is dominated by shallow asthenospheric mantle, similar to the reservoir commonly interacting due to magmatism along mid-ocean ridges. Previous studies have shown that lavas from the Basin & Range province and adjacent areas in the south-western U.S. extend to low $^{3}He/^{4}He$ ratios, reflecting the involvement of Proterozoic continental lithosphere (Graham et al., 2009). This supports the argument that the basalts were generated through asthenospheric upwelling.

Plots based on Drummond and Defant (1990) which looked at mafic crustal melts, using $La/Yb_{chondrite}$ vs. $Yb_{chondrite}$, $Sr/Y_{chondrite}$ vs. $Y_{chondrite}$, and Sr/Y_{pmn} vs. SiO_2 for SVC lavas show that the basalts do not have a eclogitic or pure amphibolite character (Figure 40a, b, c;). The plots indicate that the source melt was not from the garnet stability field but was instead from a 75-85 km hydrous spinel source (Drummond & Defant, 1990). Amphibolitic melts can only produce dacite, not basalt. A plot of Tb/Yb_{pmn} vs. Ce/Sm_{pmn} also shows that the SVC plots well within the spinel stability field (Figure 41). Likewise, middle to heavy REE patterns do not show a steep garnet stability field pattern but a curved concave-up hydrous amphibole-spinel stability field pattern which does not conform to intraplate patterns. Finally, Cr abundances within the basalts suggests that a spinel peridotite is the likely source of partial melts given the highly compatible nature of Cr and similarly because we have established garnet phases are not present. In summary, the likely source of partial melts that generated the basaltic samples in the SVC was likely derived from a subduction modified spinel peridotite.

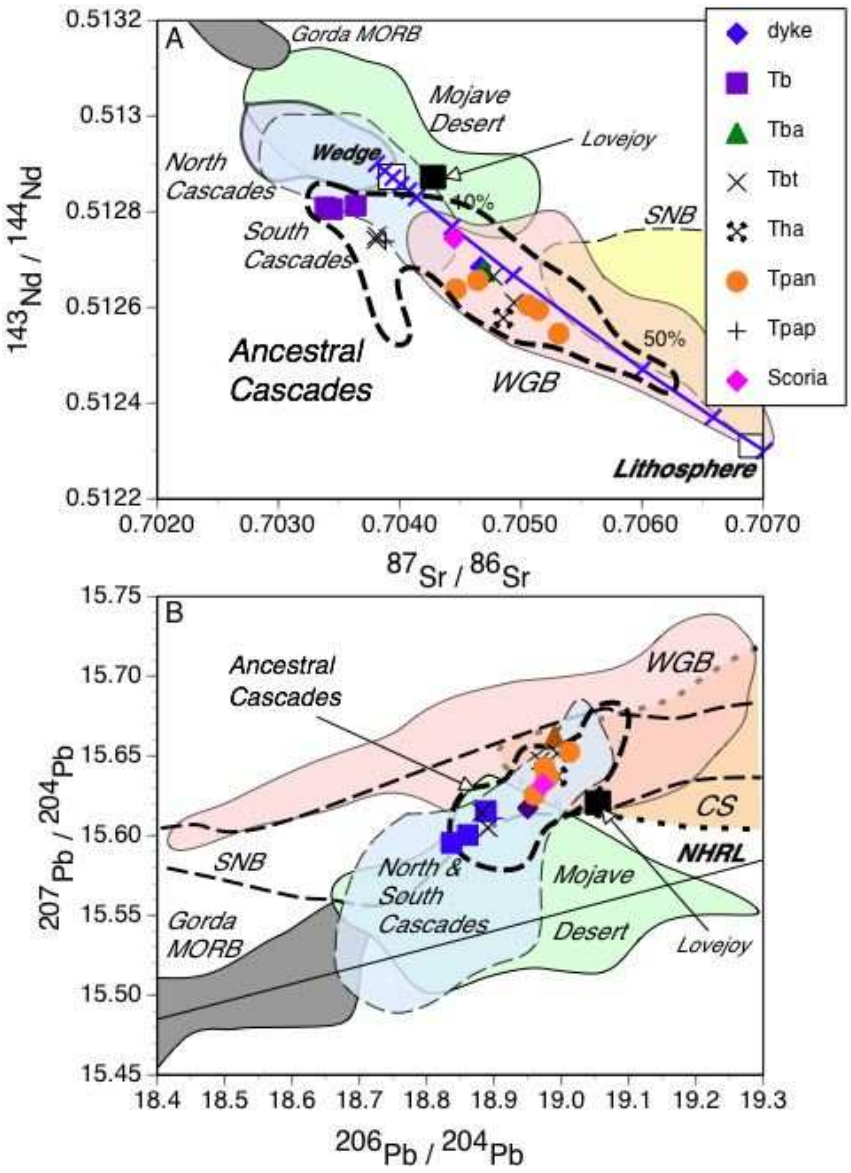

Figure 38 A: Modified from Cousens et al., (2008). Sr versus Nd isotope plot showing the relationship of SVC map units and Hetch Hetchy SNB granitoids (Barbarin et. al., 1989) to surrounding volcanic fields. Mixing curve is for melts of lithosphere (Sr =1200 ppm, Nd = 38 ppm, $^{87}Sr/^{86}Sr$ = 0.7070, $^{143}Nd/^{144}Nd$ = 0.5123) and melts of mantle wedge (Sr = 550 ppm, Nd = 15 ppm, $^{87}Sr/^{86}Sr$ = 0.7038, $^{143}Nd/^{144}Nd$ = 0.5129) with tick marks showing percentage of lithospheric melt in the mix (modified from Yogodzinski et al., 1996). B: Modified from Cousens et al., (2008). A Pb-Pb plot with corresponding fields and data points to (A). NHRL= Northern Hemisphere Reference Line for MORB and oceanic island basalt (Hart, 1984).

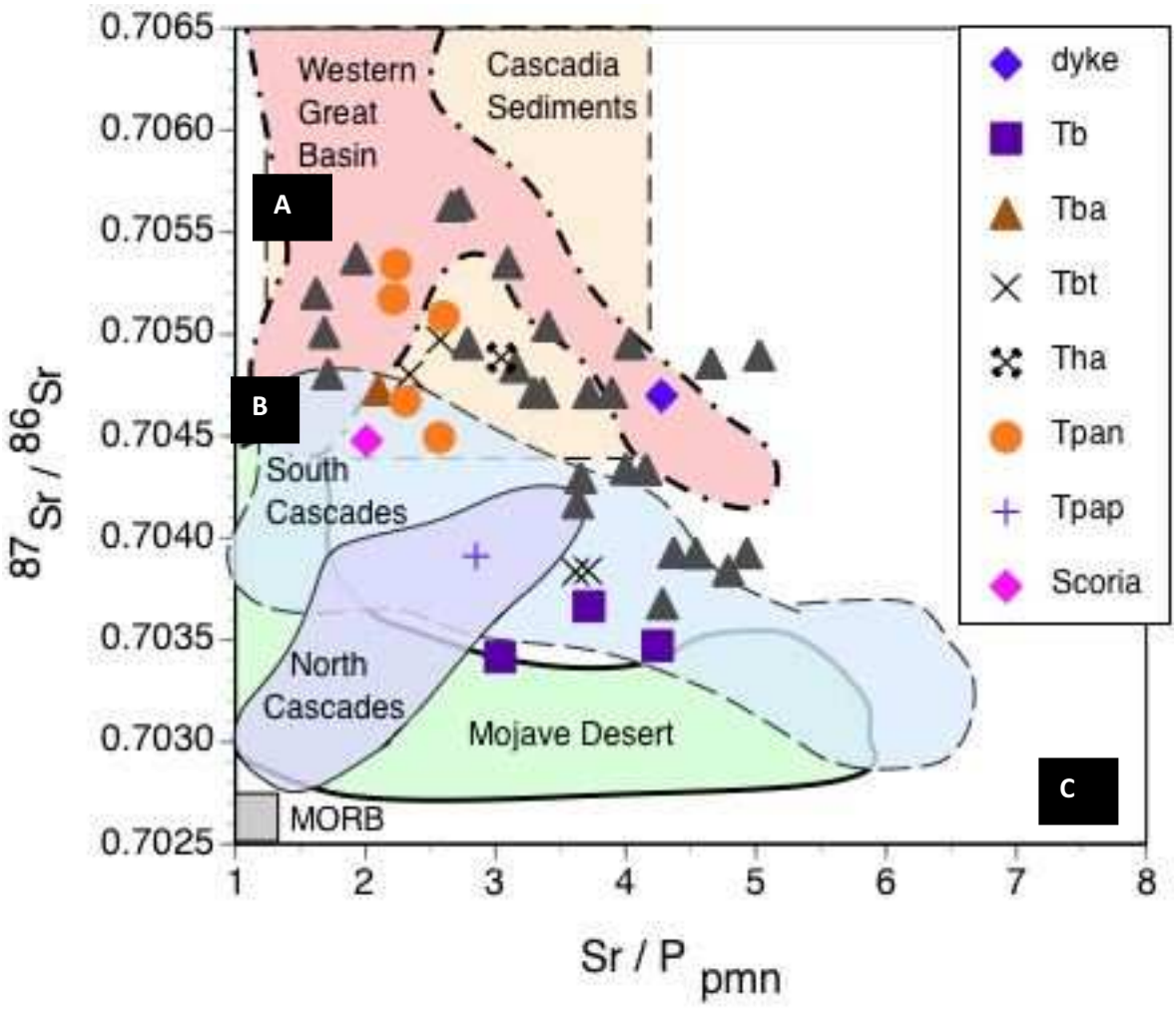

Figure 39: Primitive mantle normalized plot of Sr/P versus $^{87}Sr/^{86}Sr$ of SVC samples; black triangles represent samples from Cousens et al., (2008). Block A represents Precambrian lithospheric mantle, block B represents Phanerozoic? Mantle and block C represents mantle wedge. The basalt samples plot well within the South Cascades Field which suggests a strong mantle wedge fluid component in the basalts. The andesites overlap with the Western Great Basin which has been inferred to have been derived from older "Proterozoic" slab melts but could also be the result of crustal contamination.

4.1.2 Classification of Lava Type

From evaluating the potential sources of basaltic lavas we can begin deduce what the main lava type is within the SVC. From our literature review we know that there are three main lava types within the Cascades: HAOT lavas, intraplate lavas and calc-alkaline lavas. Intraplate lavas have been discussed in section 4.1.2.2 so we will summarise our conclusions that they do

not play a part in the SVC. Because of lower Nd isotopic ratios and a presence of a Nb-Ta anomaly the SVC does not have the necessary characteristics to be a intraplate lava. Next let us evaluate HAOT lavas as the potential primary lava for the SVC and again we can clearly see this is not the case primarily because HAOTs are tholeiites and are Low-K. This leaves us with Calc-alkaline lavas our primary lava end-member. The TAS diagram indicates that the majority of SVC samples are sub-alkaline, while the AFM diagram shows a strong calc-alkaline trend and the K_2O versus SiO_2 diagram shows our samples plot as Med-K (i.e. calc-alkaline). Likewise ratios of Ba/TiO_2 (200-700), Ba/Nb (20-100) and Sr/Y (20-100) are similar to the calc-alkalic group described by Leeman et al., (2005). Furthermore, the petrographic evidence of thick (100 µm) recrystallized amphibole (hornblende) rims in the SVC samples indicates that lavas ascended from an approximately 8 km –deep magma reservoir and that the melt was hydrous as well (Rutherford & Hill, 1983).

4.1.3 Evidence of Crustal Contamination

There are two kinds of crustal interaction that can lead to the crustal contamination of a melt: the assimilation of upper crustal granitoids or interactions with lower mafic crust. The presence of oscillatory zoning in the plagioclase and pyroxene is an indication of “non-equilibrium" crystallization and was likely triggered by magma mixing within the system. First, let us assess the possibility of upper crustal contamination. Mio-Pliocene volcanic rocks of the Ancestral Cascades arc commonly include fragments of Sierra Nevada granitoids (Cousens et al., 2008). In order to test SVC samples for upper crust contamination from Sierran granitoids, the geochemical study of Barbarin et al. (1989) was used. The Barbarin et al. (1989) study includes Sierra Nevada Batholith granitoid samples that are located near the SVC (Hetch Hetchy). Ni and

Cr abundances of SVC lavas were tested for granitoid assimilation. The SVC samples do not fall on a mixing array between high magnesium number (Mg#, Figure 42) compositions and the granitoids, as might be expected in the case of granitoid assimilation but they do cover the same range as the andesitic material (Figure 43a, b, Figure 44). Sierran granitoids are generally enriched in Th (>10 ppm) and Rb (>100 ppm) and depleted in Zr (<150 ppm), Hf (<4 ppm) and Ba (<1500 ppm) (Barbarin et al, 1989, Kistler et al., 1986). Within the SVC, the andesitic samples have Zr and Hf patterns that are flat or enriched and Ba is enriched relative to adjacent REEs (Figure 35) suggesting there was no end-member interaction since if there was an interaction we would see depletions of Zr and Hf. Furthermore, the Barbarin et al. (1989) samples are depleted in Pr, Sm and Tm relative to adjacent REEs while the SVC samples have no depletion of Pr, Sm and Tm relative to adjacent REE. If there was interaction from between the granitoids and SVC there should be comparable REE patterns which there are none. However, there is a linear correlation between incompatible elements, isotope ratios, and SiO_2 content for a majority of SVC samples with the only exception being the basalts (minus the scoria). Ratios of Ba/La and La/Nb are also high in SVC samples; depletions of HFSE are characteristic of volcanic arcs and continental crust (Reid & Ramos, 1996).

The proposed isotopic mixing line of Cousens et al., (2008; Figure 38 & Figure 44) defines a line for melts of lithospheric mantle (Sr = 1200 ppm, Nd = 38 ppm, $^{87}Sr/^{86}Sr = 0.7070$, $^{143}Nd/^{144}Nd = 0.5123$) and melts of mantle wedge (Sr = 550 ppm, Nd = 15 ppm, $^{87}Sr/^{86}Sr = 0.7038$, $^{143}Nd/^{144}Nd = 0.5129$) with tick marks showing percentage of lithospheric melt in the mix. The mixing line suggests the addition of a lithospheric end-member into a mantle melt. The SVC and the Barbarin et al., (1988) samples partially conform to this line with the only exception being the basalt units and that the andesite $^{143}Nd/^{144}Nd$ values are generally lower than

Cousens et al., (2008) samples but still follow the trend. Using the isotopic analyses of SNB granitoids sampled near the Tahoe-Truckee area and plotting them with SVC samples, a two component mixing line is observed (Hetch Hetchy samples; Barbarin et al, 1989). When $^{143}Nd/^{144}Nd$ and $^{87}Sr/^{86}Sr$ initial values are calculated as εNd and εSr respectively using the methods of Farmer & DePaolo (1983) the relationship between the basalts and the andesites shows a two component mixing line is further revealed (Figure 36d). Also, Ar-Ar age dates from the SVC show that the basalts are the youngest unit even though they have the most depleted mantle compositions which suggests that while the andesitic magmas ascended through thick stacks of lithosphere (and thus adding isotopic Sr) the basalts did not. We conclude that upper crustal contamination from Sierra Nevada granitoids is a factor in the petrogenesis of SVC andesites.

Second, there is the possibility of crustal contamination from mafic lower crust of the Sierra Nevada batholith. In general, partial melting of mafic crust produces felsic melts resulting from the intrusion of hot mafic magmas (Beard and Lofgren, 1991; Drummond & Defant, 1990; Rapp and Watson, 1995). Felsic melts are generally enriched in the LILE and light REEs, and which have negative Nb and Ta anomalies if rutile is a residual phase; if melting occurs in the garnet stability field then REE patterns in the melt may be steep with high La/Yb and Sr/Y ratios and no Eu anomaly (Martin, 1986). Figure 40a & b demonstrates the variation of $La/Yb_{chondrite}$ with $Yb_{chondrite}$, $Sr/Y_{chondrite}$ vs. $Y_{chondrite}$, and Sr/Y_{pmn} with SiO_2 for SVC lavas, following diagrams from Drummond and Defant (1990) that are commonly used to identify melts of mafic crustal rocks. Plots of SVC samples correspond with existing Ancestral Cascades Arc (ACA) analyses. The $La/Yb_{chondrite}$ with $Yb_{chondrite}$ plot shows the basalts and andesites forming two

separate flat trends that stack on top of each other (Figure 40 b, c). The $La/Yb_{chondrite}$ with $Yb_{chondrite}$ plot should have a negative linear trend moving to a high La/Yb versus low Yb hypothetical dacitic end-member if there was contamination from the lower crust. The Sr/Y ratios do not increase with silica content in the felsic range of the SVC samples (i.e. the andesites), but instead decrease due to plagioclase fractionation which also indicates contamination is not present. In Cousens et al., (2011), the ACA is shown to be on the low end of the diagrams and so they too do not have the values necessary to conform to lower crustal contamination. The SVC does not conform to the Drummond and Defant (1990) plots. What the Drummond and Defant (1990) plots indicate with regards to the SVC samples is that they did not originate within the garnet stability field. We conclude that addition of felsic partial melts from the lower crust is not an important component in SVC lavas.

Figure 40: Plots of SVC map units based on Drummond & Defant, (1990). A: Chondrite normalized plot of Yb versus La/Yb, B: Chondrite normalized plot of Y versus Sr/Y, C: Chondrite normalized plot of Y versus SiO_2.

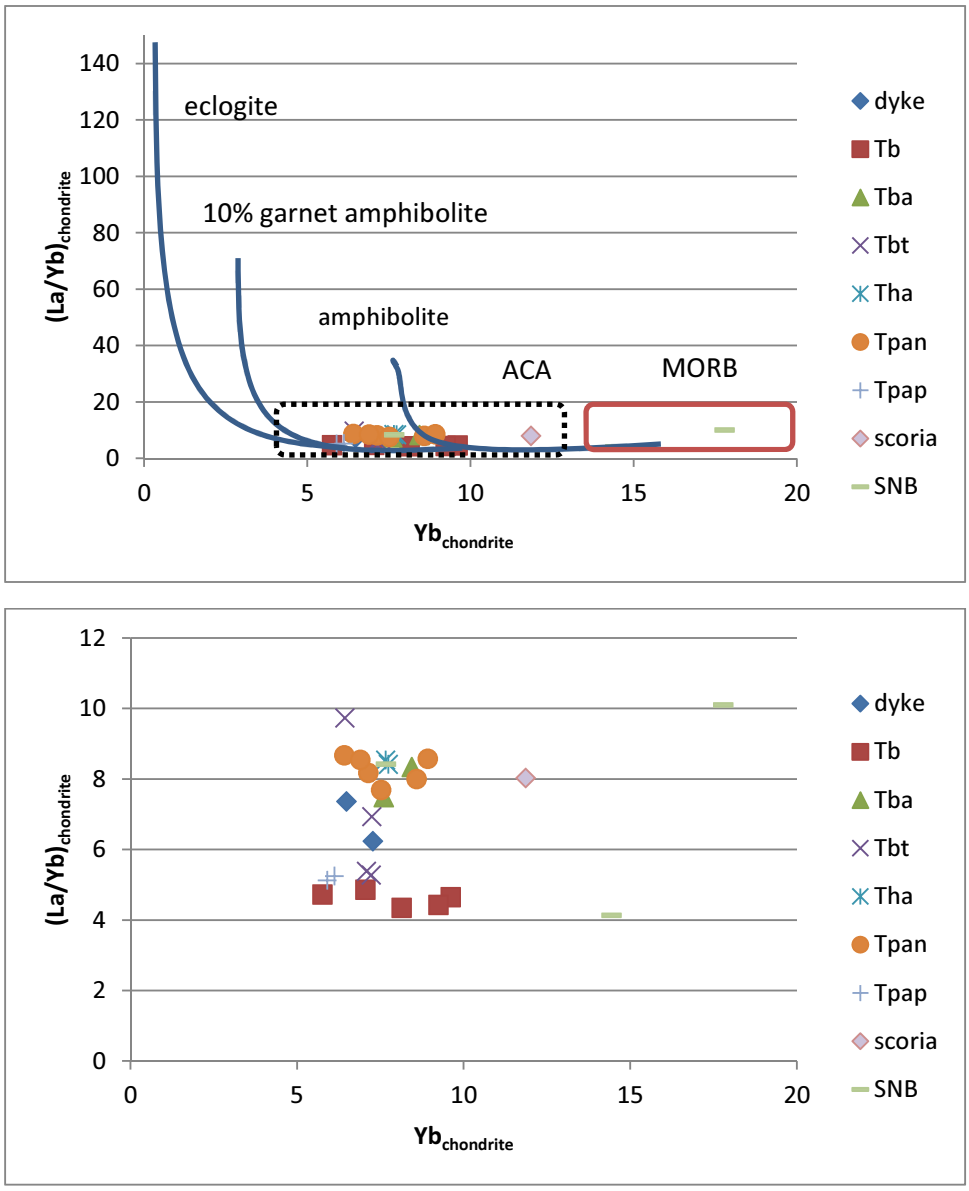

40A: Chondrite normalized plot of Yb versus La/Yb from Drummond & Defant (1990). The SVC samples plot near the amphibolite fractionation curve as does the SNB samples from Hetch Hetchy (Barbarin et al., 1989). The trend of the samples is flat indicating they are not mixing with a hypothetical dacitic end-member.

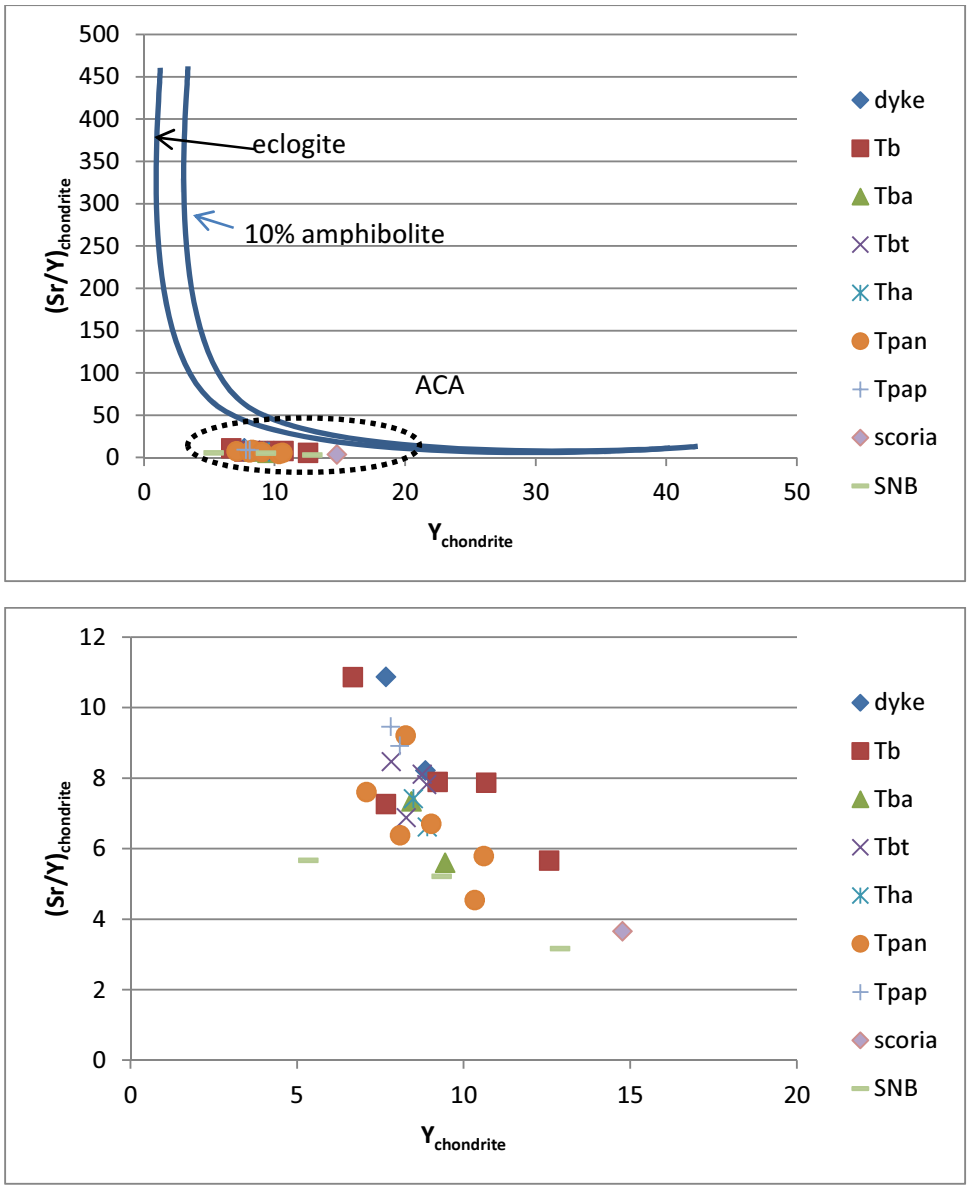

40B: Chondrite normalized plot of Y versus Sr/Y from Drummond & Defant (1990). The SVC samples plot below the overlapping fields of eclogite and 10% amphibolite; they have a negative linear trend. SNB samples from Hetch Hetchy (Barbarin et al., 1989) also overlap the SVC samples suggesting the SNB is not a lithospheric end-member to the SVC.

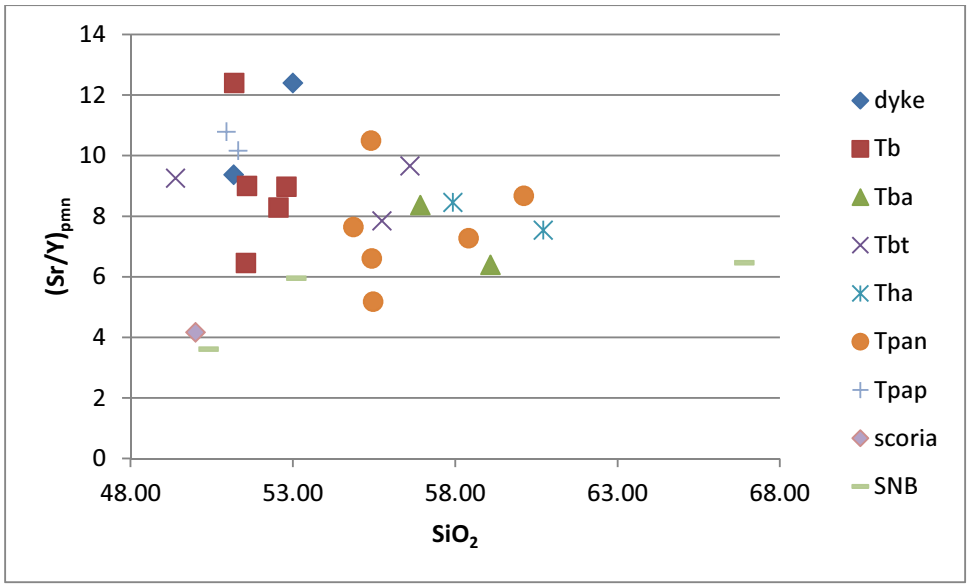

40C: Chondrite normalized plot of Sr/Y versus SiO_2 from Cousens et al., (2011). The SVC samples do not show a trend with increasing silica, indicating that mixing from felsic melts is not likely, this is also supported by Hetch Hetchy (Barbarin et al., 1989) samples overlapping the SVC sample range as well.

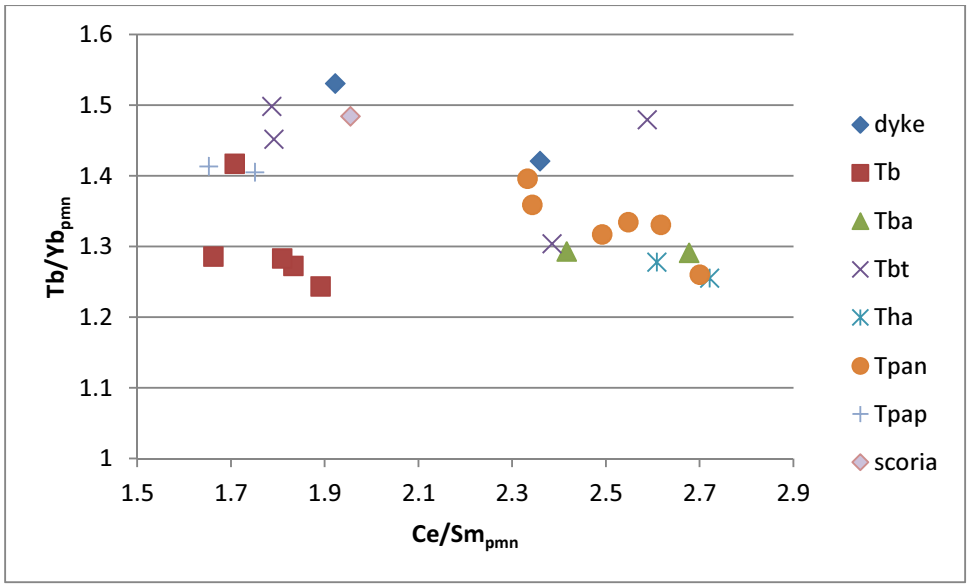

Figure 41: Primitive mantle normalized ratios of Ce/Sm versus Tb/Yb. The plot shows SVC basalt and andesite samples plotting in the garnet stability field. There is a distinct separation of the basaltic samples with the andesitic samples along the Ce/Sm_{pmn} axis suggesting crustal assimilation is occurring in the andesites and not the basalts.

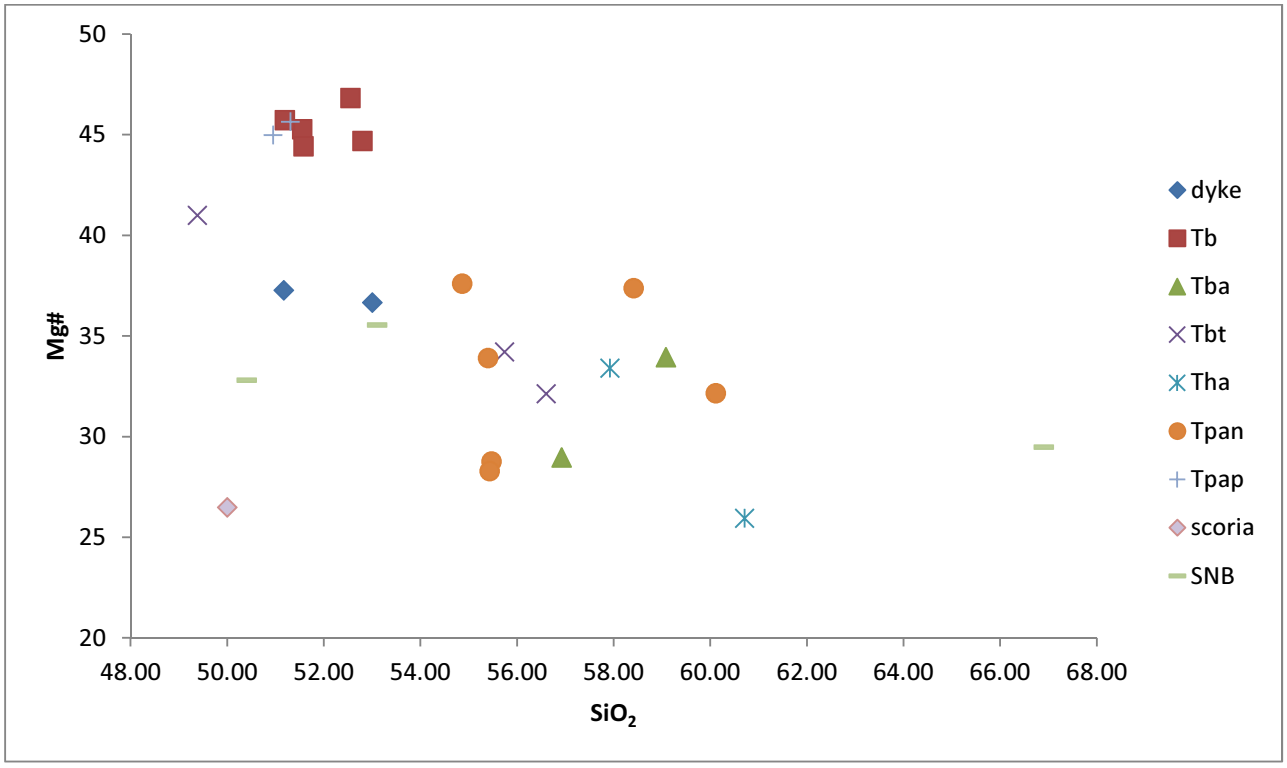

Figure 42: A plot of silica versus Mg# of SVC samples and SNB Hetch Hetchy (Barbarin et al., 1989). Samples show a weak negative linear trend of decreasing Mg# with increasing silica (i.e. crustal thickness). The SNB samples overlap the SVC andesite samples also.

Figure 43: Incompatible element plots of Sierra Nevada Batholith (SNB) analyses from the Hetch Hetchy sample site which is near the SVC (Barbarin et. al., 1989). HH1-H is a tonalite, HH4-I is an inclusion, HH6a-D is a dyke

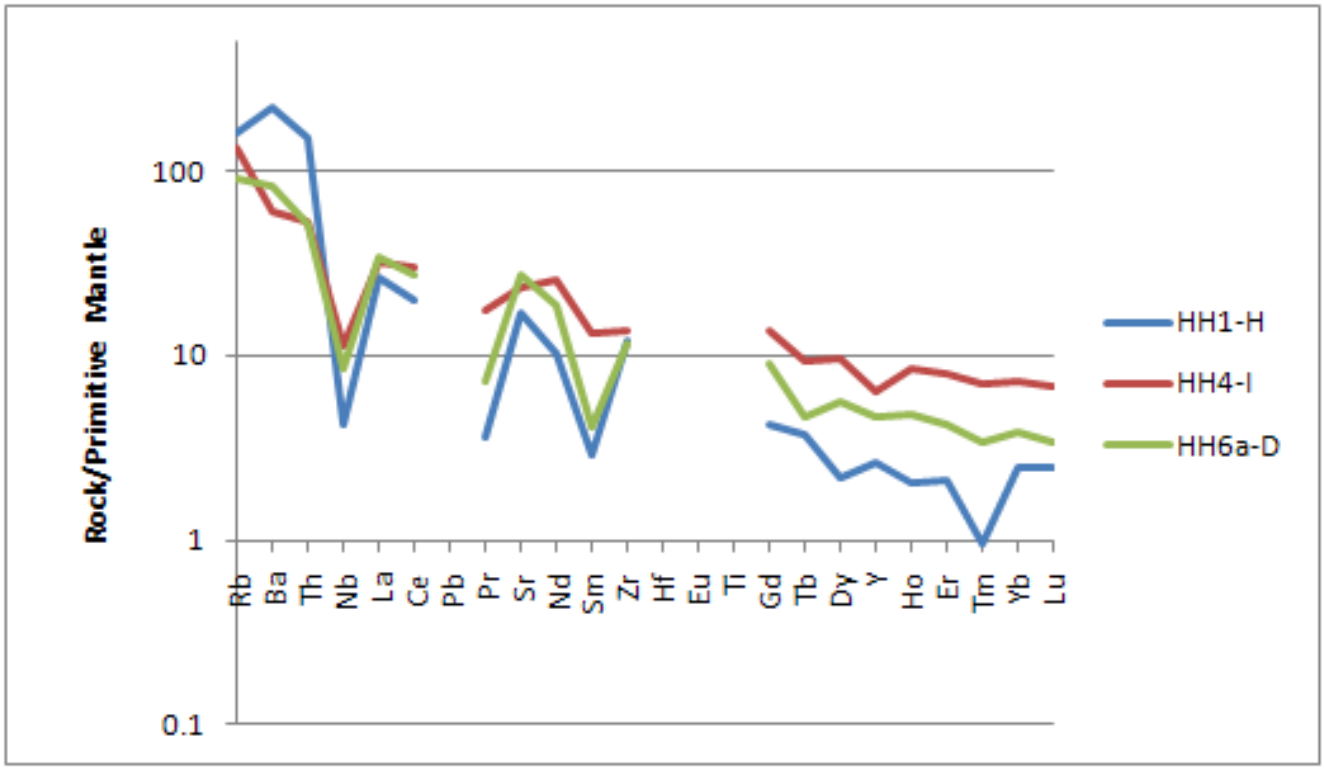

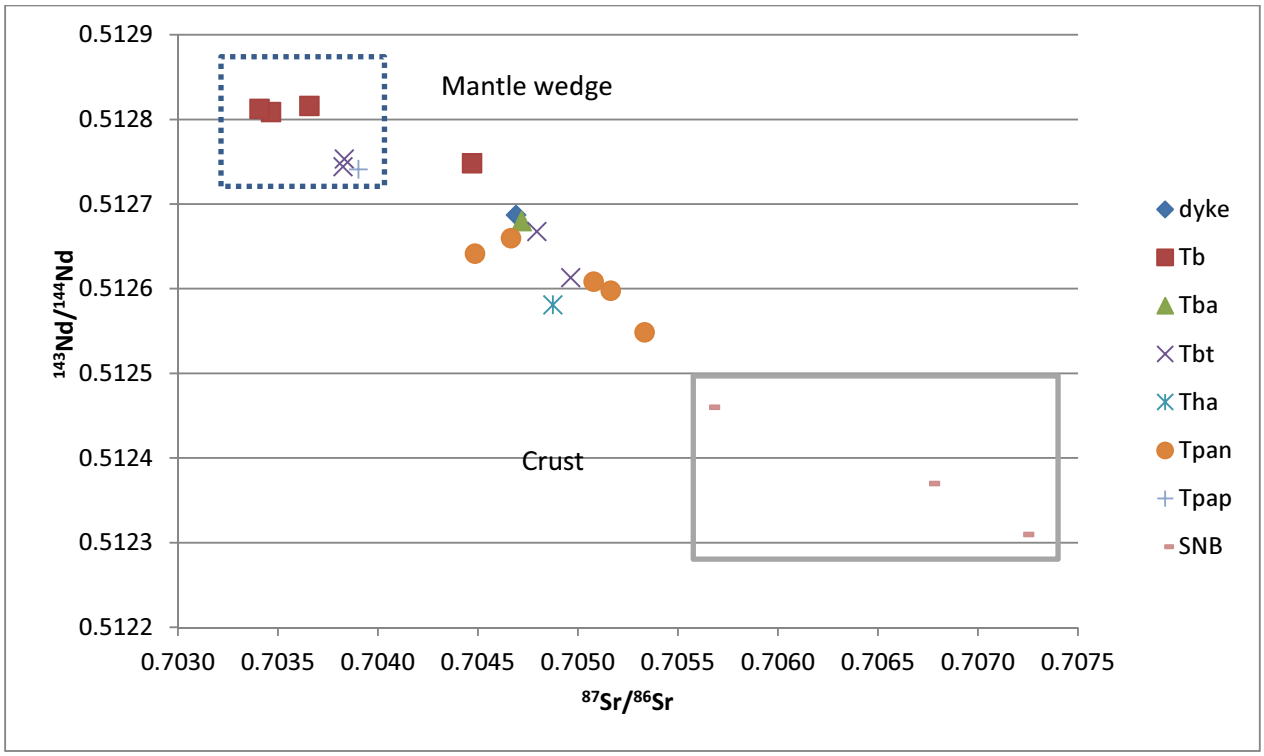

Figure 44: A plot of isotopic Sr versus Nd showing the roughly linear relationship of SVC samples to the Sierra Nevada Batholith Hetch Hetchy samples from Barbarin et al., (1989). This indicates that the SVC andesites where contaminated by SNB granitoids.

4.1.3 Geological Model

4.1.3.1 Reclassification of Samples Based on Geochemical and Petrologic Results

The geochemical results and the established map units do not correspond well. Therefore we will reclassify the samples along their petrologic and geochemical properties. This does not equate into a total re-interpretation of the Sylvester & Raines (2007) map since not every outcrop was sampled but rather to demonstrate the simplified nature of the Sagehen geological map. Samples were reclassified based on where they plotted within the alkali-silica plot; trace element patterns and isotopic $^{87}Sr/^{86}Sr$ v. $^{143}Nd/^{144}Nd$ (Figure 27, Figure 35, Figure 36a; Table 3).

There are three interpreted rock units in the SVC: basalt, basaltic-andesite and andesite. The andesite is the older unit and is also the most differentiated in terms of facies (porphyritic flows, undivided flows, nonporphyritic, and hornblende rich). Basalt in the SVC is young and is primarily basalt flows. Chemically they are distinct and can easily be distinguished as separate units while still falling under the same category as ACA rocks, that is, subalkaline. The andesites have slight enrichments of Zr and Hf while the basalts are slightly depleted relative to middle REE. Primitive mantle normalized Rb is generally highly enriched in the andesites relative to basalts; only the Tpap (pyroxene andesite flows, porphyritic) samples have Rb values comparable to the basalt. Both basalts and andesites are enriched in Pb and Sr relative to primitive mantle but generally the andesites have a higher relative abundance of Pb while the basalts are relatively more enriched in Sr. One of the two mapped basaltic andesites (Tba) when evaluated in the previous section appear to be andesite; and some map units of basalt, andesite and one temporally distinct dyke are in fact basaltic andesites (Figure 27). The normalized incompatible element diagrams reveal this differentiation as well with the Tba samples having a distinct convex curve of Sm, Zr, Hf and Eu compared to the 'convex flat top' in the andesites and the valley in the basalts over the same element range (Figure 35d). One sample from near a mapped contact (not at the contact) within the Tpap unit is a basaltic andesite which suggests that the Tba unit is potentially a mixing boundary between andesite and basalt lava flows. However, there is no observed evidence of re-melting or mingling within the outcrop.

Both basalts and andesites display Ancestral Cascades Arc petrographic and geochemical properties and appear to be part of a subduction suite related to subduction of the Juan de Fuca plate. Isotopically, $^{87}Sr/^{86}Sr$ v $^{143}Nd/^{144}Nd$ plots show three distinct groupings of samples that fall within the range of the Ancestral Cascades Arc (Figure 36A). The first group is composed of the

Tb, Tbt and Tpap map units; the second group is composed of Tba, Tpan and dyke samples that plotted as basaltic-andesites on the alkali-silica diagram while the third group is composed of Tpan and Tha samples that plotted as andesites on the alkali-silica diagram.

Finally, the scoria 10LT-04 is clearly from another suite and not part of the SVC. The scoria is depleted in Ba and is highly enriched in Th and does not have a Sr peak; it is also slightly alkaline. These properties are not present in any of the other SVC samples and it does not correspond to spider diagrams of ACA samples, although in Harker diagrams of major and trace elements it does fall within ACA sample ranges and it also follows ACA isotopic trends. The scoria is fresh and was sampled at the bottom of a quarry and we propose that it potentially represents an older arc related volcanic episode which may be part of an unmapped/eroded SVC suite.

Table 3: Map vs. Chemical (with mineralogical modifiers) classification of SVC samples

Sample	Map Unit Classification	Chemical Sample Classification
10LT-01	Olivine basalt (Tb)	Olivine bearing calc-alkaline basalt
10LT-02	Olivine basalt (Tb)	Olivine bearing calc-alkaline basalt
10LT-03	Porphyritic andesite (Tpap)	Pyroxene bearing calc-alkaline basalt
10LT-04	Porphyritic andesite (Tpap)	Alkaline basalt scoria
10LT-05	Porphyritic andesite (Tpap)	Olivine bearing calc-alkaline basalt
10LT-06	Non-porphyritic andesite (Tpan)	Andesite
10LT-07	Non-porphyritic andesite (Tpan)	Basaltic-andesite
10LT-08	Non-porphyritic andesite (Tpan)	Basaltic-andesite
10LT-09	Non-porphyritic andesite (Tpan)	Andesite
10LT-10	Hornblende andesite (Tha)	Hornblende bearing andesite
10LT-11	Basaltic tephra (Tbt)	Basaltic Volcaniclastic Flow
10LT-12	Basaltic tephra (Tbt)	Basaltic Volcaniclastic Flow
10LT-13	Basaltic tephra (Tbt)	Basaltic-andesite Volcaniclastic Flow
10LT-14	Basaltic tephra (Tbt)	Basaltic-andesite Volcaniclastic Flow
10LT-15	dyke	Basaltic-andesite dyke
10LT-16	Tpan - non-porphyritic andesite	Basaltic-andesite
10LT-17	Olivine basalt (Tb)	Olivine bearing calc-alkaline basalt
10LT-18	Basaltic andesite (Tba)	Basaltic-andesite
10LT-19	Basaltic andesite (Tba)	Andesite
10LT-20	Hornblende andesite (Tha)	Hornblende bearing andesite
10LT-21	Olivine basalt (Tb)	Olivine bearing calc-alkaline basalt
10LT-22	dyke	Basaltic dyke
10LT-23	Non-porphyritic andesite (Tpan)	Basaltic-andesite
10LT-24	Porphyritic andesite (Tpap)	Pyroxene bearing calc-alkaline basalt

4.1.3.2 Proposed Model: A Stratovolcano Complex Similar to Lassen

The proposed geologic model for the SVC is a stratovolcano complex similar to the Lassen Volcanic Centre. The primary reasons for this model being proposed is that stratovolcanoes are common within the Cascades range and are commonly associated with

abundant basaltic-andesite shield volcanoes. Furthermore, the SVC is not characterized by low viscosity basaltic lava flows similar to a Hawaiian-type shield volcano or by large volumes of scoriaceous material that one would associate with a cinder cone. The SVC is dominated by layered viscous lava flows of andesite, basaltic andesite, basalt and volcaniclastic deposits which are generally associated with a stratovolcano. A stratovolcano begins to develop when thin lava flows of basaltic andesite to dacite are erupted along with pyroclastic flows; during this period, lithologies and compositions are heterogeneous (Clynne, 1990). Later stages of stratovolcano formation are dominated by the eruption of thick homogeneous lava flows of silicic andesite to dacite (Clynne, 1990). Hydrothermal systems close to the core of the main cone are also common with their primary heat source being the silicic magma system (Clynne, 1990). Hydrothermal alteration can encourage fluvial and glacial erosion of the central cone resulting in the outer rim of the volcano, which is composed of thick cone-building lavas and flanking silicic rocks to be selectively preserved which is the case at Lassen (Clynne, 1990).

4.1.3.3 Andesite Map Units

Tpan-Pyroxene andesite, nonporphyritic & Tba-Basaltic andesite flows

- *Reclassified: Pyroxene bearing calc-alkaline andesite*

The *pyroxene andesite* (PA) unit is the lowermost andesite unit within the SVC and is also the most extensive in terms of exposed outcrop. Petrographic observations show that PA is a porphyritic pyroxene andesite with flow banding. Total alkali silica plots of PA samples fall into the subalkaline andesite field. REE plots show pa follows a concave-up trend (steep LREE slope transitioning to a flat HREE slope) and has enrichments of Ba, Zr, and Hf. When PA $^{143}Nd/^{144}Nd$ versus $^{87}Sr/^{86}Sr$ values are normalized with CHUR/UR model mantle values they plot within the

+εNd/+εSr (0-1, 0-3) quadrant indicating that the basaltic andesite samples represent a transitional phase between a depleted mantle component and an enriched crustal component. The level of εNd and εSr enrichment within the PA samples indicates that the melt was not as evolved compared to the andesites but was more evolved than the basalts in terms of incorporating crustal Sr. Pb isotopic values also show PA incorporates enriched crust. The unit PA potentially represents a slow cooling and viscous extrusive phase in the SVC. The level of enrichment within the pa samples indicates that the melt was more highly evolved suggesting that this unit was not the first eruptive unit in the SVC since one assumes lavas with a less evolved character should be erupted first be erupted first given the general evolution of volcanic centres and that the Volcaniclastic Flow (Tbt map unit) contains clasts of older volcanic units with less evolved characteristics from the geochemistry results.

Tpap-Pyroxene andesite flows, porphyritic – Reclassified: Pyroxene bearing calc-alkaline basalt

The *pyroxene basalt* (PB) unit represents the upper portions of the Tpan map unit within the SVC according to previous mapping. Ar-Ar age dating places the PB unit within the 5.65 Ma timeframe; this has been inferred to be the time when all other andesite units were emplaced as well. Petrographic observations show that PB is a porphyritic pyroxene basalt with phenocrysts of plagioclase and pyroxene and flow banding. Normalized incompatible plots show PB follows a concave-up trend and has enrichments of Ba and depletions of Zr, and Hf (Figure 35). Furthermore, incompatible element plots show that PB shares more characteristics similar to the OB (olivine basalt) unit especially in terms of Sr enrichment compared to Pb (Sr>Pb unlike in all other andesite and dyke units where Pb>Sr) and the Zr and Hf depletions. Isotopically, PB follows trends similar to OB and follows a two-component $^{143}Nd/^{144}Nd$ versus $^{87}Sr/^{86}Sr$ mixing

line similar to Cousens et al. (2008) with only slightly lower $^{143}Nd/^{144}Nd$ values. When PB $^{143}Nd/^{144}Nd$ versus $^{87}Sr/^{86}Sr$ values are normalized with CHUR/UR model mantle values they show samples that have a depleted signature (+2 εNd, –9 εSr) with a slight enrichment of isotopic Sr and depletion of Nd compared to OB samples. Pb isotopic values also show PB has a more depleted mantle signature similar to OB. The Pyroxene Basalt potentially represents a slow cooling and viscous extrusive phase in the SVC. The level of enrichment within the PB samples indicates that the melt was not evolved compared to the andesites.

Tpan-Pyroxene andesite, nonporphyritic & Tba-Basaltic andesite flows

- *Reclassified: basaltic andesite*

The Tba map unit is a poorly defined boulder field in the southeast of the SVC but four samples of Tpan and one Tba sample have basalt-andesite characteristics based on geochemical data using the total alkali-silica plot. These Basaltic Andesite (BA) samples petrographically are porphyritic with pyroxene and plagioclase phenocrysts and minor foliation. Incompatible element plots show BA follows a concave-up trend and has enrichments of Ba, Zr, and Hf and is overall similar to *pyroxene andesite* trace element patterns. Isotopically, BA follows a two-component $^{143}Nd/^{144}Nd$ versus $^{87}Sr/^{86}Sr$ mixing line similar to Cousens et al. (2008) with only slightly lower $^{143}Nd/^{144}Nd$ values. When BA $^{143}Nd/^{144}Nd$ versus $^{87}Sr/^{86}Sr$ values are normalized with CHUR/UR model mantle values they show samples that have an enriched-lithospheric signature (+εNd) with an enrichment of isotopic Sr (+εSr) indicating that melts passed through thick lithosphere; the *basaltic andesite* is more relatively enriched in continental arc than the *pyroxene andesite* which is somewhat counter-intuitive given that the *basaltic andesite* should be less evolved. Pb isotopic values also show BA incorporates enriched lithosphere. The *basaltic*

andesite samples show that the Tpan map unit has potentially lateral variability in its composition or is composed of multiple unmapped units. It is therefore difficult to resolve the *basaltic andesite's* place in the stratigraphic order (i.e. did it come before or after the 'true' andesites in the Tpan unit). What is certain is that the *basaltic andesite* is an extensive and thick unit: there is no strong flow banding in these samples and phenocryst sizes are small indicating a viscous and fast cooling lava compared to the other *pyroxene andesites*.

Tha-Hornblende andesite flows – Reclassified: hornblende bearing andesite

The *hornblende andesite* (HA) unit is the uppermost unit topographically and stratigraphically (based on Sylvester & Raines, 2007). Petrographic observations confirm that HA is a phenocrystic hornblende andesite. Incompatible element plots show HA follows a concave-up trend similar to PA and has enrichments of Ba, Zr, and Hf. Isotopically, HA lies on a two-component $^{143}Nd/^{144}Nd$ versus $^{87}Sr/^{86}Sr$ mixing line similar to Cousens et al. (2008) with only slightly lower $^{143}Nd/^{144}Nd$ values. When Tha $^{143}Nd/^{144}Nd$ versus $^{87}Sr/^{86}Sr$ values are normalized with CHUR/UR model mantle values they have an enriched mantle signature (-1 εNd, +5 εSr) indicating that melts passed through thick lithosphere. Pb isotopic values also show HA is a mixture of depleted mantle and enriched lithosphere. The *hornblende andesite* unit potentially represents a slow cooling moderately viscous extrusive phase in the SVC.

4.1.3.4 Pyroclastic Flow

Tbt- Basaltic tephra – Reclassified Volcaniclastic flow

The *volcaniclastic flow* (VF) unit contains clasts that Ar-Ar age dating places at 6.25 Ma. Since the Ar-Ar date only represents the clasts within the pyroclastic flow, the matrix of basalt is most likely closer in age to the underlying andesitic unit (Tpan) and it is potentially cross-cut by

a dyke (the dyke is in contact and cross cuts the andesite map unit Tpan) but the matrix needs to be tested to prove this. Petrographic observations confirm that VF is a volcaniclastic unit. The volcaniclastic flow is not pumice or ash rich and has large boulder sized fragments that are a result of volcaniclastic down slope movement indicating that we are looking at the bottom of the unit. In terms of REE abundances, the VF unit samples have compositions more in line with the andesite units. Geochemically and isotopically, the matrix (basalt) rich samples of VF follow trends similar to the OB unit while the clast (andesite) rich samples follow andesite trends. The deposit is, at least in part, slightly younger than the clast age. However, some clasts had radial cooling joints suggesting that part of the unit was hot when deposited. There is no clear upper time constraint to the VF unit. The VF unit could potentially represent a dome collapse occurring after the eruption of the andesite unit but in order for this to be possible the clasts and the matrix of the flow would have to be homogeneous which is not the case.

4.1.3.5 Dykes

The dykes crosscut the volcaniclastic and are inferred to underlie the Tpan andesite units (the dyke on the north shore of Independence Lake is below a cliff of Tpan) and could potentially be the youngest units in the SVC but since no multiple contact relationships have been observed we can only conclude that they are younger than the andesitic units. Geochemically the dykes are similar to Tpan basaltic andesites except for their elemental abundances of Sr (Sr≈Pb); isotopically they are similar to Tpan samples. The level of εNd/εSr enrichment within the dyke samples is similar to the basaltic andesite samples and indicates that the melt was a more transitional phase in the SVC. The dykes are more basaltic geochemically but are more similar isotopically to the Tpan andesites this could possibly mean that the dykes are feeders to the Tpan map unit.

4.1.3.6 Basalt

Tb-Basalt flows – Reclassified: olivine bearing calc-alkaline basalt (OB)

Olivine basalt flows overly the andesites and is extensive in the topographically lower portions of the north-eastern area of the SVC. Ar-Ar dating indicates that the OB unit is 4.41 Ma making the basalt the youngest major rock unit. Petrographically, the *olivine basalt* is primarily aphanitic and flow banded with minor vuggs indicating a partially volatile and viscous extrusive flow that followed topography. Geochemically, the *olivine basalt* has fractionation patterns that do not favour extensive pyroxene fractionation (CaO/Al_2O_3 vs. silica Figure 29). Incompatible element patterns show that the basalt follows a curve similar to the *pyroxene basalts* but Pb values are more highly variable (one basalt sample has a depletion of Pb) and Y also has minor enrichments compared to the andesite samples. Isotopically, the OB samples display a εNd versus εSr depleted signature (+3.5 εNd and –11-16 εSr).

The OB samples also follow a two-component mixing trend with the other SVC samples within this plot. $^{207}Pb/^{204}Pb$ versus $^{206}Pb/^{204}Pb$ plots of OB samples show the basalts plot close to the NHRL line. In $^{143}Nd/^{144}Nd$ versus $^{87}Sr/^{86}Sr$ plots the Tb samples do not follow the mixing line proposed in Cousens et al. (2008) since their $^{143}Nd/^{144}Nd$ values are too low, but ignoring the linear mixing line the OB samples fit well on a polynomial curve with the previously studied Tahoe/Truckee arc samples of Cousens et al. (2008), the evolved SVC samples and the Sierra Nevada Batholith samples from Barbarin et al. (1989). The *olivine basalt* potentially represents a fast cooling moderately viscous extrusive phase in the SVC. The OB samples indicate that the melt was derived from a highly depleted source, suggesting that this extrusive phase did not

interact with thick continental lithosphere. Given that the basalts are the youngest rock units within the SVC (dated so far) and older units have a more enriched signature its seems likely that the *olivine basalt* unit was a product of rifting, potentially as a precursor of Basin & Range extension (which began at ~3 Ma).

4.1.3.7 Summary of Geologic events within the SVC

Subduction activity in the Mesozoic led to the intrusion of the major granitic batholiths, notably the Sierra Nevada batholith. During the Laramide orogeny (Late Cretaceous to middle Eocene) arc volcanism ceased in California and Nevada which allowed the Sierra Nevada batholith to be exposed through erosion. The cause of the cessation of arc volcanism is believed to be the result of shallowing of the dip of the Juan de Fuca/Farallon plate (Dickinson & Snyder, 1979). The shallowly dipping Juan de Fuca slab detached and subsided from the overlying continental lithosphere along a roughly north-south trend in Washington and Oregon which is believed to have resulted in the resumption of arc volcanism in the Sierra Nevada Ancestral Cascades by ca. 40 Ma (Christiansen and Yeats, 1992). However, the Juan de Fuca slab remained attached near the trench through California, where magmatism did not resume until much later (Cousens et al., 2008). Some form of tear probably separated steep- and shallow-dipping slabs near the California-Oregon border (Cousens et al., 2008). The foundering slab beneath California pulled both southward and southwestward, with a significant component toward the trench, in an apparent slow attempt to re-establish steep subduction (Cousens et al., 2008). The last westward step at ca. 3 Ma from the Tahoe area to Lassen Peak most likely reflects the latest foundering and/or steepening of the slab (Cousens et al., 2008). The SVC, given Ar-Ar dating would thus enter this model in the ~6-4 Ma time frame, just prior to the final steepening of the Juan de Fuca slab. From our chemistry, we can see the distinct subduction and

ACA signature in the SVC samples so this in itself does not contradict Cousens et. al. (2008). However, the interpretation of the Miocene–Pliocene Ancestral Cascade arc in the Sierra Nevada has been controversial. Lipman (1992), and Dickinson (2002, 2004, 2006) indicated an arc along the length of the northern and central Sierra Nevada during much of the middle and late Cenozoic.

The volcanic units within the SVC describe alternating periods of volcanic εNd/εSr compositions; instead of a straight continuous evolution of volcanic units. Given the petrography of the rock units, especially with regards to the pyroclastic flow and the lack of ash/pumice deposits the Sagehen study area does not represent a distal deposition centre but a volcanic centre near the stratovolcano. The volcanic units are thick successions of crystalline, non-fragmental andesite and basalt that are primarily homogeneous in terms of REE patterns and mineralogy (amphibole-pyroxene-plagioclase) suggesting they represent a later stage of strato-cone flank deposits. There is no major structural deformation, chemical alteration or metamorphism within the SVC, indicating that the SVC is part of the outer cone of the volcanic complex where there would be no hydrothermal system. The only defining macro scale structure is distinct continuous flow banding that follows the topography. From the Ar-Ar age dates we know that the clastic units comprising the volcaniclastic flow are >6.25 Ma and incorporate several rock types indicating that there was a thick succession of basaltic and andesitic volcanic material that no longer exists in outcrop within the SVC. The subsequent inferred 5.65 Ma period of extrusive volcanism (Ar-Ar dating of the Tba unit) was characterized by emplacement of the depleted pyroxene basalt unit followed by the basaltic andesite and pyroxene andesite units and then finished by the Tha unit. The last dated volcanic activity was the extrusion of depleted olivine basaltic lava flows. The work of Hildreth and Moorbath (1988) showed that Andean style

subduction has enrichments of LILE and LREE, the SVC and Tahoe-Truckee region arc lavas also have similar LILE and LREE enrichments relative to REE abundances. In this instance, it is felt that a subduction character exists in the SVC and that geologically it developed in an Andean style subduction zone setting with a shallowly dipping slab similar to the Tahoe-Truckee region arc rock suites sampled by Cousens et al., (2008) and Stoffers, (2010). Given the style of erupted units and the similarity with the geologic development of Lassen as described by Clynne, (1990) we conclude that the SVC represents a heavily eroded late-stage Lassen-style stratovolcano because of the thick viscous homogeneous andesitic and basaltic units that appear to represent Flank lava flows and the LILE & LREE enrichments typical of a subduction zone (Figure 45). Furthermore, the disequilibrium textures seen in most of the samples indicates that the melts were derived from a 'magma reservoir' since these textures, in order to develop, would need degassing, magma mixing and prolonged crustal assimilation which is what a magma reservoir can provide.

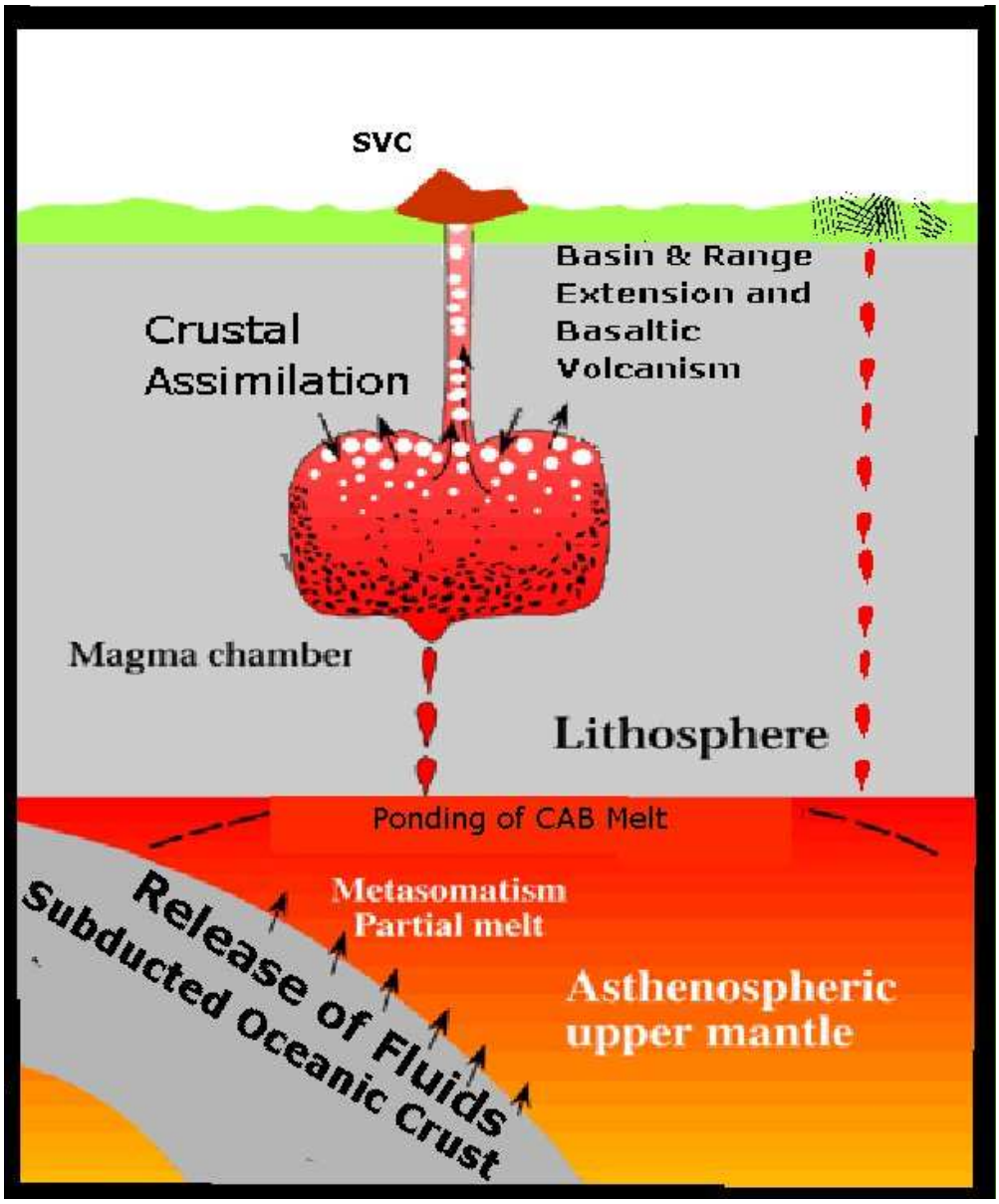

Figure 45: A simplified model of SVC lava setting modified from Strong and Wolff, (2003) (base image taken from Geomar.de and modified/redrafted) which is based on the Modern Cascades. The lines through the crust represent simplified Basin and Range faulting. SVC lavas were derived from hydrous calc-alkaline magmas. The andesitic rock units were emplaced first relative to the analyzed basalts. The andesites are relatively more enriched in crust than the basalts indicating they passed through thick units of crust relative to the basalts which is supported by the thick recrystallized hornblende rims of the hornblende andesites. What is interesting to note is that MORB, Intraplate, and LKT magmas have little to no influence within the SVC while in the Modern Cascades they are present. This implies there was some factor preventing their influence.

4.2 SVC versus Ancestral Cascades and Young Volcanism in the Western Great Basin

Sagehen Volcanic Centre lavas are in general sub-alkaline and depleted in incompatible elements with low concentrations of K_2O, Ba (fairly high LILE), the rare earth elements, and high field strength elements compared to young <3 Ma post-arc rocks. SVC basalts and andesites overlap compositionally with andesites of the Ancestral Cascades and specifically with samples from previous studies of comparable age. When SVC samples are normalized to primitive mantle, their incompatible element patterns are nearly identical to those of Ancestral Cascades arc lavas (Figure 46). Therefore the SVC appears to have a subduction-related signature and is considered to be part of the ACA.

4.2.1 Post-Arc Comparisons

The Tahoe-Truckee Volcanic Field (TTVF) overlies the Ancestral Cascades Arc and reflects volcanism after the subducting Juan de Fuca slab migrated north past Lake-Tahoe. Most TTVF lava groups show strong enrichments in most incompatible elements over Ancestral Cascade volcanic rocks (Cousens et al., 2011). The elements with the strongest enrichments are the HFSE Nb, Ta, Hf and Zr, followed by Ba, K_2O and the light- to middle- rare earth elements. Bald Mountain, Truckee River, and Tahoe City flows are particularly enriched in K_2O and P_2O_5, given their low SiO_2 contents, and these groups are also strongly enriched in Nb and Ta demonstrates the enrichment in Nb relative to Zr, La, Pb and Th (Cousens et al., 2011). All TTVF groups, except the Dry Lake flows, are up to 4 times richer in Nb at a given Zr content than Ancestral Cascade arc volcanic rocks (Cousens et al., 2011). TTVF lavas have lower Ba/La, Th/La, but higher Ce/Pb and La/Sm_{pmn} than most Ancestral Cascade lavas. Overall, TTVF lavas include less of a young subduction component than Ancestral Cascade lavas. Bald Mountain and Truckee River flows consistently have high Ce/Pb, Nb/ La, but low Ba/La; although Tahoe City

lavas also extend to high Ce/Pb. Carnelian Bay and Carson Range lavas appear to have a larger subduction signature (Cousens et. al., 2011).

The observed enrichment in incompatible elements in the TTVF only rarely correlates with changes in isotopic composition (Cousens et al., 2011). Within the TTVF array, Tahoe City and Bald Mountain lavas show better intergroup correlation, but the Truckee River and Carson Range groups are variable (Cousens et al., 2011). The Carnelian Bay group shows little variation. There is no correlation between Nb enrichment (Nb*) and isotopic composition (Cousens et al., 2011). Similarly, Ce/Pb does not co-vary with $^{206}Pb/^{204}Pb$. Th/ La shows a weak negative correlation with Pb isotope ratios (Cousens et al., 2011). It is apparent that changes in incompatible element signatures mark a decrease in the proportion of a subduction component in TTVF lavas compared to Ancestral Cascade arc volcanic rocks–are not accompanied by a consistent or distinct change in mantle source isotopic composition (Cousens et al., 2011). The only isotopic distinction between Ancestral Cascade and TTVF lavas is that the younger suite sits at the high $^{87}Sr/^{86}Sr$, $^{206}Pb/^{204}Pb$ and low $^{143}Nd/^{144}Nd$ end of the Ancestral Cascades data array (Cousens et al., 2011). The Ancestral Cascades data set is modeled by mixing of melts derived from the mantle wedge and enriched, subduction-modified lithospheric mantle (Cousens et al., 2008). Based on this model, the lithospheric mantle source dominates the isotopic character of TTVF lavas, but melts are not as rich in young subduction components compared to Ancestral Cascade arc melts.

4.2.2 Comparisons with Modern Cascade Arc volcanism

Paleo-reconstruction of the Juan de Fuca slab indicates that a continental volcanic arc should have been present along the northern Sierra Nevada in the Miocene and Pliocene (Cousens et al., 2008). Dickinson (1997, 2006) referred to this volcanic activity as the Ancestral Cascades arc that extended from British Columbia south to the California-Nevada-Arizona state boundary intersection at 15 Ma. Modeling of the movement of the trailing edge of the Juan de Fuca plate relative to North America shows that it has moved progressively northward over the past 20 Ma, leaving a slab window in its wake (Atwater & Stock, 1998). The south edge of the subducting Juan de Fuca slab reached the latitude of Lake Tahoe at ca. 6 Ma and is now (presently) stalled just north of the lake at ~39.5°N (Benz et al., 1992). The slab edge is south of the Lassen volcanic field, the generally accepted southern end of the active Cascades arc (Clynne, 1990), perhaps as a result of the highly fragmented Gorda plate being dragged southward into the slab window (Benz et al., 1992). Miocene–Pliocene volcanism in the Tahoe-Reno region broadly resembles modern south Cascade volcanism in terms of geology and petrology notably the andesite and basalt flows of the SVC. Due to the northward migration of the Juan de Fuca plate edge, Miocene–Pliocene subduction related volcanism should have progressively ceased as it moved northward in eastern California and western Nevada if the dominant process responsible for volcanic activity is the loss of fluids from the subducted slab (Cousens et al., 2008).

4.2.2.1Field and Petrographic Characteristics

There are both similarities and differences between volcanoes of the modern south Cascades (Lassen, Shasta) and the Ancestral Cascade lavas of the SVC. In the field, both the modern south Cascades and the Tahoe-Reno region include volcanic complexes composed of both

volcaniclastic rocks (and debris flow and/or lahar deposits, ex: the Tbt map unit in the SVC) and lava flows (Tpan, Tpap, Tb; Cousens et al., 2008). South Cascade andesites are commonly plagioclase-clinopyroxene-hornblende porphyritic, much like lavas of the SVC. Furthermore, within some areas in the Tahoe-Reno region, hornblende mineralization has a ring of recrystallized fine grained hornblende which we see within the SVC as well. Finally, the SVC lacks felsic pyroclastic or rhyolitic flows that are common, although volumetrically minor, in the Lassen region (Cousens et al., 2008).

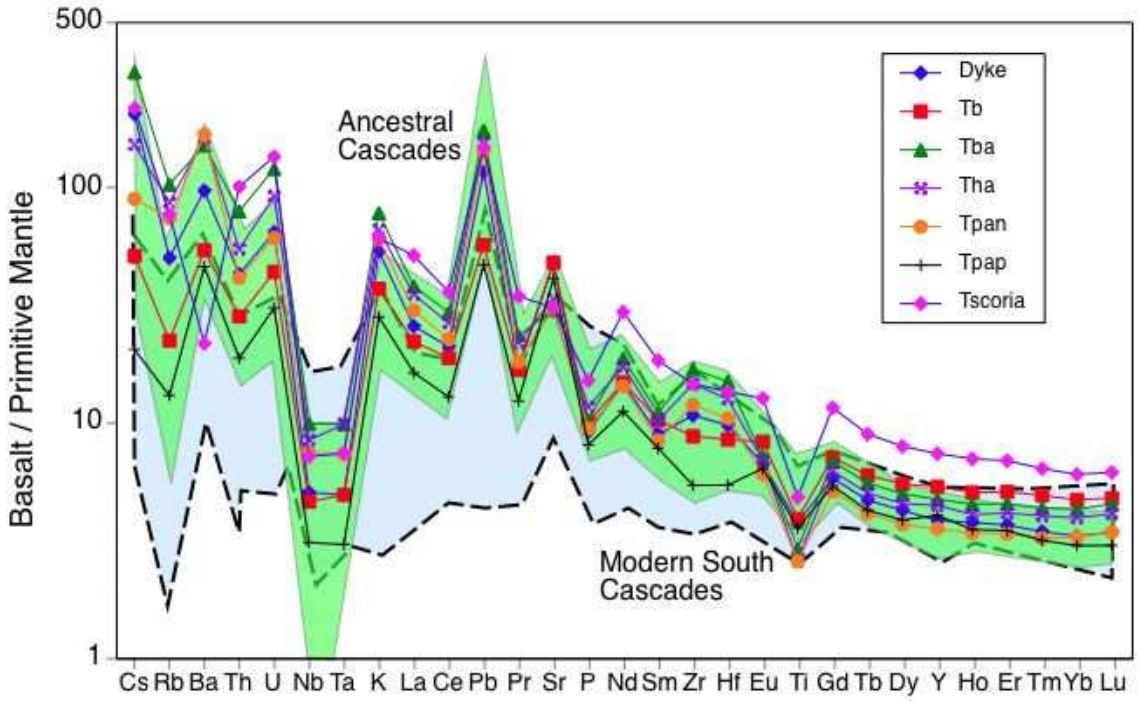

Figure 46: Comparison of primitive mantle normalized incompatible element plots for SVC samples against Ancestral and Modern South Cascades incompatible element ranges.

4.2.2.2 Trace Element and Isotopic Contrasts

Modern south Cascade basalts and Tahoe-Reno region/SVC mafic lavas show large differences in incompatible element characteristics (Figure 46). Although some overlap exists and

patterns are similar in shape, many modern Cascade basalts have lower abundances of the more incompatible elements but similar abundances of the heavy REEs to the ACA and SVC (Cousens et al., 2008). The higher incompatible element abundances in Tahoe-Reno region lavas is also consistent with the model of Putirka and Busby (2007), who showed that Miocene–Pliocene Sierran lavas are derived by lower degrees of partial melting than Lassen area lavas. In particular, Tahoe-Reno lavas (including SVC) are enriched in Ba, Th, Pb, and Sr relative to modern Cascade lavas. Figure 36 demonstrates the variation in Sr relative to P at a given $^{87}Sr/^{86}Sr$ in Tahoe-Reno region basalts compared to other basaltic rocks of the western United States. At Lassen Peak, Sr/P_{pmn} is interpreted to reflect variable slab-derived fluid addition to the mantle wedge: lavas with low Sr/P_{pmn} were interpreted as melts of unmodified mantle wedge peridotite, whereas lavas with high Sr/P_{pmn} imply melting of hydrous, Sr-enriched, metasomatized mantle peridotite (Borg et al., 1997). Sr/P_{pmn} also correlates with trace element ratios, such as Ba/Nb, that are also sensitive to fluid addition from the subducting slab. At Lassen, lavas with low $^{87}Sr/^{86}Sr$ have high Sr/P_{pmn}, suggesting that slab-derived fluids have mid-ocean ridge basalt (MORB)-like Sr isotope ratios, whereas lavas with high $^{87}Sr/^{86}Sr$ have low Sr/P_{pmn}, consistent with melts from an enriched, intraplate mantle source but trace element patterns do not correspond (Cousens et al., 2008). The Sr/P_{pmn} plots of SVC basalts also fall within the range of South Cascades basalts. No high-alumina olivine tholeiite (HAOT) or Low Potassium Tholeiites (LKT) have been found in any volcanic sequences in the Tahoe-Reno region including the SVC (Cousens et. al., 2008). The HAOTs and LKTs represent melts of unmetasomatized lithospheric mantle (but some can have very low $^{87}Sr/^{86}Sr$) or asthenosphere which potentially means that arc volcanism occurred before the subducting slab detached from the North American plate (Bacon et al., 1997; Cousens et al., 2008). This is a significant

geochemical difference between Miocene–Pliocene Tahoe-Reno region lavas and volcanic rocks of the modern south Cascades.

4.2.3 Potential Basin and Range Extension in the SVC?

One of the questions that arose during our sampling on the Sagehen property was whether the Tb basalts, the youngest dated rock unit, could have been associated with Basin and Range extension. Our initial reasoning for this was the age of the basalts (4 Ma, Basin and Range Extension would have begun at 3 Ma), their stratigraphic position with relation to their less evolved character (they overlie evolved andesites which is counter to standard volcanic successions) and their topographic position being on the eastern flank of the property similar to Lassen volcanic centre extension related volcanism. In order to evaluate our theory we have compared our basalt samples to samples analyzed previously that have been suggested to be associated with Basin and Range extension. These samples are from the Boca Reservoir, Ellis Peak, Squaw Peak and Henness Pass (Cousens et al., 2008; Saucedo & Wagner, 1992). The historic samples when compared to the SVC basalts are highly similar and display the same relative abundances in the major oxides, and in the trace elements as well except: Sc is twice as abundant in SVC basalts than in the historic samples and Cr abundances are less than half in the Ellis peak and Boca samples when compared to the SVC and Squaw peak samples. Isotopically, the SVC and Historic samples fall along the same line almost perfectly (Figure 47). Therefore, it seems possible that the eruption of SVC basalts could have been influenced by Basin & Range Extension. However, the SVC basalts displays these same similarities and overall trends with other ACA samples (albeit to a lesser degree), even the historic samples associated with Basin & Range Extension show evidence of crustal assimilation which is curious as this would mean fast

rising basaltic melts dues to rifting would be able to assimilate that much isotopic Sr from the crust.

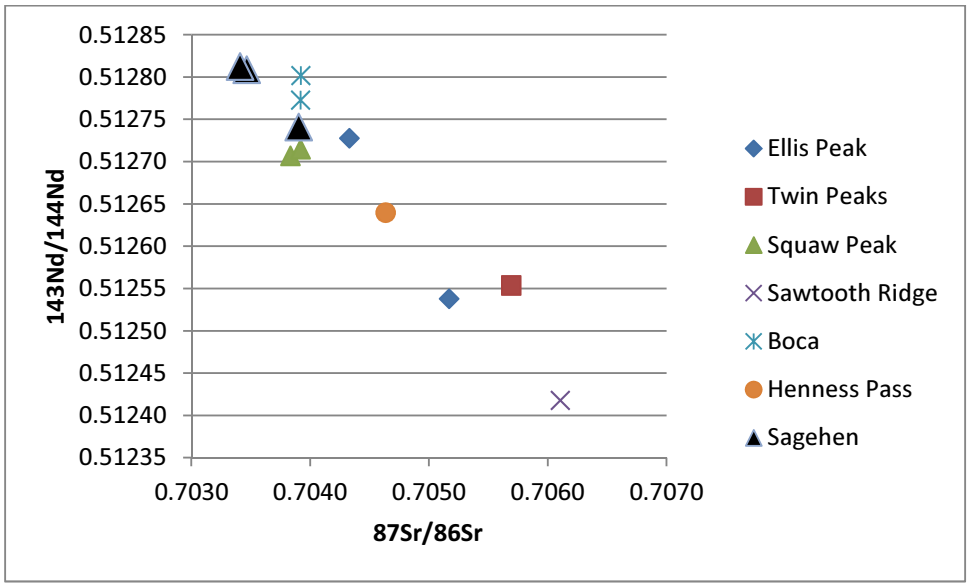

Figure 47: A plot of isotopic Sr versus Nd showing the linear relationship of SVC basalt samples to other ca. 4-5 Ma basalt samples associated with Basin & Range Extension.

5. Conclusions

This study has shown that volcanic rocks of the Sagehen Volcanic Centre in the Tahoe-Truckee region are calc-alkaline basalts through andesites and range in age from 6.25-4.41 Ma. Volcanic edifices are lava flows or blocky volcaniclastic flows that have a dominant plagioclase-pyroxene-hornblende phyric composition. The more evolved andesite units show strong evidence of interaction with Sierra Nevada Batholith granitoids such that major element characteristics, incompatible element ratios, and isotope ratios (Sr, Nd & Pb) all covary with increasing SiO_2,while depleted basalts and the andesite porphyritic unit (Tpap) are less affected. The source for SVC lavas appears to be calc-alkaline melts produced from mantle wedge peridotites.

Isotopic evidence shows that the volcanic units in the SVC follow a linear two component mixing trend between lithosphere (Sierra Nevada Granites) and mantle wedge but this trend is not temporally linear with the volcanic units pulsing between crustal and mantle wedge compositions. The non-porphyritic pyroxene andesite unit Tpan displays a primarily basalt-andesite geochemical trend (except for two samples) whereas the Tba unit (mapped as a basaltic andesite) is actually an andesite. Furthermore, the disequilibrium textures seen in most of the samples indicates that the melts were derived from a 'magma reservoir' since these textures, in order to develop, would need degassing, magma mixing and prolonged crustal assimilation which is what a magma reservoir can provide. The restricted timeframe of the units supporst this assertion as well since we can easily distinguish crustal contamination. The SVC basalts also have isotopic compositions and major oxide and trace element abundances similar to previously sampled ca. 4-5 Ma basaltic volcanic rocks in the area but the differences in age and location suggest these samples may share a similar source but not a similar eruptive centre. Likewise, the eruption of the basalts could potentially be the result of Basin and Range extension in the area given the similarity of the SVC basalts to historic samples believed to be associated with the Basin and Range province and the restricted age of the SVC samples which allows us to see specific processes. Finally, the SVC displays geochemical and petrographic similarities to the Lassen volcanic centre leading us to conclude that the SVC was potentially a stratovolcano.

At the beginning of this thesis, we brought forward the idea that a better understanding of Ancestral Cascades Arc volcanism can help us have a better understanding of modern processes and future events within the Cascades. From this study we can glean the following: that if current plate motions remain the same in the Juan de Fuca plate; an equivalent SVC/LVC style volcanic

centre will potentially develop within the Cascades in Oregon when the southern edge of the Juan de Fuca plate passes through the state a few million years from now.

5.1 Further Work

The stratigraphy within the SVC is still poorly understood making a drill program and the study of drillcore an important next step in the understanding of the volcanic assemblages. The presence of the 6.25 Ma volcanic clasts within the Tbt unit suggests that the SVC is more extensive than previously thought. This observation leads us to recommend more geochronology of the volcanic units within the SVC and reconnaissance further to the east and north of the SVC. Furthermore, within the southern outcrops of Tha there was a strong magnetic anomaly that distorted compass navigation. Samples from that area had a preponderance of Fe minerals within them as well. The magnetic anomaly could represent a conductor that could be an indicator for a mineral deposit thus making the SVC a likely candidate for a geophysical survey.

6. References

Acocella, V. and F. Funiciello (2010). "Kinematic setting and structural control of arc volcanism." Earth and Planetary Science Letters **289**: 43-53.

Amelin, Y., C. Li, O. Valeyev and A. J. Naldrett (2000). "Nd-Pb-Sr Isotope Systematics of Crustal Assimilation in the Voisey's Bay and Mushuau Intrusions, Labrador, Canada." Economic Geology **96**: 815-830.

Bacon, C. R., P. E. Bruggman, R. L. Christiansen, M. A. Clynne, J. M. Donnelly-Nolan and W. Hildreth (1997). "Primitive Magmas at Five Cascade Volcanic Fields: Melts from Hot, Heterogeneous Sub-Arc Mantle." Canadian Mineralogist **35**: 397-423.

Benz, H. M., G. Zandt and D. H. Oppenheimer (1992). "Lithospheric Structure of Northern California from Teleseismic Images of the Upper Mantle." Journal of Geophysical Research **97**(B4): 4791-4807.

Birkeland, P. W. (1963). "Pleistocene Volcanism and Deformation of the Truckee Area, North of Lake Tahoe, California." GSA Bulletin **74**: 1453-1464.

Borg, L. E., J. Blichert-Toft and M. A. Clynne (2002). "Ancient and modern subduction zone contributions to the mantle sources of lavas from the Lassen region of California inferred from Lu-Hf isotopic systematics." Journal of Petrology **43**: 705-723.

Borg, L. E. and M. A. Clynne (1998). "The petrogenesis of felsic calc-alkaline magmas from the southernmost Cascades, California: Origin by partial melting of basaltic lower crust." Journal of Petrology **39**: 1197-1222.

Borg, L. E., M. A. Clynne and T. A. Bullen (1997). "The Variable Role of Slab-Derived Fluids in the Generation of a Suite of Primitive Calc-Alkaline Lavas from the Southernmost Cascades, California." Canadian Mineralogist **35**: 425-452.

Carr, M. J. (1984). "Symmetrical and segmented variation of physical and geochemical characteristics of the central American volcanic front." Journal of Volcanology and Geothermal Research **20**: 231-252.

Carr, M. J., M. D. Feigenson and E. A. Bennett (1990). "Incompatible element and isotopic evidence for tectonic control of source mixing and melt extraction along the Central American arc." Contributions to Mineralogy and Petrology **105**: 369-380.

Chambers, L. M., M. S. Pringle and R. R. Parrish (2005). "Rapid formation of the Small Isles Tertiary centre constrained by precise 40Ar/39Ar and U–Pb ages." Lithos **79**: 367-384.

Claiborne, L. L., C. F. Miller and J. L. Wooden (2010). "Trace element composition of igneous zircon: a thermal and compositional record of the accumulation and evolution of a large silicic batholith, Spirit Mountain, Nevada." Contributions to Mineralogy and Petrology **2010**: 511-531.

Clynne, M. A. (1990). "Stratigraphic, Lithologic, and Major Element Geochemical Constraints on Magmatic Evolution at Lassen Volcanic Center, California." Journal of Geophysical Research **95**(no. B12): 19,651-19,669.

Cole, R. B. and B. W. Stewart (2009). "Continental margin volcanism at sites of spreading ridge subduction: Examples from southern Alaska and western California." Tectonophysics **464**: 118-136.

Colgan, J. P., A. E. Egger, D. A. John, B. Cousens, R. J. Fleck and C. D. Henry (2011). "Oligocene and Miocene arc volcanism in northeastern California: Evidence for post-Eocene segmentation of the subducting Farallon plate." Geosphere **7**(no. 3): 733-755.

Conliffe, J., D. Selby, S. J. Porter and M. Feely (2010). "Re–Os molybdenite dates from the Ballachulish and Kilmelford Igneous Complexes (Scottish Highlands): age constraints for late Caledonian magmatism." Journal of the Geological Society **167**: 297-302.

Cousens, B. (1996). "Magmatic evolution of Quaternary mafic magmas at Long Valley Caldera and the Devils Postpile, California: Effects of crustal contamination on lithospheric mantle-derived magmas." Journal of Geophysical Research **101**(B12): 27,673-27,689.

Cousens, B., C. D. Henry, B. J. Harvey, T. Brownrigg, J. Prytulak and J. F. Allan (2011). "Secular variations in magmatism during a continental arc to post-arc transition: Plio-Pleistocene volcanism in the Lake Tahoe/Truckee area, Northern Sierra Nevada, California." Lithos **123**: 225-242.

Cousens, B., J. Prytulak, C. Henry, A. Alcazar and T. Brownrigg (2008). "Geology, geochronology, and geochemistry of the Miocene–Pliocene Ancestral Cascades arc, northern Sierra Nevada, California and Nevada: The roles of the upper mantle, subducting slab, and the Sierra Nevada lithosphere." Geosphere **4**(5): 829–853.

Dickinson, W. R. (1997). "Tectonic implications of Cenozoic volcanism in coastal California." GSA Bulletin **109**(8): 936-954.

Dickinson, W. R. (2008). "Accretionary Mesozoic–Cenozoic expansion of the Cordilleran continental margin in California and adjacent Oregon." Geosphere **4**(2): 329–353.

Drummond, M. S. and M. J. Defant (1990). "A Model for Trondhjemite-Tonalite-Dacite Genesis and Crustal Growth via Slab Melting: Archean to Modern Comparisons." Journal of Geophysical Research **95**(B13): 21,503-21,521.

Ducea, M. and J. Saleeby (1998). "Crustal recycling beneath continental arcs: silica-ricj glass inclusions in ultramafic xenoliths from the Sierra Nevada, California." Earth and Planetary Science Letters **156**: 101-116.

Dunning, G. R. and R. B. Pedersen (1988). "U/Pb ages of ophiolites and arc-related plutons of the Norwegian Caledonides: implications for the development of Iapetus." Contributions to Mineralogy and Petrology **98**: 13-23.

Ellam, R. M. and C. J. Hawkesworth (1988). "Is average continental crust generated at subduction zones?" Geology **16**: 314-317.

Farmer, G. L. and D. J. DePaolo (1983). "Origin of Mesozoic and Tertiary Granite in the Western United States and Implications for Pre-Mesozoic Crustal Structure 1. Nd and Sr Isotopic Studies in the Geocline of the Northern Great Basin." Journal of Geophysical Research **88**(B4): 3379-3401.

Farmer, G. L., A. F. Glazner, H. G. Wilshire, J. L. Wooden, W. J. Pickthorn and M. Katz (1995). "Origin of late Cenozoic basalts at the Cima volcanic field, Mojave Desert, California." Journal of Geophysical Research **100**(No. B5): 8399-8415.

Farver, J. R. and B. J. Giletti (1989). "Oxygen and strontium diffusion kinetics in apatite and potential applications to thermal history determinations." Geochimica et Cosmochimica Acta **53**: 1621-1631.

Fowler, M. B. (1988). "Ach'uaine hybrid appinite pipes: Evidence for mantle-derived shoshonitic parent magmas in Caledonian granite genesis." Geology **16**: 1026-1030.

Fowler, M. B. and P. J. Henney (1996). "Mixed Caledonian appinite magmas: implications for lamprophyre fractionation and high Ba-Sr granite genesis." Contributions to Mineralogy and Petrology **126**: 199-215.

Fraser, G., D. Ellis and S. Eggins (1997). "Zirconium abundance in granulite-facies minerals, with implications for zircon geochronology in high grade rocks." Geology **25**(7): 607-610.

Fraser, G. L., D. R. M. Pattison and L. M. Heaman (2004). "Age of the Ballachulish and Glencoe Igneous Complexes (Scottish Highlands), and paragenesis of zircon, monazite and baddeleyite in the Ballachulish Aureole." Journal of the Geological Society **161**: 447-462.

Garcia, M. O., L. Swinnard, D. Weis, A. R. Greene, T. Tagami, H. Sano and C. E. Gandy (2010). "Petrology, Geochemistry and Geochronology of Kaua‘i Lavas over 4·5 Myr: Implications for the Origin of RejuvenatedVolcanism and the Evolution of the Hawaiian Plume." Journal of Petrology **51**(7): 1507-1540.

Garrison, N. J., C. J. Busby, P. B. Gans, K. Putirka and D. L. Wagner (2008). "A mantle plume beneath California? The mid-Miocene Lovejoy flood basalt, northern California." Geological Society of America Special Paper **438**: 22 pages.

Gerlach, D. C. and T. L. Grove (1982). "Petrology of the Medicine Lake Highland Volcanics: Characterization of Endmembers of Magma Mixing." Contributions to Mineralogy and Petrology **80**: 147-159.

Godfrey, J. D. (1962). "The deuterium content of hydrous minerals from the East-Central Sierra Nevada and Yosemite National Park." Geochimica et Cosmochimica Acta **26**: 1215-1245.

Graham, D. W., M. R. Reid, B. T. Jordan, A. L. Grunder, W. P. Leeman and J. E. Lupton (2009). "Mantle source provinces beneath the Northwestern USA delimited by helium isotopes in young basalts." Journal of Volcanology and Geothermal Research **188**: 128-140.

Gromet, L. P. (1983). "Rare earth element distributions among minerals in a granodiorite and their petrogenetic implications." Geochimica et Cosmochimica Acta **47**: 925-939.

Guffanti, M., M. A. Clynne, J. G. Smith, L. J. P. Muffler and T. D. Bullen (1990). "Late Cenozoic Volcanism, Subduction, and Extension in the Lassen Region of California, Southern Cascade Range." Journal of Geophysical Research **95**(B12): 19,453-19,464.

Halliday, A. N. and W. E. Stephens (1984). "Crustal controls on the genesis of the 400 Ma old Caledonian granites." Physics of the Earth and Planetary Interiors **35**: 89-104.

Hawkesworth, C. J., P. D. Kempton, N. W. Rogers, R. M. Ellam and P. W. van Calsteren (1990). "Continental mantle lithosphere and shallow level enrichment processes in the Earth's mantle." Earth and Planetary Science Letters **96**: 256-268.

Henry, C. D. and M. E. Perkins (2001). "Sierra Nevada–Basin and Range transition near Reno, Nevada: Two-stage development at 12 and 3 Ma." Geology **29**: 719-722.

Hiekey-Vargas, R. and M. K. Reagan (1987). "Temporal variation of isotope and rare earth element abundances in volcanic rocks from Guam: implications for the evolution of the Mariana Arc." Contributions to Mineralogy and Petrology **97**: 497-508.

Hildreth, W. and S. Moorbath (1988). "Crustal contributions to arc magmatism in the Andes of Central Chile." Contributions to Mineralogy and Petrology **98**: 455-489.

Holbrook, W. S., D. Lizarralde, S. McGeary, N. Bangs and J. Diebold (1999). "Structure and composition of the Aleutian island arc and implications for continental crustal growth." Geology **27**: 31-34.

Irvine, T.N. and W.R.A. Barager (1971). "A guide to the chemical classification of the common volcanic rocks. Canadian Journal of Earth Sciences **8**: 523-548.

Jerram, D. A., K. M. Goodenough and V. R. Troll (2009). "Introduction: from the British Tertiary into the future – modern perspectives on the British Palaeogene and North Atlantic Igneous provinces." Geol. Mag. **146**(3): 305-308.

Kaczor, S. M., G. N. Hanson and Z. E. Peterman (1988). "Disequilibrium Melting of Granite at the Contact with a Basic Plug: A Geochemical and Petrographic Study." The Journal of Geology **96**(1): 61-78.

Kistler, R. W., B. W. Chappell, D. L. Peck and P. C. Bateman (1986). "Isotopic variation in the Tuolumne Intrusive Suite, central Sierra Nevada, California." Contributions to Mineralogy and Petrology **94**: 205-220.

Lawton, T. F. and N. J. McMillan (1999). "Arc abandonment as a cause for passive continental rifting: Comparison of the Jurassic Mexican Borderland rift and the Cenozoic Rio Grande rift." Geology **27**(9): 779-782.

Leeman, W. P., J. F. Lewis, R. C. Evarts, R. M. Conrey and M. J. Streck (2005). "Petrologic contraints on the thermal structure of the Cascades arc." Journal of Volcanology and Geothermal Research **140**: 67-105.

Leventhal, J. A., M. R. Reid, A. Montana and P. Holden (1995). "Mesozoic invasion of crust by MORB-source asthenospheric magmas, U.S. Cordilleran interior." Geology **23**(5): 399-402.

Lin, P. N., R. J. Stern, J. Morris and S. H. Bloomer (1990). "Nd- and Sr-isotopic compositions of lavas from the northern Mariana and southern Volcano arcs: implications for the origin of island arc melts." Contributions to Mineralogy and Petrology **105**: 381-392.

McCall, G. J. H. (1963). "Classification of Calderas: 'Krakatoan' and 'Glencoe Types." Nature **197**: 136-138.

McCrory, P. A., D. S. Wilson and R. G. Stanley (2009). "Continuing evolution of the Pacific–Juan de Fuca–North America slab window system —A trench–ridge–transform example from the Pacific Rim." Tectonophysics **464**: 30-42.

McIntosh, W. C., M. Heizler, L. Peters and R. Esser (2003). "$^{40}Ar/^{39}Ar$ geochronology at the New Mexico Bureau of Geology and Mineral Resources." New Mexico Bureau of Geology and Mineral Resources **Open File Report OF-AR-1**: 7.

Menzies, M. A., P. R. Kyle, M. Jones and G. Ingram (1991). "Enriched and Depleted Source Components for Tholeiitic and Alkaline Lavas from Zuni-Bandera, New Mexico:

Inferences About Intraplate Processes and Stratified Lithosphere." Journal of Geophysical Research **96**(B8): 13,645-13,671.

Mysen, B. (1979). "Trace-element partitioning between garnet peridotite minerals and water-rich vapour: experimental data from 5 to 30kbar." American Mineralogist **64**: 274-287.

Nelson, B. K. and D. J. DePaolo (1985). "Rapid production of continental crust 1.7 to 1.9 b.y. ago: Nd isotopic evidence from the basement of the North American mid-continent." Geological Society of America Bulletin **96**: 746-754.

Ormerod, D. S., N. W. Rogers and C. J. Hawkesworth (1991). "Melting in the lithospheric mantle: Inverse modelling of alkali-olivine basalts from the Big Pine Volcanic Field, California." Contributions to Mineralogy and Petrology **108**: 305-317.

Ort, M. H., B. L. Coira and M. M. Mazzoni (1996). "Generation of a crust-mantle magma mixture: magma sources and contamination at Cerro Panizos, central Andes." Contributions to Mineralogy and Petrology **123**: 308-322.

Paterson, B. A., G. Rogers and W. E. Stephens (1992). "Evidence for inherited Sm- Nd isotopes in granitoid zircons." Contributions to Mineralogy and Petrology **111**: 378-390.

Pearce, J. A. (1983). Role of the Sub-continental Lithosphere in Magma Genesis at Active Continental Margins. Continental Basalts and Mantle Xenoliths. C. J. Hawkesworth and M. J. Norry. Cambridge, MA, Birkhauser Boston Inc.

Pearce, J. A. and M. J. Norry (1979). "Petrogenetic Implications of Ti, Zr, Y, and Nb Variations in Volcanic Rocks." Contributions to Mineralogy and Petrology **69**: 33-47.

Putirka, K. and C. J. Busby (2007). "The tectonic significance of high K2O volcanism in the Sierra Nevada, California." Geology **35**: 923-926.

Reid, M. R. and F. C. Ramos (1996). "Chemical dynamics of enriched mantle in the southwestern United States: Thorium isotope evidence." Earth and Planetary Science Letters **138**: 67-81.

Reiners, P. W., P. E. Hammond, J. M. McKenna and R. A. Duncan (2000). "Young basalts of the central Washington Cascades, flux melting of the mantle, and trace element signatures of primary arc magmas." Contributions to Mineralogy and Petrology **138**: 249-264.

Renne, P. R., C. Swisher, III , D. B. Deino, D. B. Karner, T. Owens and D. J. DePaolo (1998). "Intercalibration of standards, absolute ages, and uncertainties in $^{40}Ar/^{39}Ar$ dating." Chemical Geology **145**: 117-152.

Richter, F. M., A. M. Davis, D. J. DePaolo and E. B. Watson (2003). "Isotope fractionation by chemical diffusion between molten basalt and rhyolite." Geochimica et Cosmochimica Acta **67**(20): 3905-3923.

Righter, K. (2000). "A comparison of basaltic volcanism in the Cascades and western Mexico: compositional diversity in continental arcs." Tectonophysics **318**: 99-117.

Roberts, J. L. (1966). "Ignimbrite Eruptions in the Volcanic History of the Glencoe Cauldron Subsidence." Geol. J. Vol. **5**(Pt. 1): 173-184.

Russell, J. K. and J. Nicholls (1988). "Analysis of petrologic hypotheses with Pearce element ratios." Contributions to Mineralogy and Petrology **99**: 25-35.

Rutherford, M. J. and P. M. Hill (1993). "Magma Ascent Rates From Amphibole Breakdown An Experimental Applied to the Mount St. Helens Eruptions." Journal of Geophysical Research **98**(B11): 19,667-19,685.

Rutherford, M. J., H. Sigurdsson, S. Carey and A. Davis (1985). "The May 18, 1980, Eruption of Mount St. Helens 1. Melt composition and Experimental Phase Equilibria." Journal of Geophysical Research **90**(B4): 2929-2947.

Salisbury, M. J., W. A. Bohrson, M. A. Clynne, F. C. Ramos and P. Hoskin (2008). "Multiple Plagioclase Crystal Populations Identified by Crystal Size Distribution and in situ Chemical Data: Implications forTimescales of Magma Chamber Processes Associated with the 1915 Eruption of Lassen Peak, CAy A. B." Journal of Petrology **49**(10): 1755-1780.

Sawka, W. N. and B. W. Chappell (1988). "Fractionation of uranium, thorium and rare earth elements in a vertically zoned granodiorite: Implications for heat production distributions in the Sierra Nevada batholith, California, U.S.A." Geochimica et Cosmochimica Acta **52**: 1131-1143.

Spencer, J. E., S. M. Richard, G. E. Gehrels, J. D. Gleason and W. R. Dickinson (2011). "Age and tectonic setting of the Mesozoic McCoy Mountains Formation in western Arizona, USA." Geological Society of America Bulletin **123**(7/8): 1258-1274.

Stephens, W. E. (2001). "Polycrystalline amphibole aggregates (clots) in granites as potential I-type restite: an ion microprobe study of rare-earth distributions." Australian Journal of Earth Sciences **48**: 591-601.

Stern, C. R. and R. Kilian (1996). "Role of the subducted slab, mantle wedge and continental crust in the generation of adakites from the Andean Austral Volcanic Zone." Contributions to Mineralogy and Petrology **123**: 263-281.

Stieger, R.H., and Jager, E., (1977). Subcommission on Geochronology: Convention on the use of decay constants in geo- and cosmochronology. " Earth and Planetary Science Letters 36: 359-362.

Stoffers, A. J. (2010). Geochemical Transition from Miocene – Pliocene to Quaternary Arc Volcanism in the Sierra Nevada, Northern California. Department of Earth Sciences. Ottawa, Carleton University**:** 128.

Sun, S. and W. F. McDonough (1989). "Chemical and isotopic systematics of oceanic basalts: implications for mantle composition and processes." Geological Society Special Publication(42): 313-345.

Tepley, F. J., J. P. Davidson and M. A. Clynne (1999). "Magmatic Interactions as Recorded in Plagioclase Phenocrysts of Chaos Crags, Lassen Volcanic Center, California." Journal of Petrology **40**(5): 787-806.

Thirwall, M. F. (1983). "Isotope Geochemistry and Origin of Calc-Alkaline Lavas From A Caledonian Continental Margin Volcanic Arc." Journal of Volcanology and Geothermal Research **18**: 589-631.

Ussler, W. and A. F. Glazner (1989). "Phase equilibria along a basalt-rhyolite mixing line: implications for the origin of calc-alkaline intermediate magmas." Contributions to Mineralogy and Petrology **101**: 232-244.

Viruete, J. E., M. Joubert, P. Urien, R. Friedman, D. Weis, T. Ullrich and A. Pérez-Estaún (2008). "Caribbean island-arc rifting and back-arc basin development in the Late Cretaceous: Geochemical, isotopic and geochronological evidence from Central Hispaniola." Lithos **104**: 378-404.

Vroon, P. Z., M. J. van Bergen, W. M. White and J. C. Varekamp (1993). "Sr-Nd-Pb Isotope Systematics of the Banda Arc, Indonesia: Combined Subduction and Assimilation of Continental Material." Journal of Geophysical Research **98**(No.B12): 22,349-22,366.

Watson, E. B. and T. M. Harrison (1983). "Zircon saturation revisited' temperature and composition effects in a variety of crustal magma types." Earth and Planetary Science Letters **64**: 295-304.

Xiong, X.-L. (2006). "Trace element evidence for growth of early continental crust by melting of rutile-bearing hydrous eclogite." Geology **34**: 945-948.

Appendix 1: GPS Locations of Samples

Sample	Latitude N	Longitude W
10LT01	39.44923	-120.236
10LT02	39.45874	-120.246
10LT03	39.4543	-120.264
10LT04	39.47298	-120.251
10LT05	39.47298	-120.251
10LT06	39.4354	-120.267
10LT07	39.42547	-120.312
10LT08	39.42645	-120.312
10LT09	39.41343	-120.319
10LT10	39.41334	-120.32
10LT11	39.41895	-120.323
10LT12	39.41901	-120.323
10LT13	39.41925	-120.323
10LT14	39.41813	-120.324
10LT15	39.41791	-120.324
10LT16	39.43918	-120.219
10LT17	39.44403	-120.209
10LT18	39.40917	-120.24
10LT19	39.41822	-120.239
10LT20	39.41339	-120.253
10LT21	39.44035	-120.205
10LT22	39.43693	-120.327
10LT23	39.44649	-120.312
10LT24	39.44351	-120.221

Appendix 2: Major and Trace Element data

Analyses above TiO_2 are XRF results from Ottawa U; below is from OGS ICP

Sample	10LT01	10LT02	10LT03	10LT04	10LT05	10LT06	10LT07	10LT08	10LT09
Map Unit	Tb	Tb	Tpap	Tb	Tb	Tpan	Tpan	Tpan	Tpan
SiO_2	51.55	52.8	50.95	50	52.55	58.41	55.47	55.43	60.11
Al_2O_3	16.22	17.02	15.9	18.12	15.74	17.39	19.67	16.75	17.88
CaO	9.95	10.33	9.84	6.44	9.95	7.03	7.15	5.89	6
K_2O	1.145	1.105	0.921	1.818	1.11	2.164	2.088	1.802	1.81
MgO	6.88	7	6.82	2.97	7.37	3.63	2.33	2.2	2.53
MnO	0.166	0.173	0.155	0.138	0.152	0.116	0.099	0.121	0.114
Na_2O	2.47	2.58	2.51	2.93	2.34	3.2	3.42	3.58	3.71
P_2O_5	0.218	0.216	0.165	0.325	0.145	0.195	0.276	0.203	0.2
Fe_2O_3(T)	9.241	9.626	9.268	9.159	9.302	6.759	6.411	6.197	5.932
Zn	73	83	84	89	78	76	74	81	77
TiO_2	0.801	0.835	0.745	1.033	0.708	0.656	0.753	0.55	0.527
Ba	402.9	374	363.2	150.1	374.8	1057.9	1168.9	1162.1	1106.3
Be	0.78	0.76	0.69	1.33	0.68	1.11	1.23	1.11	1.09
Bi	0.024	0.024	0.033	<0.009	0.08	0.075	0.1	0.03	0.02
Cd	0.13	0.3	0.16	0.15	0.11	0.15	0.13	0.11	0.13
Ce	30.1	33.12	23.94	63.13	25.85	48.91	57.24	39.83	43.31
Co	35.2	39.6	38	26.8	37.4	20.7	18.8	16.2	14.1
Cr	206	219	212	36	287	92	30	39	<24
Cs	0.25	0.4	0.29	1.7	0.37	1.92	1.81	0.7	0.96
Cu	69	54	140	152	92	64	114	23	17
Dy	4.34	4	2.88	5.79	3.01	3.81	4	2.69	3.16
Er	2.65	2.41	1.65	3.27	1.82	2.29	2.33	1.6	1.87
Eu	1.42	1.38	1.04	2.11	1.05	1.18	1.34	1	1.1
Ga	18.58	21.65	18.97	21.17	18.57	18.56	21.21	19.45	20.13
Gd	4.61	4.19	3.2	6.83	3.18	4.21	4.5	3.01	3.46
Hf	2.48	2.59	1.74	4.14	1.93	4.55	4.47	3.19	4.25
Ho	0.91	0.82	0.58	1.14	0.62	0.77	0.8	0.55	0.63
La	16.4	15.03	11.78	34.96	12.57	25.2	28.1	20.41	21.41
Li	7.5	9.1	8.5	12.9	8.1	15.2	14.2	17.7	13.5
Lu	0.37	0.35	0.23	0.45	0.27	0.33	0.34	0.25	0.28
Mo	0.42	0.67	0.66	1.45	0.71	1.99	2.12	1.14	1.73
Nb	2.82	3.25	2.39	5.07	2.11	6.23	6.85	5.25	5.4
Nd	20.92	19.88	15.42	39.69	15.14	24.9	29.02	19.12	20.89
Ni	31	34	48	21	43	29	24	19	6
Pb	2.8	4	5.4	10.4	7	9.9	13.6	10	7.6
Pr	4.65	4.58	3.47	9.43	3.53	6.25	7.33	4.95	5.32
Rb	13.64	14.04	12.42	48.38	14.22	58.17	60.13	46.59	54.79
Sb	0.21	0.28	0.33	0.42	0.15	0.49	0.54	0.55	0.48
Sc	41.9	46.8	40.1	30.1	45.3	23.5	18.4	14.8	12.9
Sm	4.53	4.52	3.42	8.08	3.42	4.91	5.62	3.69	4.14
Sn	0.93	0.95	0.72	1.82	0.8	1.18	1.26	0.91	1.12
Sr	847	1000	879	643	663	559	731	641	614
Ta	0.2	0.2	<0.2	0.3	<0.2	0.3	0.4	0.3	0.3
Tb	0.671	0.639	0.467	0.956	0.476	0.614	0.647	0.439	0.516
Th	2.21	2.38	1.86	8.49	3.83	5.52	6.58	3.46	3.93
Ti	5077.4	5871.14	4764.21	6272.61	4381.84	3872.51	4760.17	3231.65	3500.36
Tl	0.06	0.04	0.03	0.05	0.05	0.24	0.21	0.17	0.26
Tm	0.38	0.359	0.24	0.467	0.269	0.333	0.338	0.236	0.272
U	0.93	0.91	0.77	2.81	1.45	2.24	2.66	1.27	1.59
V	290.76	329.7	301.27	276.08	304.47	176.19	210.82	123.38	129.28
W	<0.5	<0.5	<0.5	0.52	<0.5	0.51	0.64	<0.5	<0.5
Y	28.27	24.01	17.56	33.22	17.24	23.24	23.85	15.93	18.19
Yb	2.382	2.292	1.517	2.94	1.747	2.128	2.213	1.59	1.77
Zn	79.57	97.1	90.5	94.05	81.26	75.9	78.23	80.83	86.61
Zr	92	97	64	162	71	188	186	132	181

Sample	10LT10	10LT011	10LT012	10LT013	10LT014	10LT015a	10LT016	10LT017	10LT018
Map Unit	Tha	Tbt	Tbt	Tbt	Tbt	dyke	Tpan	Tb	Tba
SiO_2	60.71	49.38	47.92	56.6	55.74	53	55.4	51.58	59.08
Al_2O_3	18.24	17.12	16.41	18.36	18.63	18.27	18.23	16.35	17.65
CaO	5.65	10.53	10.47	6.36	7.43	8.29	7.65	10.24	6.15
K_2O	1.969	1.208	1.185	2.432	1.355	1.597	1.392	1.127	2.323
MgO	1.95	5.97	6.26	2.39	3.58	4.31	3.76	6.79	2.97
MnO	0.128	0.126	0.132	0.09	0.136	0.148	0.139	0.168	0.119
Na_2O	3.57	2.62	2.51	3.46	3.34	2.73	3.29	2.45	3.36
P_2O_5	0.251	0.193	0.189	0.271	0.207	0.197	0.228	0.218	0.221
Fe_2O_3(T)	6.185	9.551	9.266	5.608	7.651	8.272	8.146	9.439	6.42
Zn	89	76	74	78	92	84	91	80	84
TiO_2	0.554	1.037	0.998	0.675	0.651	0.807	0.735	0.814	0.624
Ba	1123.6	469.8	474.4	1043	776.2	671.2	780.9	368.3	1046.3
Be	1.29	0.71	0.73	1.23	0.94	0.83	1.06	0.66	1.2
Bi	0.015	0.016	0.036	0.032	0.084	0.11	0.11	0.018	0.085
Cd	0.18	0.13	0.17	0.14	0.13	0.18	0.14	0.14	0.17
Ce	46.61	30.86	30.29	44.38	37.75	36.97	41.87	29.36	51.69
Co	11.8	37.8	38.1	16.4	20.6	27.4	23.9	34.8	16.2
Cr	<24	150	147	<24	<24	42	<24	201	<24
Cs	1.19	1.27	1.38	2.26	0.91	1.61	0.65	0.26	2.42
Cu	11	104	99	31	25	80	47	41	28
Dy	3.3	3.55	3.55	3.1	3.2	3.09	3.19	3.57	3.63
Er	1.96	2.02	1.97	1.73	1.9	1.74	1.83	2.14	2.15
Eu	1.15	1.24	1.22	1.19	1.09	1.11	1.26	1.25	1.19
Ga	21	19.66	19.54	21.18	20.98	20.53	21.49	18.64	19.33
Gd	3.66	3.85	3.87	3.58	3.44	3.43	3.7	3.74	4.03
Hf	3.85	2.38	2.37	3.58	2.86	2.98	2.85	2.52	4.57
Ho	0.66	0.72	0.71	0.6	0.65	0.61	0.64	0.73	0.73
La	23.89	13.98	14	22.97	18.44	17.5	21.63	12.99	25.85
Li	17.2	9.3	9.5	10.5	13.9	9.5	12	7.7	17.6
Lu	0.3	0.27	0.27	0.25	0.28	0.25	0.27	0.31	0.33
Mo	1.72	0.81	0.72	1.76	0.86	1.01	1.22	0.57	2.68
Nb	5.95	3.24	3.12	5.6	4.52	3.56	4.5	2.84	6.98
Nd	23.2	18.67	18.5	22.48	19.52	19.65	22.64	18	25.15
Ni	5	42	38	15	10	25	12	29	12
Pb	10.9	5	5.3	12.4	8.7	8.2	9.5	5.2	12.3
Pr	5.98	4.27	4.15	5.62	4.84	4.77	5.52	4.1	6.41
Rb	54.28	23.2	22.43	57.48	34.69	31.59	26.35	12.11	64.77
Sb	0.37	0.37	0.37	0.64	0.24	0.28	0.61	0.18	0.55
Sc	12.6	47	47.5	14.8	18.9	32.4	22.6	42.2	15.8
Sm	4.47	4.32	4.23	4.29	3.96	3.92	4.49	4.06	4.83
Sn	1.12	0.88	0.73	1.03	1.04	1.01	0.99	0.61	1.21
Sr	701	846	827	789	678	992	905	866	630
Ta	0.4	0.2	0.2	0.4	0.2	0.2	0.2	0.2	0.4
Tb	0.537	0.576	0.57	0.517	0.513	0.5	0.523	0.567	0.592
Th	4.6	3.13	3.07	3.97	3.71	3.6	4.54	1.98	6.67
Ti	3413.84	6288.26	6408.81	4275.45	3946.86	4991.4	4531.55	5066.61	3709.86
Tl	0.32	0.02	0.03	0.32	0.16	0.24	0.11	0.05	0.35
Tm	0.294	0.282	0.285	0.247	0.277	0.252	0.265	0.31	0.318
U	1.91	1.2	1.16	1.68	1.34	1.34	1.62	0.82	2.5
V	118.59	377.66	380.34	153.2	178.55	292.33	217.16	293.24	140.28
W	<0.5	<0.5	<0.5	0.55	<0.5	<0.5	<0.5	<0.5	0.64
Y	20.03	19.7	20	17.61	18.62	17.25	18.58	20.73	21.24
Yb	1.918	1.755	1.792	1.595	1.796	1.606	1.71	2.017	2.093
Zn	97.89	76.93	78.79	84.38	95.39	89.1	102.4	84.32	84.87
Zr	162	89	87	151	114	119	115	94	187

Sample	10LT019	10LT020b	10LT021	10LT022	10LT023	10LT024
Map Unit	Tba	Tha	Tb	dyke	Tpan	Tpap
SiO_2	56.92	57.92	51.19	51.17	54.86	51.31
Al_2O_3	18.32	18.08	15.98	18.88	18.15	15.99
CaO	6.86	6.7	10.56	8.41	7.34	10.59
K_2O	1.537	1.713	0.855	1.341	1.347	0.84
MgO	2.99	3.01	7.14	4.73	4.27	7.2
MnO	0.154	0.131	0.155	0.14	0.138	0.157
Na_2O	3.61	3.56	2.5	3.08	3.42	2.49
P_2O_5	0.288	0.259	0.172	0.254	0.259	0.173
Fe_2O_3(T)	8.148	6.67	9.416	8.848	7.874	9.525
Zn	94	83	81	92	91	84
TiO_2	0.656	0.613	0.762	1.022	0.78	0.765
Ba	937	927.2	312.2	629.8	832.4	318.5
Be	1.24	1.09	0.64	1.09	1.12	0.64
Bi	0.058	0.029	0.032	0.041	0.082	0.063
Cd	0.14	0.14	0.13	0.16	0.19	0.14
Ce	42.89	46.88	22.53	36.19	40.37	22.59
Co	19.6	17.7	38.1	28.9	24.7	37.6
Cr	<24	<24	214	24	42	213
Cs	1.03	0.78	0.16	2.13	1.05	0.16
Cu	33	50	51	77	39	81
Dy	3.32	3.23	2.71	3.56	3.39	2.81
Er	1.97	1.91	1.57	2.01	1.97	1.65
Eu	1.26	1.17	1.02	1.28	1.22	1.06
Ga	20.86	19.92	18.64	21.98	19.68	18.39
Gd	3.67	3.57	2.97	4.11	3.76	3.17
Hf	3.04	3.57	1.65	3.21	3.01	1.66
Ho	0.66	0.66	0.55	0.7	0.67	0.57
La	20.89	23.98	9.98	16.66	21.22	11.1
Li	14.2	13.9	7.3	13.8	12.2	6.8
Lu	0.29	0.29	0.22	0.27	0.29	0.22
Mo	1.36	1.17	0.52	1.46	1.68	0.54
Nb	4.52	5.32	2.18	4.3	5.86	2.18
Nd	22.45	22.5	14.53	21.42	21.96	14.97
Ni	6	13	43	32	23	45
Pb	12.2	9	3.3	9	13	3.3
Pr	5.59	5.84	3.27	4.97	5.41	3.38
Rb	41.43	42.38	8.48	33.49	32.86	8.2
Sb	0.39	0.62	0.31	0.52	0.39	0.24
Sc	15.5	16.8	44.3	26	21.1	44.2
Sm	4.44	4.31	3.3	4.71	4.31	3.42
Sn	1.03	1.1	0.77	0.85	1.06	0.86
Sr	737	749	863	865	720	857
Ta	0.3	0.3	<0.2	0.2	0.3	<0.2
Tb	0.534	0.522	0.443	0.605	0.555	0.453
Th	4.19	4.47	1.6	3.85	3.21	1.58
Ti	3940.15	3613.24	4671.82	6093.17	4693.6	4627.24
Tl	0.19	0.2	0.03	0.13	0.17	0.02
Tm	0.289	0.287	0.221	0.281	0.285	0.231
U	1.76	1.73	0.66	1.51	1.26	0.64
V	176.5	151.87	306.63	255.83	183.11	305.98
W	<0.5	<0.5	<0.5	<0.5	<0.5	<0.5
Y	18.98	19.09	15.01	19.9	20.3	18.17
Yb	1.885	1.898	1.427	1.804	1.864	1.463
Zn	100.03	87.38	87.33	99.79	94.61	89.31
Zr	119	147	60	123	124	60

Appendix 3: Isotopic Values of Samples

Note: 2sigma based on reproducibility of standards, $^{87}Sr/^{86}Sr$±0.000015, $^{143}Nd/^{144}Nd$±0.000008, $^{206}Pb/^{204}Pb$±0.002

Sample	10LT01	10LT02	10LT03	10LT04	10LT05	10LT07	10LT08	10LT09	10LT10
Map Unit	Tb	Tb	Tpap	Tb	Tb	Tpan	Tpan	Tpan	Tha
$^{208}Pb/^{204}Pb$	38.4809	38.4584	38.5583	38.6859	38.5614	38.7000	38.8011	38.7271	38.7313
$^{207}Pb/^{204}Pb$	15.6003	15.5953	15.6107	15.6319	15.6151	15.6351	15.6524	15.6428	15.6370
$^{206}Pb/^{204}Pb$	18.8606	18.8368	18.9015	18.9734	18.8876	18.9771	19.0116	18.9748	18.9939
$^{208}Pb/^{206}Pb$	2.0396	2.0409	2.0392	2.0382	2.0409	2.0386	2.0402	2.0402	2.0384
$^{207}Pb/^{206}Pb$	0.8269	0.8277	0.8257	0.8237	0.8265	0.8237	0.8231	0.8242	0.8230
$^{87}Sr/^{86}Sr$	0.703465	0.703408	0.703903	0.704470	0.703658	0.704665	0.705333	0.705079	0.704875
$^{143}Nd/^{144}Nd$	0.512809	0.512813	0.512741	0.512749	0.512816	0.512660	0.512549	0.512609	0.512581

Sample	10LT11	10LT12	10LT13	10LT14	10LT16	10LT19	10LT22	10LT23
Map Unit	Tbt	Tbt	Tbt	Tbt	Tpan	Tba	dyke	Tpan
$^{208}Pb/^{204}Pb$	38.5593	38.7747	38.7290	38.5413	38.6663	38.7860	38.6238	38.7090
$^{207}Pb/^{204}Pb$	15.6144	15.6513	15.6467	15.6048	15.6255	15.6621	15.6170	15.6369
$^{206}Pb/^{204}Pb$	18.8817	18.9944	18.9689	18.8911	18.9600	18.9903	18.9495	18.9811
$^{208}Pb/^{206}Pb$	2.0414	2.0406	2.0410	2.0395	2.0386	2.0417	2.0375	2.0386
$^{207}Pb/^{206}Pb$	0.8267	0.8238	0.8246	0.8258	0.8239	0.8245	0.8239	0.8236
$^{87}Sr/^{86}Sr$	0.703832	0.703826	0.704794	0.704964	0.704485	0.704718	0.704690	0.705164
$^{143}Nd/^{144}Nd$	0.512753	0.512744	0.512668	0.512613	0.512642	0.512680	0.512687	0.512598

Appendix 4: Field Descriptions and Photography

Table 4: Sample Descriptions

Sample	Outcrop Description
10LT-01	Tb map unit. Olivine basalt. Sampled near HO7-140 dated sample. Speckly foliation (weak few cm). Minor vuggs. Flow direction ~50 degrees. Weathering light brown. Fresh dark gray black. See Plate 7.
10LT-02	Tb map unit. Olivine basalt. Vuggs are more pronounced but are more localized to various parts of the outcrop than 10LT-01, foliated 1-8 cm length. Flow direction 120 degrees.
10LT-03	Tpap map unit (andesite). Porphyritic basalt. Pyroxene, olivine?, phenocrysts. Olivine has pyroxene rims (green cores brown rims). Pyroxene black-brown or brown colouration ~3-4 mm size. Weak foliation (weaker than Tb). See Plate 3.
10LT-04	Quarry in Tpap map unit. Lots of boulders of varying types similar to the above units. Rock types: frothy obsidian (10LT-04), flow banded basalt similar to Tb (underlying unit?) (10LT-05). See Plate 8.
10LT-05	
10LT-06	Tpan map unit. However the outcrop is a porphyritic pyroxene andesite. Plagioclase phenocrysts ~5 mm. Pyroxene phenocrysts ~3 mm. Some weathered out vesicles in the matrix. Brown weathering rind. Vesicles have some secondary mineralization of feldspar. Vesicles ~5 mm.
10LT-07	Tpan map unit: a few meters down from 10LT-06 the andesite develops big flow bands that shallowly dip prograding to a near vertical dip. Flow bands have a north-south strike.
10LT-08	Rubble pile on top of a ridge in unit Tpan. Porphyritic pyroxene andesite boulders. Rare pyroxene phenocrysts ~3 mm. Plagioclase grains ~3 mm. Plagioclase is more bladey/acicular than 10LT-06/07
10LT-09	Tpan map unit here is slightly different from last stop. Pyroxene is better formed and more abundant. Plagioclase is less abundant. See Plate 2
10LT-10	Carpenter ridge weather station unit. Hornblende andesite (Tha). Aphanitic matrix with fissile flow bands. Plag ~3-4 mm (rare as phenocrysts). Hornblende ~2 mm euhedral or rounded more abundant than plagioclase. Looking to the other side of Carpenter Valley we can see an extensive granite exposure and normal fault. Fresh=light grey. Weathered=rose red-brown. 10LT-10 taken from adjacent hill less than 100 m away appears to be the margin of a dyke. Vesicles are prevalent and weathered. Walking back to the car I came across 2 outcrops: one had a large hornblende crystal (2-3 cm) the other had large 3-5 cm rounded xenocrysts. See Plate 5.

Sample	Outcrop Description
10LT-11	The cliff itself is a pyroclastic flow (unit Tbt). Clasts are rounded-angular. Boulder to pebble size. Likely flank flow. Polymict: glassy rocks/basalt, hornblende andesites, frothy basalts, pyroxene andesites. No distinct bedding but there is clumping of small and large clasts in areas. On one side (east) there appears to be vertical flows. Bottom of cliff contains larger clasts (but still has small clasts). Top of cliff is framework support dominates and clasts are generally smaller. Bottom of cliff is pyroxene dominated (basaltic?) andesite (10LT11, 10LT12). Top is a plagioclase rich vesicular andesite (10LT13). Southwest and 100 m from Tbt is a more coherent flow with more angular clasts (10LT-14). Primarily a rhyodacite? Possible quartz grains (disputed). See Plate 1.
10LT-12	
10LT-13	
10LT-14	
10LT-15	Continuing SW we start ascending a new peak and reach a dyke on the east side of the mountain. The dyke has a heavily thermally altered pyroclastic flow beside it. The dyke has columnar jointing. Samples: 10LT15a-west side of dyke (darker colouration). 10LT15b-east side of dyke (more vesicular and sheared). See Plate 6.
10LT-16	Searched for map unit Tb but only found andesite float (sample taken). Map unit Tpan. Undifferentiated andesite with minor foliation, vugs and vapour phase. Plagioclase dominates not pyroxene, this is different from the other Tpan samples where pyroxene dominates: 20-30% plagioclase (<1 mm grain size), 2-5% pyroxene.
10LT-17	East side of Hwy 89 looking for Tb and Tpa. 10LT17: olivine basalt. Olivine is <1 mm (unlike other Tb samples). Unit is also light grey colour. There are weak foliations. There are vertical flowbands in outcrop. Sample 10LT17b was taken from across the logging road at another outcrop. This sample is unit Tb but olivine is more abundant (~15% more). There is also ramping and boulder (pillow?) structures. Flow bands are present (<20°).
10LT-18	No outcrop but lots of homogenous boulders. Basaltic andesite map unit? Porphyritic (pyroxene, plagioclase). Some foliation. Olivine? See Plate 4.
10LT-19	Tba: weather station. Two outcrops with near vertical dip. Looks different from the boulder sample 10LT-18 (lighter colour, less phenocrysts). Very fissile. Cuspate cleavage. 3-4 mm plagioclase crystals. There is a weak foliation of the plagioclase grains.
10LT-20	Tha: Big outcrop/ridge. Hornblende andesite. Magnetic! (Strong). Fissile cleavage is 1-3 cm. Multiple dip directions (all compass points). Red oxidation. The outcrop lithology is highly variable in a small area. One area has little to no phenocrysts- 10LT20a. Another area has a typical Tha composition, not a lot of plagioclase and lots of hornblende– 10LT20b. The final area has large >2 cm scale hornblende and plagioclase – 10LT20c.

Sample	Outcrop Description
10LT-21	Tpan on ridge east of Hwy 89. Pyroxene 5-10 mm angular some rounded. Minor amounts of olivine (<5%). It is possible that this outcrop is map unit Tb i.e. no Tpan in this area.
10LT-22	Independence Lake. Searched for Tpan but no luck, sampled a Tpan boulder (10LT23) that appears to have fallen from a cliff above the lake (not possible to climb up). Found a mafic dyke almost directly along strike and dip of the dyke I sampled two days ago on top of carpenter ridge (10LT22). Contains pyroxene. Also plenty of granitic/dacitic boulders in the area.
10LT-23	
10LT-24	Tpan on East Road to Sagehen camp. Similar to Tpan from Independence Lake (compositionally). Pyroxene phenocrysts, minor plagioclase (not phenocrystic).

Appendix 4.1 Representative Photos of Map Units

Plate 2: Tbt lower portion of outcrop (upper portion not well exposed due to lichen). Polymict boulder to pebble clasts within a fine-coarse grained matrix (matrix is not pumiceous or ash rich).

Plate 3: Tpan 10LT-09. Plagioclase phenocrysts within an aphanitic matrix

Plate 4: Tpap 10LT-03. 2-3 mm sized phenocrysts of pyroxene that are green, brown and black.

Plate 5: Tba 10LT-18. Boulder with plagioclase phenocrysts.

Plate 6: Tha 10LT-10. 2-4 mm phenorysts of plagioclase and hornblende.

Plate 7: Dyke 10LT-15. A mafic dyke margin with moderate alteration.

Plate 8: Tb 10LT-01. Olivine basalt with flow banding and foliated vuggs.

Plate 9: Tb 10LT-04 scoria. The sample was found at the bottom of the quarry within the Tpap map unit. It was inferred to be Tb at the time of sampling.